UNIVERSITEIT GENT

FACULTY OF VETERINARY MEDICINE
approved by EAEVE

The Role of Joint Biomechanics in the Development of Tarsocrural Osteochondrosis in Dogs

WALTER BENJAMIN DINGEMANSE

Thesis submitted in fulfilment of the requirements for the degree of
Doctor of Philosophy (PhD) in Veterinary Sciences,
Faculty of Veterinary Medicine, Ghent University

2017

Promoters:
Dr. Ingrid Gielen
Prof. Dr. Ilse Jonkers
Prof. Dr. Bernadette Van Ryssen
Prof. Dr. Magdalena Müller-Gerbl

Department of Veterinary Medical Imaging and Small Animal Orthopaedics
Faculty of Veterinary Medicine
Ghent University

The Role of Joint Biomechanics in the Development of Osteochondrosis in Dogs

Walter Benjamin Dingemanse

Vakgroep Medische Beeldvorming van de Huisdieren en Orthopedie van de Kleine Huisdieren

Faculteit Diergeneeskunde

Universiteit Gent

Cover design by Michael Edmond Nico Van Waegevelde

PhD supported by a grant from IWT

I MAY NOT HAVE GONE WHERE I INTENDED TO GO

BUT I THINK I HAVE ENDED UP WHERE I

NEEDED TO BE

- DOUGLAS ADAMS -

EXAMINATION BOARD

Chair:

Prof. dr. Hilde de Rooster

Faculty of Veterinary Medicine, Ghent University, BE

Secretary:

Prof. dr. Wim Van den Broeck

Faculty of Veterinary Medicine, Ghent University, BE

Members:

Prof. dr. Robert Colborne

Institute of Veterinary, Animal & Biomedical Sciences, Massey University, NZ

Dr. Evelien de Bakker

Faculty of Veterinary Medicine, Ghent University, BE

Dr. Maarten Oosterlinck

Faculty of Veterinary Medicine, Ghent University, BE

Prof. dr. Benedicte Vanwanseele

Faculty of Kinesiology and Rehabilitation Sciences, KU Leuven, BE

Prof. dr. Jos Vander Sloten

Faculty of Engineering Science, KU Leuven, BE

TABLE OF CONTENTS

LIST OF ABBREVIATIONS

3D	three-dimensional
ACLT	anterior cruciate ligament transsection
CT	computed tomography
DOF	degrees of freedom
FOV	field of view
GRF	ground reaction force
HU	Hounsfield Unit
ID	inverse dynamics
IK	inverse kinematics
kV	kilovoltage
L	lateral
LCS	local coordinate system
mAs	milliampere-seconds
MPR	multi-planar reconstruction
MRI	magnetic resonance imaging
MSM	musculoskeletal model
M	medial
N	Newton
N/A	not available
OC	osteochondrosis
PMMA	polymethylmethacrylate
PSCA	physical cross sectional area
ROI	region of interest
SO	static optimization

GENERAL INTRODUCTION

CHAPTER ONE

Subchondral Bone – Morphology, Density, and Density Evaluation

W. Dingemanse [1], M. Müller-Gerbl [2], H. van Bree [1], I. Gielen [1]

[1] Department of Medical Imaging of Domestic Animals and Orthopaedics of Small Animals Faculty of Veterinary Medicine, Ghent University. Merelbeke, Belgium

[2] Institute of Anatomy, Basel University. Basel, Switzerland

BONE AND BONE ADAPTATION

Bones provide a solid structure for muscle attachment and protect the most vital organs. Bones are also made of living cells that function like an organ, whose structure continually changes, and adapts to current needs. Mature bone tissue is composed of 60–70% mineral substance and 30–40% organic matrix, mainly (85–90%) type I collagen fibrils. The osteoblasts are the main cells responsible for bone formation and secrete important constituents of the extra-cellular matrix (ECM). Calcium hydroxyl apatite crystals are deposited within the triple helix of the collagen type I fibrils [1]. The mineral substance does not only have a biomechanical role (strength), it also has an important metabolic role (mineral homeostasis and reservoir function for many different ions) [2].

The mechanical loads and associated strains, help to control and guide bone morphology [3]. This response to bone strains not only dictates general bone anatomy, it also allows for adaptations to changes in loading. The adaptations are done through modeling and remodeling of bone. This is a result of local strains either staying below the remodelling threshold or exceeding the modelling threshold [3]. The loading of bones leads to a certain degree of deformation, even though this degree is low, since it is a hard, mineralised tissue. The deformation generates strains, and when these strains exceed the modeling threshold, bone modeling is signalled to increase bone strength (locally), and thereby reducing later strains [3].

The need for these adaptations is signalled through the different bone cells, which are mechanosensitive [4]. The conversion of a mechanical stimulus to into a cellular response is called mechanotransduction [5]. The four important cells in bone include (1) osteoclasts, which are of hematopoietic origin and resorb bone, (2) osteoblasts, mesenchymal-derived and form bone, (3) terminally differentiated osteoblasts embedded in the bone, called osteocytes, and (4) the mesenchymal stem cell (MSC), which are the osteoprogenitor cells [4]. These cells can detect mechanical signals independently and interact with each other through different pathways to regulate bone modeling and remodeling. The osteocytes form a network through their

canalicular projections, and the movement of fluid within these canaliculi generates shear forces that play a role in the mechanotransduction of bone loading to cell-level information cells [4]. On a cell level, the surface proteoglycan layer is the primary sensor of mechanical signals. The cell membrane deformations are transmitted to the cytoskeleton through integrin and cadherin proteins [5]. The different intra-cellular signalling pathways that are part of the adaptive response are beyond the scope of this work, they have however been described in detail elsewhere [5-7].

SUBCHONDRAL BONE

Definitions

The subchondral bone plate is defined as the bony lamella immediately below the calcified articular cartilage. The line separating these two structures is known as the 'cement line'. At the level of the cartilage, a second line i.e. the 'tidemark' separates the articular cartilage and the underlying calcified articular cartilage [8]. The subchondral bone plate receives additional support from the subchondral trabeculae and which are grouped together as 'subchondral bone' [8].

Morphology

The subchondral bone plays an important role in the transfer of loads across the joint surface. Thus, the morphology of the subchondral bone is dictated by the compressive forces acting upon it. As in all bones, the structure is continually adapted to current needs. At the level of the joints, these needs are predominantly the transduction of (compressive) forces from the proximal to the distal bones forming a specific joint [9,8]. These forces give rise to local strains and stresses and induce modelling and remodelling of the subchondral bone, as discussed above.

The thickness of the subchondral bone plate varies among joint and has regional variations within a joint [8]. These variations in thickness are associated with joint loading and the loading regime [10] and have been correlated with joint pathology [11].

Density

The density of the subchondral bone at any given time is the result of the bone functional adaptation [8,12]. It is a heterogeneously mineralized material described by the apparent density and the mineral density.

$$Apparent\ density\ = \frac{mineralised\ mass}{sample\ volume}$$

$$Material\ density\ = \frac{mineralised\ mass}{volume\ of\ the\ material\ itself}$$

The difference between these two density measures is geometrical, and is due to the presence of pores [13,14]. The biomechanical properties of the subchondral bone are characterized by mineral density, collagen content, and ash fraction [14]. In general subchondral bone density can be adapted by changing the apparent density, the material density, or a combination of both. These biomechanical properties can change through modeling and remodeling of the articulating bones, guided by local strains [7,15]. The material properties are tissue level properties and by definition independent of the size of the bone [14].

Increased joint loading leads to increased local strains and bone modelling ensures an increase in subchondral bone density to withstand the increased loading [3,16]. In addition, altered joint biomechanics lead to altered joint loading distribution, leading in turn to alterations in the subchondral bone density distribution [17,18]. This ability to adapt is summarized in the term ‘bone functional adaptation’. This allows us to indirectly evaluate joint loading based on the subchondral bone density.

JOINT LOADING AND SUBCHONDRAL BONE DENSITY

Joint loading

The evaluation of actual joint loading is very difficult *in vivo*, since it requires the use of intra-articular pressure films [19]. Invasive (*in vitro*) methods to study joint loading include the description of pressure distribution and contact areas on cadavers [20,21]. However, these techniques require a certain degree of dissection, which will ultimately alter the joint kinematics. As demonstrated in humans, the subchondral bone density distribution is highly correlated with joint loading and reflects the loading history of the joint [8,18,22]. Thus, subchondral bone density provides an opportunity for non-invasive research of joint loading [8,12].

Imaging bone material properties

The subchondral bone density distribution can be evaluated non-invasively using computer tomographic osteoabsorptiometry (CTOAM) [9,18,23]. It is important to note that the density evaluation using CT images is based on apparent density. The formation of CT images is based on tissue attenuation and is therefore a representation of both the material density and material porosity.

For the description of bone porosity, MRI techniques evaluating differences in mobile and bound water can be used [24,25]. Mobile water consists of hydrogen atoms occupying the canaliculi and lacunae within the bone and represents the bone porosity. Bound water is attached to the Collagen molecules or forms a hydratation shell based on the bone mineral surface charges (Ca^{2+} and PO^{4-}). The relaxation time of covalently bound hydrogen atoms, i.e. those present in the Collagen amino acids or minerals, is much faster than that of water molecules (H2O), which are exhibiting van der Waals interactions. These differences in relaxation time allow both mobile and bound water to be imaged using MRI [24].

The subchondral bone density distribution can be visualized and quantified using computer tomographic osteoabsorptiometry (CTOAM) [18,22,23]. The CTOAM workflow includes several different steps. In the first step, the bone of interest is segmented

using the segmentation algorithm in 'Analyze'. Based on the segmented images, one or more different three-dimensional (3D) views of the can be reconstructed.

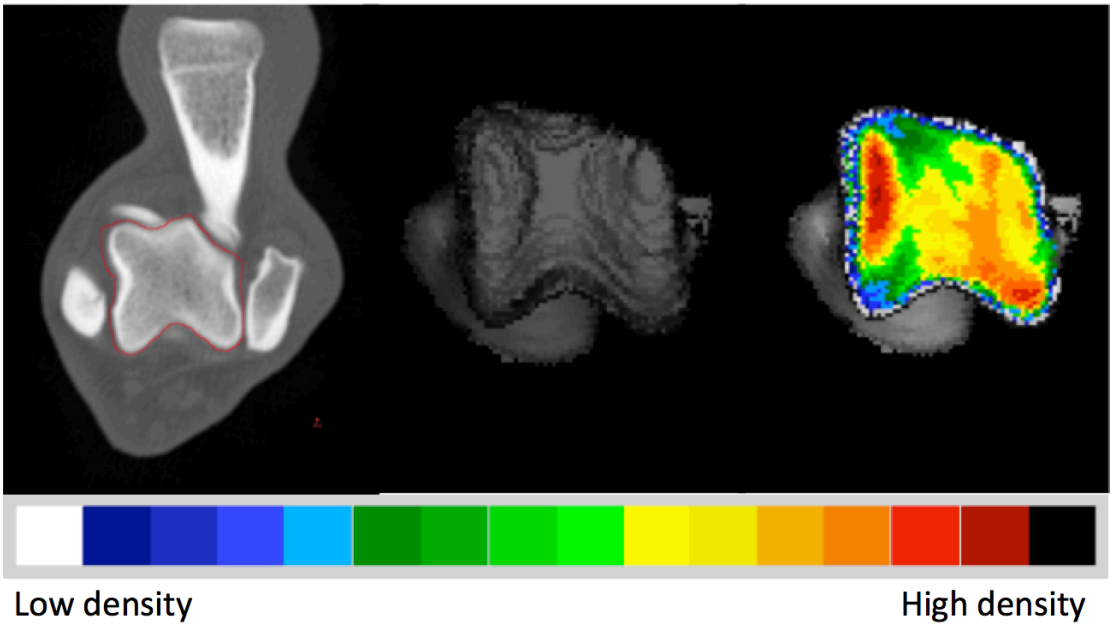

Figure 1: CTOAM workflow in Analyze. From left to right: segmentation of the talus; 3D rendering of the proximal view; overlay of the false-colour map of the subchondral bone density distribution.

Subsequently, the subchondral bone plate of the articulating surface is isolated and reconstructed in exactly the same orientations. The maximum bone density is projected onto the articular surface using a maximum intensity projection (MIP). With a MIP, the three-dimensional (3D) data volume (in voxels) of the subchondral bone plate is converted to a 2D image (in pixels) in which each pixel represents the maximum value (based on the HU). This maximum value is obtained from the voxels along the line perpendicular to the pixel in the 2D image. The length of this line, i.e. the depth of the MIP, is based on the thickness of the subchondral bone plate and was set at 1.5 mm. This MIP view is then converted to a false colour scale, where the range of 200 – 1200 Hounsfield Units (HU) is divided in value ranges of 100 HU each representing a colour. In descending order these colours are black, dark red, light red, orange, yellow, dark green, light green, dark blue, light blue, and white. This results in a densitogram, which displays lines of isodensities, i.e. lines connecting regions of equal density. This densitogram is a visual representation of the apparent

density distribution and can be used to further describe and quantify the subchondral bone density distribution.

CTOAM of the canine talus

Specifically for the evaluation of the subchondral bone density distribution of the canine talus, two different views are reconstructed. A proximal view is reconstructed first, and the distal view is obtained by tilting the proximal view backwards approximately 90 degrees. This allows the evaluation of the entire proximal trochlear joint surface of the lateral and medial trochlear ridge (Figure 2).

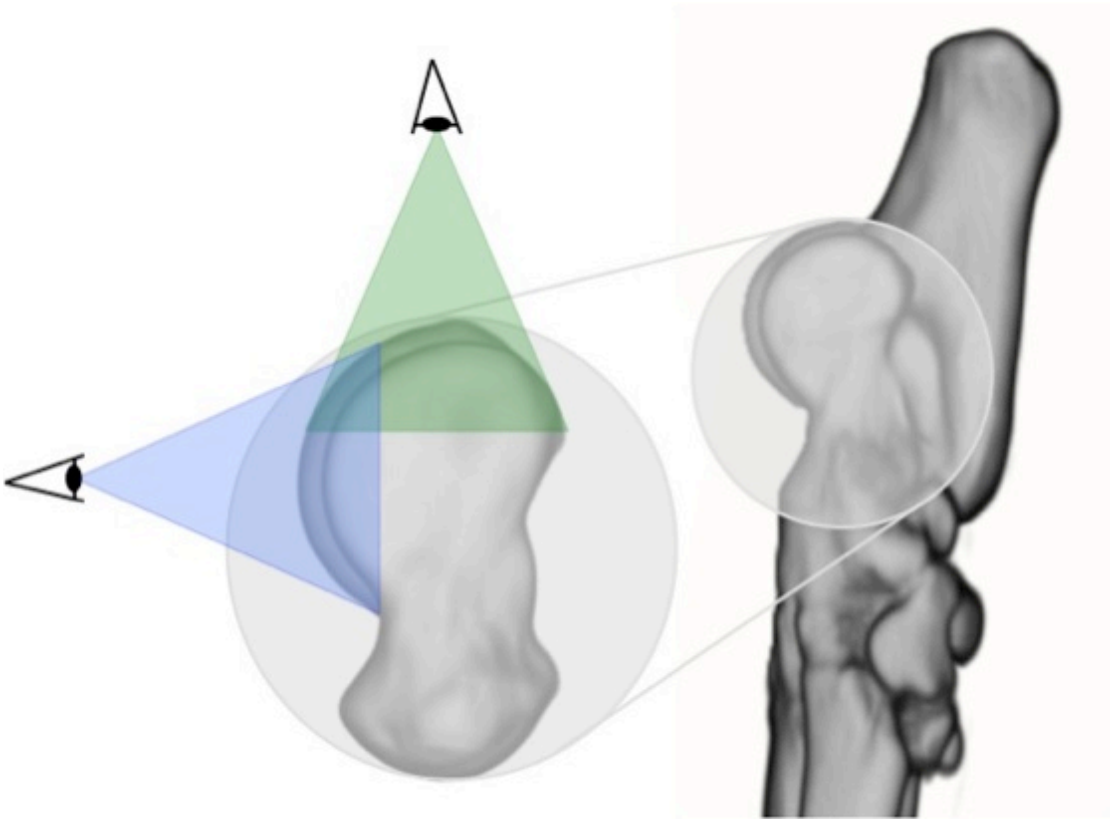

Figure 2: Three dimensional reconstruction of the tarsal and metatarsal bones of the right foot, medial view. Line of sight for the two 3D reconstructions, proximal view (green) and distal view (blue). The use of these two views provides full visualisation of the trochlear ridges.

REFERENCES

1. Sapir-Koren R, Livshits G: Bone Mineralization and Regulation of Phosphate Homeostasis. International Bone & Mineral Society 8:286-300, 2011.

2. Clarke B: Normal Bone Anatomy and Physiology. Clinical Journal of the American Society of Nephrology 3:S131-S139, 2008.

3. Frost HM: The Utah paradigm of skeletal physiology: an overview of its insights for bone, cartilage and collagenous tissue organs. Journal of Bone and Mineral Metabolism 18:305-316, 2000.

4. Thompson WR, Rubin CT, Rubin J: Mechanical regulation of signaling pathways in bone. Gene 503:179-193, 2012.

5. Liedert A, Kaspar D, Blakytny R, et al: Signal transduction pathways involved in mechanotransduction in bone cells. Biochemical and Biophysical Research Communications 349:1-5, 2006.

6. Ehrlich PJ, Lanyon LE: Mechanical strain and bone cell function: A review. Osteoporosis International 13:688-700, 2002.

7. Rayfield EJ: Finite element analysis and understanding the biomechanics and evolution of living and fossil organisms. Annual Review of Earth and Planetary Sciences 35:541-576, 2007

8. Madry H, van Dijk CN, Mueller-Gerbl M: The basic science of the subchondral bone. Knee Surgery Sports Traumatology Arthroscopy 18:419-433, 2010.

9. Eckstein F, Jacobs CR, Merz BR: Mechanobiological adaptation of subchondral bone as a function of joint incongruity and loading. Medical Engineering & Physics 19:720-728, 1997.

10. Murray RC, Branch MV, Dyson SJ, et al: How does exercise intensity and type affect equine distal tarsal subchondral bone thickness? Journal of Applied Physiology 102:2194-2200, 2007.

11. Branch MV, Murray RC, Dyson SJ, et al: Alteration of distal tarsal subchondral bone thickness pattern in horses with tarsal pain. Equine Veterinary Journal 39:101-105, 2007.

12. Patel BA, Carlson KJ: Habitual use of the primate forelimb is reflected in the material properties of subchondral bone in the distal radius. Journal of Anatomy:659-670, 2006.

13. Berli M, Borau C, Decco O, et al: Localized tissue mineralization regulated by bone remodelling: A computational approach. Plos One 12, 2017.

14. van der Meulen MCH, Jepsen KJ, Mikic B: Understanding bone strength: Size isn't everything. Bone 29:101-104, 2001.

15. Ruff C, Holt B, Trinkaus E: Who's afraid of the big bad wolff? "Wolff is law" and bone functional adaptation. American Journal of Physical Anthropology 129:484-498, 2006.

16. Burton NJ, Ellis JR, Burton KJ, et al: An ex vivo investigation of the effect of the TATE canine elbow arthroplasty system on kinematics of the elbow. Journal of Small Animal Practice 54:240-247, 2013.

17. Giunta RE, Krimmer H, Krapohl B, et al: Patterns of subchondral bone mineralization in the wrist after midcarpal fusion. Journal of Hand Surgery-American Volume:138-147, 1999.

18. Müller-Gerbl M, Putz R, Hodapp N, et al: Computed-tomography-osteoabsorptiometry - A method of assessing the mechanical condition of major joint in a living subject. Clinical Biomechanics 5:193-198, 1990.

19. Coughlin KM, Peura GD, Fleming BC, et al: In vivo loads in the medial compartment of the rabbit knee. Clinical Biomechanics 20:1007-1009, 2005.

20. Mason DR, Schulz KS, Fujita Y, et al: Measurement of humeroradial and humeroulnar transarticular joint forces in the canine elbow joint after humeral wedge and humeral slide osteotomies. Veterinary Surgery 37:63-70, 2008.

21. Preston CA, Schulz KS, Kass PH: In vitro determination of contact areas in the normal elbow joint of dogs. American Journal of Veterinary Research 61:1315-1321, 2000.

22. Müller-Gerbl M, Putz R, Kenn R: Demonstation of subchondral bone density patterns by three-dimensional CT osteoabsorptiometry as a noninvasive method for in vivo assessment of individual long-term stresses in joints. Journal of Bone and Mineral Research 7:411-418, 1992.

23. Dingemanse W, Muller-Gerbl M, Jonkers I, et al: Subchondral bone density distribution of the talus in clinically normal Labrador Retrievers. Bmc Veterinary Research 12, 2016.

24. Nyman JS, Ni QW, Nicolella DP, et al: Measurements of mobile and bound water by nuclear magnetic resonance correlate with mechanical properties of bone. Bone 42:193-199, 2008.

25. Zhao X, Song HK, Seifert AC, et al: Feasibility of assessing bone matrix and mineral properties in vivo by combined solid-state H-1 and P-31 MRI. Plos One 12, 2017.

CHAPTER TWO

Diagnosis and Treatment of Tarsocrural Osteochondrosis in Dogs

Walter B. Dingemanse[1], Ingrid M.V.L. Gielen[1], B. Van Ryssen[1], Henri J.J. van Bree[1]

[1] Department of Medical Imaging and Small Animal Orthopaedics, Ghent University, 9820 Merelbeke, Belgium

Adapted from: W. Dingemanse, I. Gielen, H. van Bree. Diagnose en behandeling van tarsocrurale osteochondrose bij de hond. Vlaams Diergeneeskundig Tijdschrift (Flemish Veterinary Journal) 80. (2011). 223-232.

And:

W. Dingemanse, I. Gielen, B. Van Ryssen, H. van Bree. An update on canine tarsocrural osteochondrosis. In preparation.

ABSTRACT

Background: Osteochondrosis in dogs is an orthopaedic condition occurring in different joints. After the shoulder and elbow joint, the tarsal joint is the third most commonly affected joint (4-9 %).

Diagnosis: Diagnosis on radiography is often challenging due to the complexity of the tarsocrural joint. Computed tomography provides additional information on the exact number of fragments and the location of the lesions on the trochlear ridge.

Treatment: Minimally invasive surgery, such as arthroscopy, if necessary combined with mini-arthrotomy gives better long-term results than the more invasive treatment using arthrotomy.

BACKGROUND

Osteochondrosis is a multifactorial condition, in which diet, genetics, and biomechanics play a role. A disruption in the enchondral ossification, the process of cartilage turnover into bone, is considered to be the main pathogenesis of canine OC [1-3]. This failure in the ossification process is focal and a specific area of growth cartilage is not converted to bone, due to failure of matrix calcification and vascular invasion [3]. More specifically, the primary event is most likely a local disruption of the epiphyseal cartilage canals during growth, leading to ischemic necrosis of the growth cartilage (Figure 1) [1]. These cartilage canals harbour microscopic vessels that invade the epiphyseal growth cartilage. Cartilage canals regress naturally during growth, a process called chondrification, as the growth cartilage is replaced with bone [1,4].

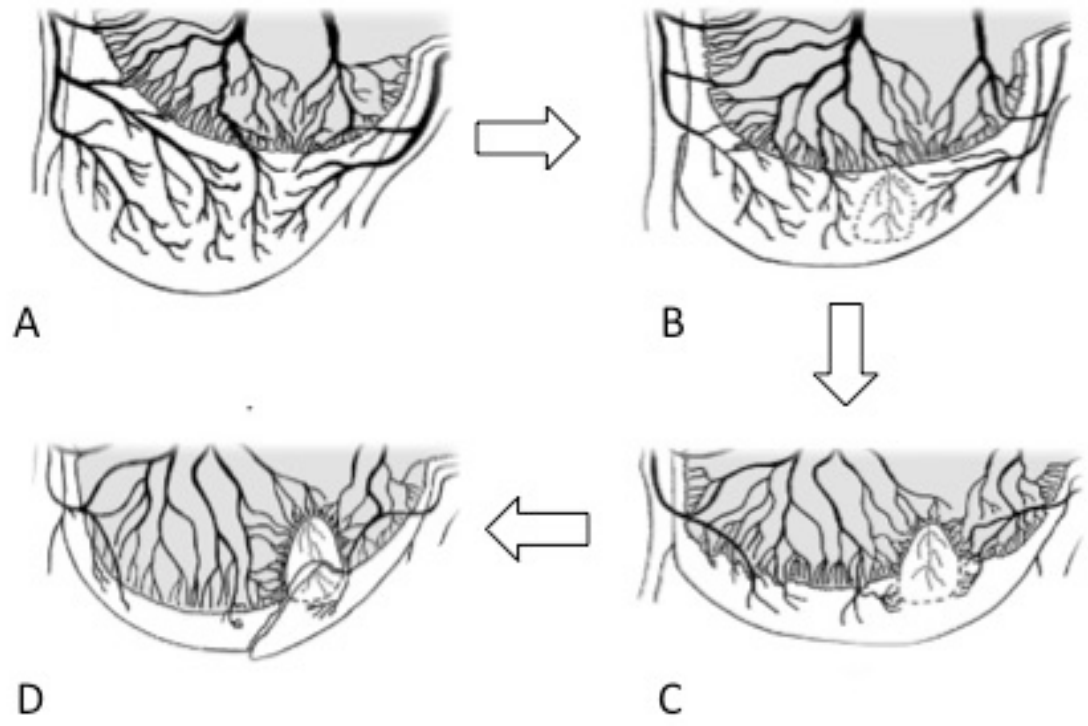

Figure 1. A) Normal joint with epiphysial cartilage vascularized through the cartilage canals. B) Focal interruption of the cartilage canal vessels leading to avascular necrosis of a part of the epiphysial cartilage. C) Disturbance of osteochondral ossification and the formation of a osteochondral lesion. D) Rupture of the overlying cartilage, leading to a cartilage flap. From Ytrehus et al., 2007.

Joint loading and the associated tensile and compressive stresses play an important role in subchondral bone physiology and pathology in general [5,6]. The morphological characteristics of canine osteochondrosis lesions, with their location being constant within a joint, has led to the hypothesis that joint loading plays an important role in the development of canine osteochondrosis. Similar to humans, a mismatch in biomechanical properties can be the start of a cascade leading to the development of osteochondrosis lesions [7,8]. In pigs it has been found that the location of cartilage canal necrosis is at the cartilage-bone interface. This region that is most likely to suffer from differences in biomechanical properties, and this might lead to damage to the cartilage canal and cartilage canal necrosis [4,9]. The damage of cartilage canals due to micro trauma also explains the site specificity of osteochondrosis lesions, as areas that undergo higher loads are more likely to suffer from micro trauma [1]. When the condition progresses, a subchondral bone defect and cartilage flap develop, which can lead to a loose fragment. At this stage the condition is commonly called osteochondrosis dissecans [1].

Osteochondrosis is a condition that can occur in different joints, including the shoulder, elbow, tarsus and stifle [6]. The tarsocrural joint is affected in 4-9 % of the cases of canine OC, making it the third most commonly affected joint [6,7].

Osteochondrosis is a condition that can occur in different joints, including the shoulder, elbow, tarsus and knee [10]. The tarsocrural joint is affected in 4-9 % of the cases of canine OC, making it the third most commonly affected joint [10,11].

Tarsocrural OC is most commonly seen in Rottweilers and Labrador Retrievers, but has also been diagnosed in a variety of other breeds [10,12]. The lesions can occur on both the lateral and medial trochlear ridges (Figure 2). The medial trochlear ridge is affected in about 80 % of the cases and the lateral trochlear ridge in about 20 %. Additionally, the medial malleolus (tibia) can also be affected [13-15]. The trochlear ridges can be divided into proximal, dorsal, and distal parts (Figure 3). Most lesions on the medial trochlear ridge occur on the proximal part [16,17], although some researchers report more lesions on the dorsal part [18]. On the lateral trochlear ridge,

most lesions are located at the proximal part of the talar ridge, although they can also occur on the dorsal and distal parts [18-20].

Most animals are presented between six and twelve months of age with intermittent or continuous lameness [10,21]. In about 50 % of cases the lesions are bilateral [14], but only about 30 % of the dogs with bilateral lesions display bilateral lameness [22]. Some authors note no sex predisposition [15], whilst others mention a male [14] or female [10,12] predisposition.

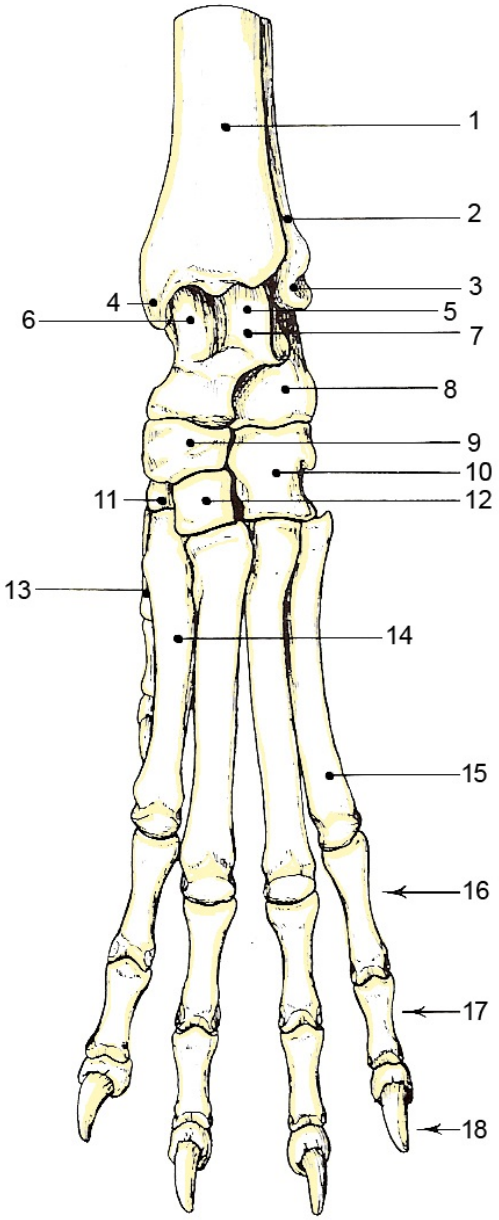

Figure 2. Dorsal view of the tarsocrural joint. Distal tibia (1), distal fibula (2), lateral malleolus (3), medial malleolus (4), lateral trochlear ridge (5), medial trochlear ridge (6), talus (7), calcaneus (8), Os centrale (9),Os tarsale IV (10), Os tarsale II (11), Os tarsale III (12), Os metatarsale I (13), Os metatarsale II (14), Os metatarsale V (15), Phalanx proximale (16), Phalanx mediale (17), Phalanx distale (18) (adapted from Barone, 1999).

The definitive diagnosis is often made about 2-3 months after the symptoms start [21]. Due to the complexity of the tarsocrural joint, the diagnosis and treatment is often challenging. This article provides an overview of the diagnostics and treatment methods for tarsocrural osteochondrosis in dogs.

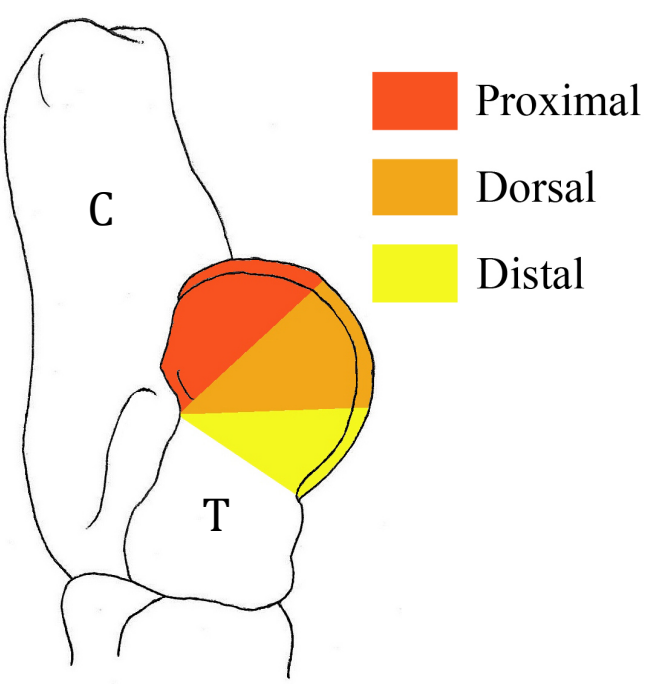

Figure 3. Lateral view of the talus (T) and calcaneus (C) with the devision of the trochlear ridges into proximal, dorsal and distal parts (adapted from Barone, 1999; Gielen et al., 2002).

DIAGNOSIS

Early diagnosis leads to an early surgical treatment, which possibly improves the long-term prognosis [21]. Comparable with the Berndt and Harty classification used in human medicine [23], a classification has been developed to describe lesions in a standardized way. This classification is based on the involvement of the talar ridges and the accompanying fragment [18].

History and clinical examination

In the history of the dog, several elements can be present, indicating tarsocrural OC. Symptoms that are often seen include hind limb lameness, pain, swelling and decreased range of motion of the tarsal joint, especially in young large breed dogs [21]. When trauma is present in the history, fragmentation of the lateral talar ridge should be included in the differential [24]. These avulsion fractures of the *ligamentum collaterale tarsi laterale breve, pars talofibularis* cause osteochondral defects, mimicking OC lesions. Following trauma, fractures of the talus and damage to the collataral ligaments is also possible [15]. Fragmentation of the medial malleolus can be seen with or without OC lesions in the tarsal joint [25]. It is likely this fragmentation can be considered a form of osteochondrosis, as it is in horses and humans [15].

Upon inspection, swelling of the entire tarsal joint can be noted, especially on the medial side, in addition to hyperextension of the affected joint (Figure 4) [13,21]. Dogs with bilateral lesions can display unilateral lameness, highlighting the importance of evaluating both joints [22].

Palpation of the joint can reveal decreased range of motion, especially flexion of the joint [26]. Forced flexion or extension can be painful, and increased lameness can be seen after joint flexion [13,14]. In some cases crepitation can be felt [12]. In chronic cases the joint has fibrous thickening and the swelling may extend over the entire tarsal joint [12,14].

Figure 4. Hyperextension of the tarsocrural joint (arrow) in a dog with tarsocrural OC.

Radiography

The projections used to evaluation the tarsocrural joint include the mediolateral, dorsoplantar, dorsolateral-plantaromedial oblique, and dorsomedial-plantarolateral oblique projection [10,13]. The oblique projections are best taken in flexion and extension [21]. A third oblique projection, a dorsoplantar projection with the joint in flexion, with an angle of 10-15 degrees to the X-ray beam can also be useful (Figure 5) [27]. This projection is also called the skyline projection (Figure 6) and has the advantage that the lateral talar ridge can be evaluated without superposition of the calcaneus [10].

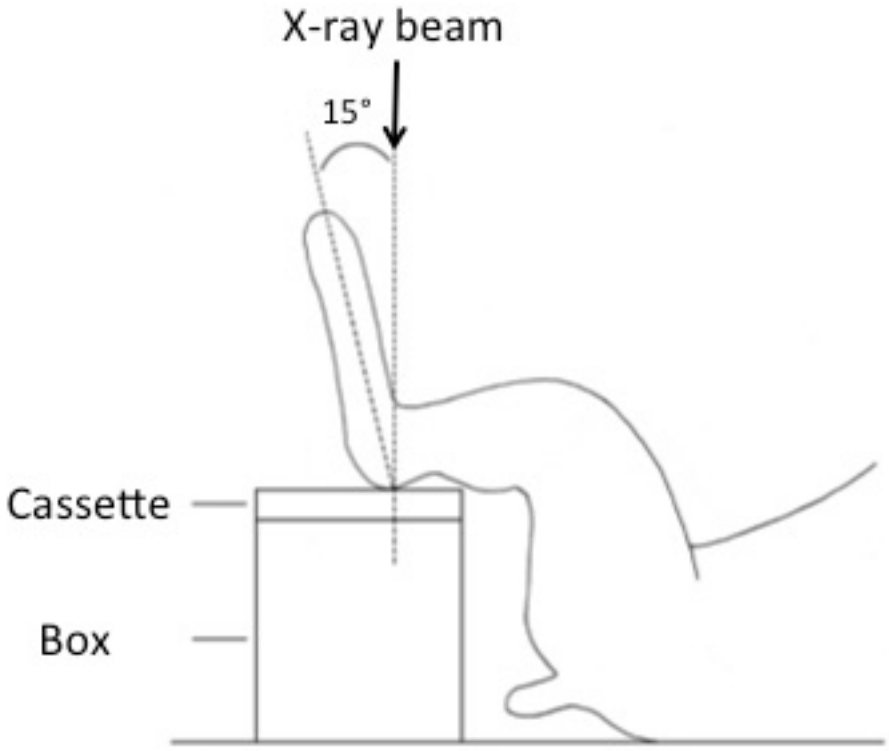

Figure 5. Positioning of the tarsal joint for the skyline projection.

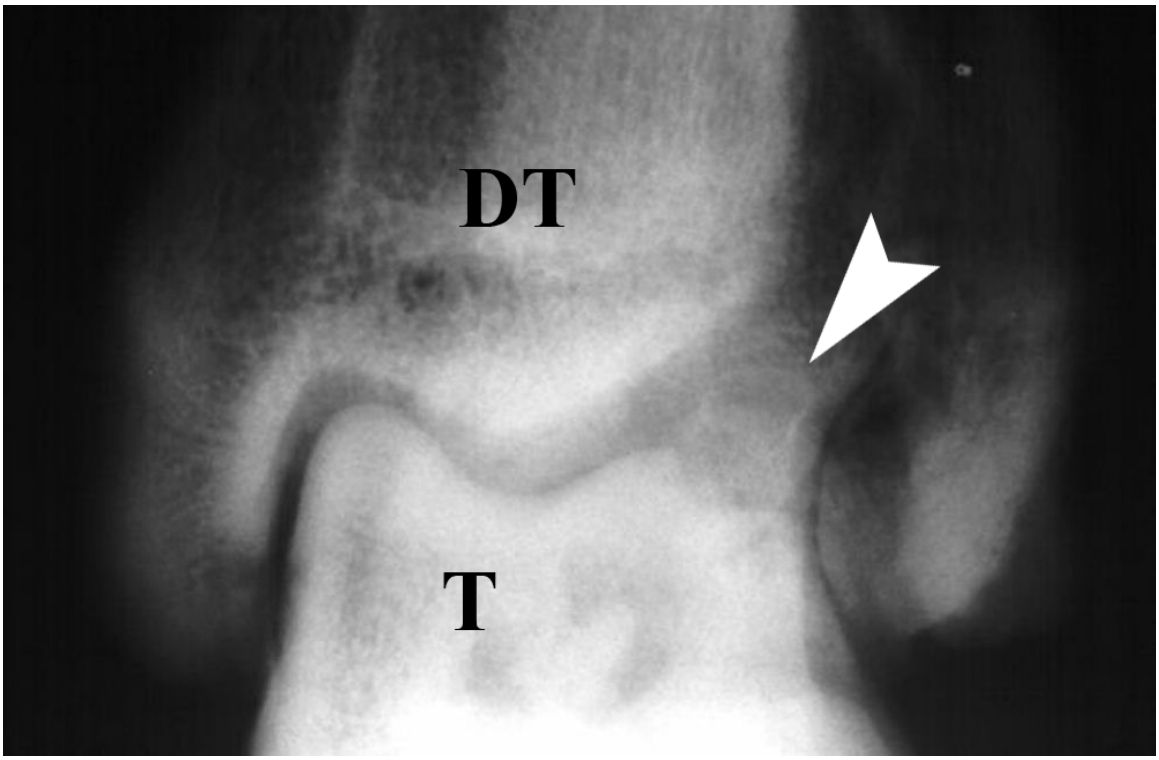

Figure 6. Radiography, skyline projection of the tarsocrural joint. The distal tibia (DT), talus (T) and a large fragment at the level of the lateral trochlear ridge (arrowhead) are indicated.
The oblique projections are used to reduce the superposition of surrounding structures and thus increase the visibility of degenerative changes at the level of the talus [13,21], and should always be included in the radiological examination [28].

The medial trochlear ridge and medial malleolus can be visualised best on the dorsoplantar and dorsolateral-plantaromedial oblique projection [13,21,27]. Lesions on the lateral trochlear ridge can be demonstrated on the mediolateral, plantarolateral-dorsomedial oblique, and skyline projection [17,20,29]. The diagnosis on the dorsoplantar projection is difficult due to the superposition of the calcaneus and other structures on the lateral trochlear ridge [28]. Even with all six projections, subtile lesions on the lateral trochlear ridge can be missed, especially in young dogs [18]. In about 25 % of cases the diagnosis of lateral trochlear ridge tarsocrural OC can not be made based on radiographic examination [20]. When the radiographic examination is limited to the dorsoplantar and mediolateral projection in extension, as often is the case in general practice, the diagnosis of lateral trochlear ridge lesions is missed in 72 % of the cases [20]. In some cases the intra-articular injection of contrast (arthrography) can be useful, especially in cases with a cartilage flap [19], although it is rarely done in the tarsocrural joint.

Mineralized cartilage fragments in the tendon sheath of the deep digital flexor tendon can be visualised on the dorsoplantar and lateral projection in flexion and extension [30].

In many cases, a widening of the tibiotarsal joint space can be seen due to flattening of the medial trochlear ridge and subchondral bone erosion [13,14]. In most cases, subchondral bone sclerosis is also present, in addition to soft tissue swelling on the medial side of the tarsocrural joint [12,26]. In addition, loose fragments (Figure 7) and osteophytes can be seen [12,14]. In very early stages it is possible no degenerative changes can be seen, but these will develop during follow-up. In the early stage of osteoarthrosis, osteophytes are formed at the level of the caudodistal tibia and the

medial part of the tarsocrural joint. In later stages, osteoarthrosis can be seen throughout the entire tarsal joint [12,13]. However, even when these typical changes are not visible on radiography, an OC defect can not be ruled out, since primary degenerative changes are rare in dogs this age [2,26].

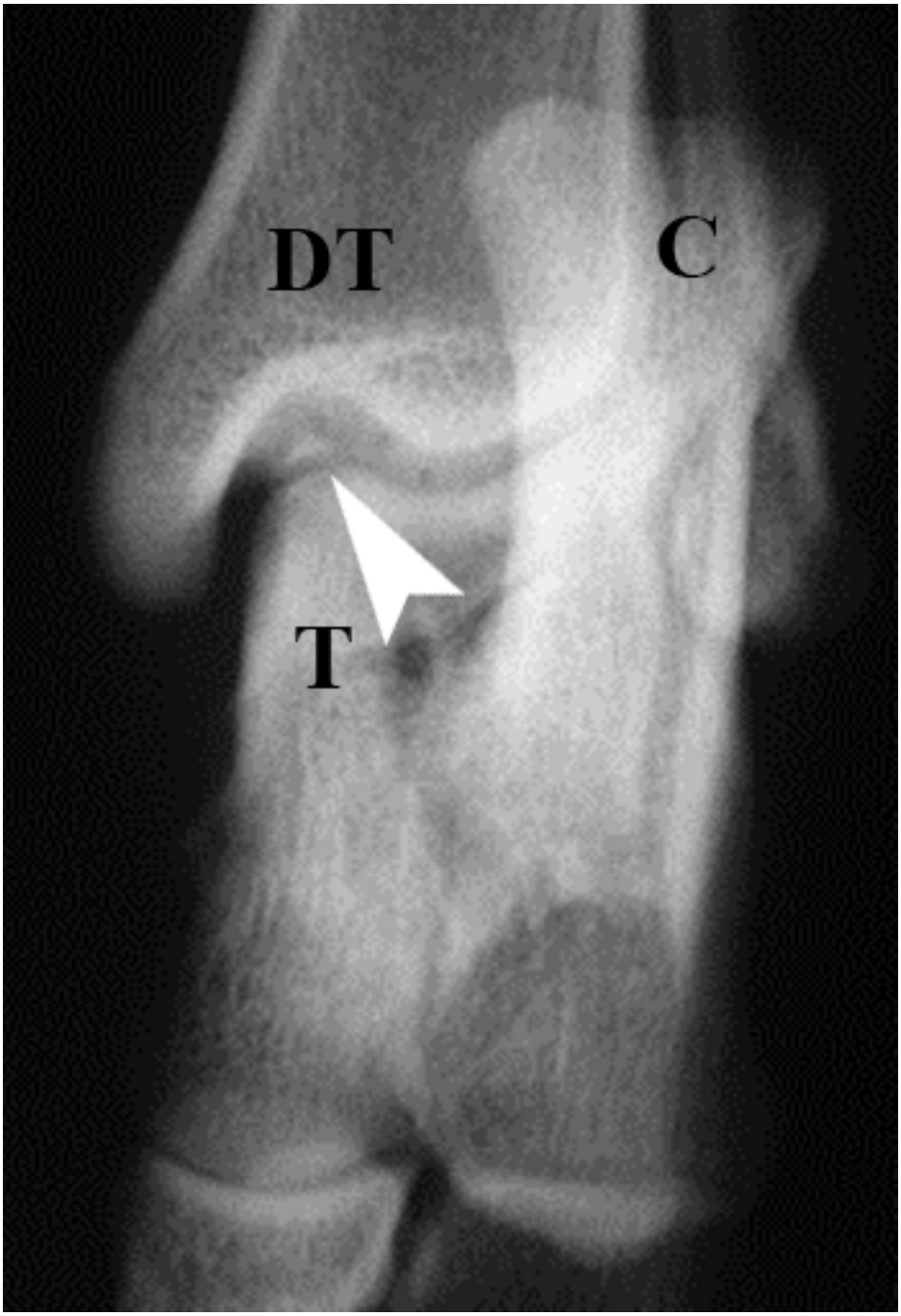

Figure 7. Radiography, dorsomedial-plantarolateral projection of the tarsal joint. The distal tibia (DT), talus (T), calcaneus (C), and a fragment at the level of the medial trochlear ridge (arrowhead) is indicated. The joint space is clearly enlarged.

In OC lesions of the lateral trochlear ridge, similar changes can be seen. In addition to subchondral sclerosis of the trochlear ridge, a subchondral radiolucent area can be present at the level of the lateral malleolus. Lateral trochlear ridge fragments are quite large, and have a thin, shell-like appearance on radiography [28].

A radiolucent line can indicate the presence of a cartilage flap [13]. In older animals, a mineralized flap can be seen, whilst in younger animals the flap is often not visible and only the filling of the defect can be seen [12].

Compared to OC in the shoulder joint, degenerative changes occur much sooner in the tarsal joint [26]. Even after surgical treatment, the degenerative changes continue to progress [13]. Despite the variation in clinical symptoms, most dogs display similar radiographical changes, and during follow-up it is difficult to correlate the amount of osteoarthrosis to the clinical symptoms [12,13].

Computed tomography

Computed tomography (CT) provides the possibility of a definitive diagnosis when the radiographical examination is inconclusive [18,31]. The use of CT eliminates the superposition of bony structures and provides a better visualization of the lesions. In addition, more lesions can be detected compared to radiography, and the size, exact location (Figure 8), and fragmentation of the medial malleolus can be evaluated better. All fragments can be visualized, whilst during arthrotomy or arthroscopy smaller fragments can be missed due to synovitis or their location [18].

Especially when lesions are located on the lateral trochlear ridge, the radiographical diagnosis is challenging, as described above. The exact location and size of the lesion can be evaluated on the transverse, and reformatted images (Figure 8) in different anatomical planes [18]. This provides valuable treatment information and can be used to decide on the surgical approach [18,31]. Using reformatted images, the joint congruity can also be evaluated better. Dogs with clinical symptoms often have larger fragments, resulting in more incongruity and more instability of the joint [32].

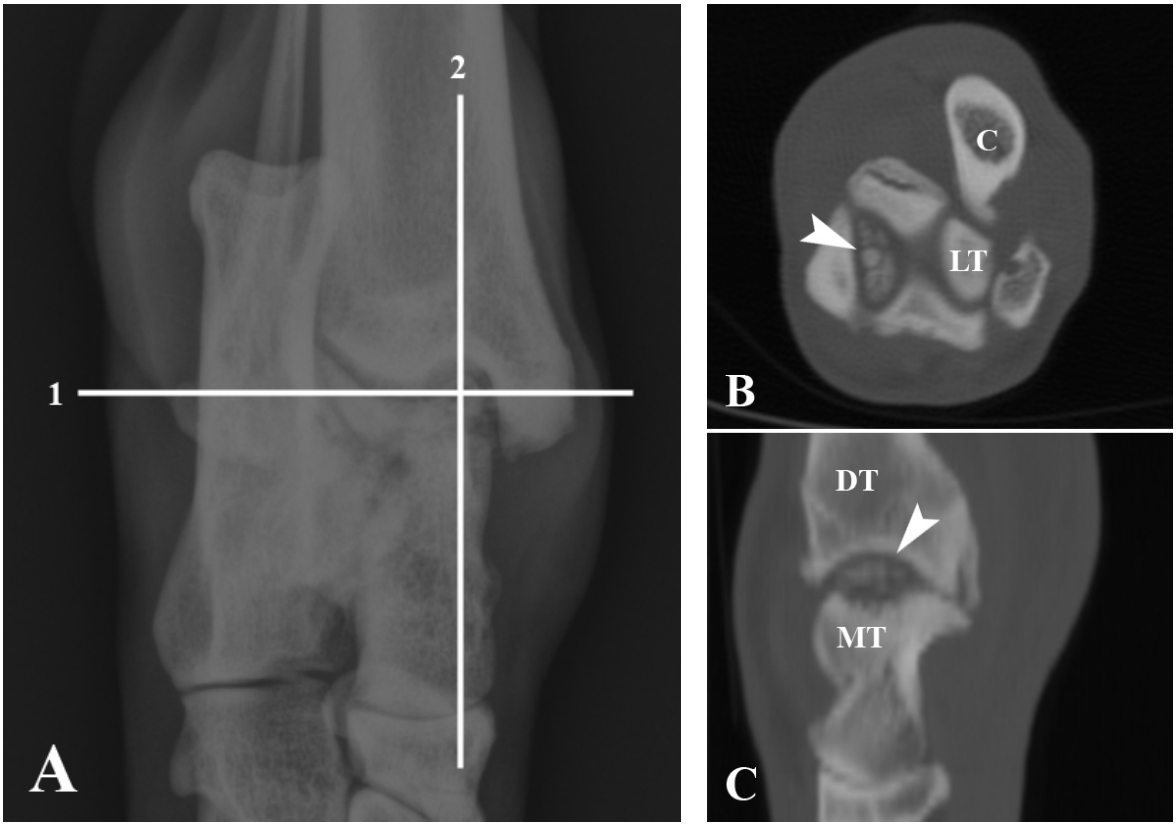

Figure 8. A: Dorsoplantar radiographic projection of the tarsocrural joint. The white line (1) indicates the location of the transverse CT image (B), line (2) incidates the location of the sagittal reformatted image (C). B: Computer tomographic image of the tarsal joint. The calcaneus (C), lateral trochlear ridge (LT) and an OC lesion at the level of the medial trochlear ridge (arrowhead) are indicated. C: Sagittal reformatted image at the level of the medial trochlear ridge (MT). A fragment (arrowhead) can be seen just distal to the distal tibia (DT).

Disadvantages of CT include higher costs compared to radiographic examination, and the need for or general anaesthesia. However, the time necessary to complete the CT is shorter than a full radiographic examination consisting of six projections [20].

In most cases the lesions on the trochlear ridge are easily seen and fragments can be localized with great precision. In some cases, an irregular trochlear ridge and some degenerative changes are the only findings. In chronic cases, osteophytes can be seen at the level of the distal tibia, lateral and medial malleolus and talus [12].

Magnetic resonance imaging

When using magnetic resonance imaging (MRI) in humans, abnormalities at the level of the articular cartilage can be seen as changes in signal intensity and/or morphology [33]. An increase or decrease in the amount of water in the articular cartilage, due to inflammation or other causes, influences the signal intensity. Cartilage defects can be visible as irregularities at the surface of the joint cartilage [33]. In human medicine, MRI is routinely used in the diagnosis of cartilage lesions. In veterinary medicine its application is more limited due to the small thickness of the cartilage, making it difficult to visualise the cartilage. In dogs, the cartilage is so thin that it is almost impossible to visualise with MRI [34].

Ultrasound

Using ultrasound, about 75 % of the surface of the trochlear ridges can be evaluated. The remaining 25 % is located at the proximal part of the trochlear ridges [35]. The evaluation of the cartilage is difficult, but because all dogs with tarsocrural OC also have lesions of the subchondral bone, or have cartilage fragments present, the evaluation of the cartilage itself is less important [20,35]. In the diagnosis of tarsocrural OC, the use of ultrasound has been limited, and the clinical application remains subject to further research. A potential disadvantage is the need for sedation, because uncomfortable flexion and extension of the tarsal joint is necessary for a full evaluation [35]

Arthrocenthesis

To evaluate other abnormalities, such as inflammation, arthrocenthesis can be used. Findings on cytology of the synovial fluid, suggesting secondary osteoarthrosis due to intra-articular pathology include the presence of light-grey, amorphous material in macrophages, and free amorphous material in the synovial fluid. This amorphous material matches articular cartilage [36]. In pathological cases, often more than 1 mL synovial fluid is present and displays a decreased viscosity [15].

Arthrotomy

The canine tarsal joint is very small and offers limited visibility of different structures, even during arthroscopy. Therefore, exploratory arthrotomy is often used to inspect the tarsocrural joint [17,19]. However, the visibility can still be limited due to synovitis, and smaller fragments can be missed [18]. Reduced range of motion of the tarsal joint in dogs with tarsocrural OC can also lead to decreased visualisation of certain areas of the tarsocrural joint. Under general anaesthesia however, usually a normal range of motion can be acquired.

Arthroscopy

Arthroscopy can be used to diagnose lesions at the level of the tarsocrural joint and to evaluate the size and localisation of the OC lesions. Defects can be seen on arthroscopy earlier then on radiography, because the latter shows the secondary bony changes. Additionally, arthroscopy can provide valuable information regarding the surgical treatment [37,38]. The use of arthroscopy can also prevent the invasive approach using arthrotomy, as it can replace the arthrotomy in early stages without specific radiographic changes, but also in advanced cases in which arthrotomy can lead to severe degenerative changes. Important advantages include a low change of post-operative complications and a swift return to full function of the joint[37]. When using a minimally invasive technique such as arthroscopy, the information provided by the CT examination can be used to determine the best entry port for the arthroscope [18].

Synovial villi can reduce visibility during arthroscopy, and smaller fragments can be missed [18]. This can be partially fixed by a higher intra-articular pressure or by performing a partial synovectomy to increase lesion visibility [36]. The entry of the needle, trocard, or canula can lead to minor cartilage damage. These small lesions often do not cause any clinical problems and occur less with increasing surgical experience [38].

TREATMENT

The treatment goal of tarsocrural OC is minimizing the degenerative changes and maintaining joint congruity [39].

Conservative treatment

Conservative treatment generally consists of weightloss, medication (painkillers and anti-inflammatory), and exercise restriction [36]. This approach can be effective in a limited number of cases [12], but some authors claim it will not be effective due to the rapid development of degenerative changes [26]. Conservative treatment can be an option in cases with severe degenerative changes, where surgical treatment offers little additional value [40].

Surgical treatment

Surgical treatment in an early stages is necessary to improve clinical symptoms and to decrease the progression of degenerative changes [21]. Fixating the loose fragment is possibly better than removing fragments or conservative treatment, but the treatment is technically very difficult and in most cases the fragments are too small [19,21,40]. Internal fixation with a cortical screw is possible for attaching large trochlear fragments, regardless of their aetiology. Results of more cases and long-term follow-up will have to show is this technique is indeed suited to treat trochlear fragments [41]. In most cases surgical treatment leads to a decrease of clinical symptoms [12,21]. Treatment can consist of removing the fragment combined with curettage, or it can be attempted to fill the defect with collagen replacements or artificial grafts [36].

Avulsion fractures of the lateral trochlear ridge should be anatomically and functionally reconstructed to ensure joint stability and congruity. Due to the large size of these fragments, the intra-articular localisation and the involvement of ligaments, it is unlikely conservative treatment or removal of the fragment will lead to good long-term results [24].

Arthrotomy

The medial approach with osteotomy of the medial malleolus provides a good visibility of the medial trochlear ridge and the distal tibia. Although some authors mention osteotomy in combination with tenotomy of the collateral ligaments, this is not necessary in most cases [21], the visibility of the medial trochlear ridge is highly increased when using an osteotomy [19,40]. In about 50 % of the cases, there are complication with the osteotomy, including incorrect positioning and insufficient fixation of the osteotomy leading to incongruity, instability and severe degenerative changes [12,21].

A better visualisation can also be realised through hyperextension and hyperflexion of the tibiotarsal joint, or by applying valgus or varus pressure to the joint [21].

The lateral approach provides good visualisation of the lateral trochlear ridge, with exception of the proximal part. The lateral malleolus and the cochlea tibiae cover the proximal part of the trochlear ridge, even when the tibiotarsal joint is fully extended [19]. The dorsolateral and plantarolateral approach can also be used to inspect the lateral trochlear ridge. Additional visualisation can be realised through similar methods as described for the medial approach. Osteotomy of the lateral malleolus is not recommended, due to a tight connection with the tendons of the m*usculus fibularis longus*, the *musculus fibularis brevis*, and the *musculus extensor digitorum longus* [21].

During an exploratory arthrotomy the lesions can be treated surgically. When results after arthrotomy and conservative treatment are compared, there were no significant differences found in the prognosis and progression of degenerative changes [21,40]. A mini-arthrotomy can be done after arthroscopic assessment of the articular cartilage. This minimally invasive technique prevents damage to the medial collateral ligaments, and causes less postoperative instability (REF *Van Bree en Van Ryssen, 1998).*

When fragments are removed from the tendon sheath after tenosynovectomy, an arthrotomy to check for other fragments can be omitted when a preoperative CT is done [30].

Arthroscopy

The success of the arthroscopic treatment depends on the size of the dog, the size of the tarsal joint, and the size of the fragment [22,36]. The technique can be used on both younger and older dogs, and for lesions on the lateral and medial trochlear ridge [36]. Because the articular cartilage, the collateral ligament, and the synovia can be evaluated, the treatment can be optimally adjusted to the individual patient [42].

A dorsolateral or dorsomedial approach can be used to evaluate the dorsal part of the lateral and medial trochlear ridge. To visualise the planter part of the trochlear ridges, a plantarolateral approach is necessary [38]. By using a small arthroscope (1.9 mm), it is often passible to also add an instrumental canula [37,38,42].

Fragments can be removed during arthroscopy, but it is often necessary to remove the fragments in multiple loose parts. After removal of the fragment, the lesion can be curetted arthroscopically [36]. Some authors claim it is not possible to treat lesions arthroscopically because the fragments are too big or the location is out or reach, for instance on the lateral trochlear ridge when the lesions is covered by the tibia [37,42]. In these cases the fragment can be removed with a mini-arthrotomy, since the exact location of the fragment be determined, especially with the combination of arthroscopy and CT examination [18]. For a mini-arthrotomy the stab incision for the arthroscopic instruments is sharply enlarged to about 15 mm in order to remove the fragment under arthroscopy guidance [42]. This approach can still be considered a minimally invasive approach.

Tenosynovectomy

When OC fragments are present in the tendon sheath of the deep digital flexor tendon, these can be removed using a medial tenosynovectomy. The fragments are

usually not attached to the tendon sheath and removal of the fragments leads to significant improvement of the clinical symptoms [30].

PROGNOSIS

Historically only 25 % of dogs treated for OC lesions on the medial trochlear ridge made a full recovery [12]. In more recent studies, full recovery is seen in 44 % of the cases, and improvement in 53 % of the cases after minimally invasive surgery, i.e. arthroscopy of mini-arthrotomy [22]. Because many different factors play a role in the prognosis of OC, it is difficult to correctly evaluate treatment and prognosis [43]. Clinical parameters such as age, weight, and duration of symptoms can influence the clinical result [12,13,26]. About the influence of these parameters a lot of discussion exists. Some authors noted a higher chance for full recovery, and thus a better prognosis, when dogs are treated shortly after the beginning of symptoms[12,21,26]. These studies use an arthrotomy as treatment and note many complications. In a more recent study, using minimally invasive techniques (arthroscopy and mini-arthrotomy), no significant correlation was found long-term, between the duration of symptoms, age, and weight [22].

In large lesions in general a worse clinical result is seen after treatment. Lesions on the medial trochlear ridge with a volume of 588 mm^3 or more, or with a length of 12 mm often have a worse result, compared to similar lesions on the lateral trochlear ridge, which usually have a better long term result [22]. An explanation might be that the lateral trochlear ridge can be visualized more easily, leading to less trauma and manipulation of the tarsocrural joint [21].

The surgical technique is another factor that can play a role in the success of the treatment [43]. An open arthrotomy has a negative effect on the long-term result, because damage to the medial collateral ligaments causes joint instability [36]. Minimally invasive treatment has the advantage of a speedy recovery [36,37]. Some researchers however note that the advantage of arthroscopic treatment is mainly a

short-term advantage and that long-term results are similar to traditional arthrotomy [42].

Arthroscopy can also be used to re-evaluate the prognosis, in combination with clinical and radiographic examination [42]. With the use of minimally invasive treatment, good results are possible even in adult dogs and dogs with chronic lameness. The prognosis of dogs with bilateral lesions is similar to dogs with unilateral lesions [21,22].

After surgical treatment, progression of degenerative changes is seen in almost all dogs, regardless of the type of treatment [21,22,40]. Despite severe degenerative changes, the clinical symptoms are often minimal [10,13]. The progression of degenerative changes is probably due to continuous joint instability. This instability is due to flattening of the medial trochlear ridge, especially after curettage of the lesion [13]. Another important cause of joint instability is the removal of a large fragment. When a large part of the medial trochlear ridge is removed, the result is severe joint incongruity and instability [43]. Fragments of the lateral trochlear ridge are quite large, so surgical removal is not indicated [28]. The clinical result do not seem to differ between lesions on the lateral or medial trochlear ridge [22].

CONCLUSION

Osteochondrosis is a multifactorial condition affecting different joints, including the tarsocrural joint [10]. Both the medial and lateral trochlear ridge can be affected. Lameness and pain located in the tarsocrural joint are the most typical symptoms, caused by the primary OC lesions as well as the secondary degenerative changes [13,21].

Using different radiographic projections, the diagnosis can be made in the majority of the cases, but in 25 % of the cases the lesion can be missed, especially when the lesion is located on the lateral trochlear ridge [20]. The use of CT eliminated the

problem of bony superposition and has a higher sensitivity for the detection of lesions compared to radiography. In addition, the size and exact location of the lesion, as well as fragmentation of the medial malleolus can be evaluated. Smaller fragments that can be missed during arthrotomy or arthroscopy, can be clearly visualised with CT [18].

Arthrotomy is an invasive treatment technique with a high complication rate [12,21]. By using minimally invasive surgery, i.e. arthroscopy or mini-arthrotomy, an improvement of clinical signs or even full recovery can be accomplished in the majority of cases, including adult dogs and dogs with chronic lameness [18,22].

REFERENCES

1. Ytrehus B, Carlson CS, Ekman S: Etiology and pathogenesis of osteochondrosis. Veterinary Pathology 44:429-448, 2007.

2. Richardson DC, Zentek J: Nutrition and osteochondrosis. Veterinary Clinics of North America-Small Animal Practice 28:115-135, 1998.

3. Ekman S, Carlson CS: The pathophysiology of osteochondrosis. Veterinary Clinics of North America-Small Animal Practice 28:17-21, 1998.

4. Ytrehus B, Haga HA, Mellum CN, et al: Experimental ischemia of porcine growth cartilage produces lesions of osteochondrosis. Journal of Orthopaedic Research 22:1201-1209, 2004.

5. Frost HM: The Utah paradigm of skeletal physiology: an overview of its insights for bone, cartilage and collagenous tissue organs. Journal of Bone and Mineral Metabolism 18:305-316, 2000.

6. Turner CH: Three rules for bone adaptation to mechanical stimuli. Bone 23:399-407, 1998.

7. Athanasiou KA, Niederauer GG, Schenck RC: Biomechanical Topography of Human Ankle Cartilage. Annals of Biomedical Engineering 23:697-704, 1995.

8. Schenck RC, Goodnight JM: Current Concept Review - Osteochondritis Dissecans. The Journal of Bone and Joint Surgery 78:439-456, 1998.

9. Carlson CS, Meuten DJ, Richardson DC: Ischemic Necrosis of Cartilage in Spontaneous and Experimental Lesions of Osteochondrosis. Journal of Orthopaedic Research 9:317-329, 1991.

10. Montgomery RD, Hathcock JT, Milton JL, et al: Osteochondritis dissecans of the canine tarsal joint. Compendium on Continuing Education for the Practicing Veterinarian 16:835-845, 1994.

11. Necas A, Dvorak M, Zatloukal J: Incidence of osteochondrosis in dogs and its late diagnosis. Acta Veterinaria Brno 68:131-139, 1999.

12. Breur GJ, Spaulding KA, Braden TD: Osteochondritis dissecans of the medial trochlear ridge of the talus in the dog. Veterinary and Comparative Orthopaedics and Traumatology 12:168-176, 1989.

13. Rosenblum GP, Robins GM, Carlisle CH: steochondritis dissecans of the tibio tarsal joint in the dog. Journal of Small Animal Practice 19:759-767, 1978.

14. Denny HR, Gibbs C: Osteochondritis dissecans of the canine stifle joint. Journal of Small Animal Practice 21:317-322, 1980.

15. Fitch RB, Beale BS: Osteochondrosis of the canine tibiotarsal joint. Veterinary Clinics of North America-Small Animal Practice 28:95-104, 1998.

16. Johnson KA, Howlett CR, Pettit GD: Osteochondrosis in the hock joints in dogs. Journal of the American Animal Hospital Association 16:103-113, 1980.

17. Robins GM, Read RA, Carlisle CH, et al: Osteochondritis dissecans of the lateral ridge of the trochlea of the tibial tarsal bone in the dog. Journal of Small Animal Practice 24:675-685, 1983.

18. Gielen I, van Bree H, Van Ryssen B, et al: Radiographic, computed tomographic and arthroscopic findings in 23 dogs with osteochondrosis of the tarsocrural joint. Veterinary Record 150:442-447, 2002.

19. van Ee RT, Gibson K, Roberts ED: Osteochondritis dissecans of the lateral ridge of the talus in a dog. Journal of the American Veterinary Medical Association 193:1284-1286, 1988.

20. Gielen I, van Ryssen B, van Bree H: Computerized tomography compared with radiography in the diagnosis of lateral trochlear ridge talar osteochondritis dissecans in dogs. Veterinary and Comparative Orthopaedics and Traumatology 18:77-82, 2005.

21. Beale BS, Goring RL, Herrington J, et al: A prospective evaluation of 4 surgical approaches to the talus of the dog used in the treatment of osteochondritis dissecans. Journal of the American Animal Hospital Association 27:221-229, 1991.

22. Gielen I, Van Bree H, Coopman F, et al: The value of computed tomography in the clinical course of canine tarsocrural osteochondrosis. Veterinary Radiology and Ultrasound 253:188-194, 2003.

23. Berndt AL, Harty M: Transchondral fractures (Osteochondritis dissecans) of the talus. Journal of Bone and Joint Surgery-American Volume 41:988-1020, 1959.

24. Sjostrom L, Hakanson N: Traumatic injuries associated with the short lateral collateral ligaments of the talocrural joint of the dog. Journal of Small Animal Practice 35:163-168, 1994.

25. Newell SM, Mahaffey MB, Aron DN: Fragmentation of the medial malleolus of dogs with and without tarsal osteochondrosis. Veterinary Radiology & Ultrasound 35:5-9, 1994.

26. Mason TA, Lavelle RB: Osteochondritis dissecans of the tibial tarsal bone in dogs. Journal of Small Animal Practice 20:423-432, 1979.

27. Miyabayashi T, Biller DS, Manley PA, et al: Use of a Flexed Dorsoplantar Radiographic View of the Talocrural Joint to Evaluate Lameness in 2 Dogs. Journal of the American Veterinary Medical Association 199:598-600, 1991.

28. Wisner ER, Berry CR, Morgan JP, et al: Osteochondrosis of the Lateral Trochlear Ridge of the Talus in 7 Rottweiler Dogs. Veterinary Surgery 19:435-439, 1990.

29. Aron DN, Purinton PT: Collateral ligaments of the tarsocrural joint - an anatomic and functional study. Veterinary Surgery 14:173-177, 1985.

30. Post C, Guerrero T, Ohlerth S, et al: Joint mice migration into the deep digital flexor tendon sheath in dogs Clinical cases and anatomical study. Veterinary and Comparative Orthopaedics and Traumatology 21:440-445, 2008.

31. Zinman C, Reis ND: Osteochondritis dissecans of the talus - use of the high-resolution computed-tomography scanner. Acta Orthopaedica Scandinavica 53:697-700, 1982.

32. Gielen I, Van Ryssen B, Coopman F, et al: Comparison of subchondral lesion size between clinical and non-clinical medial trochlear ridge talar osteochondritis dissecans in dogs. Veterinary and Comparative Orthopaedics and Traumatology 20:8-11, 2007.

33. Hodler J, Resnick D: Current status of imaging of articular cartilage. Skeletal Radiology 25:703-709, 1996.

34. Probst A, Modler F, Kunzel W, et al: Demonstration of the articular cartilage of the canine ulnar trochlear notch using high-field magnetic resonance imaging. Veterinary Journal 177:63-70, 2008.

35. Liuti T, Saunders JH, Gielen I, et al: Ultrasound approach to the canine distal tibia and trochlear ridges of the talus. Veterinary Radiology & Ultrasound 48:361-367, 2007.

36. Cook JL, Tomlinson JL, Stoll MR, et al: Arthroscopic removal and curettage of osteochondrosis lesions on the lateral and medial trochlear ridges of the talus in two dogs. Journal of the American Animal Hospital Association 37:75-80, 2001.

37. van Bree HJJ, Van Ryssen B: Diagnostic and surgical arthroscopy in osteochondrosis lesions. Veterinary Clinics of North America-Small Animal Practice 28:161-169, 1998.

38. Vanryssen B, Vanbree H, Vyt P: Arthroscopy of the canine hock joint. Journal of the American Animal Hospital Association 29:107-115, 1993.

39. Siffert RS: Classification of the osteochondroses. Clinical Orthopaedics and Related Research:10-18, 1981.

40. Smith CW: Osteochondrosis in the dog - diagnosis, treatment, and prognosis. Canine Practice 16:15-17, 1991.

41. Maley JR, Dvorak LD, Bahr A: Diagnosis and management of a fracture of the lateral trochlear ridge of the talus in a dog. Veterinary and Comparative Orthopaedics and Traumatology 23:284-288, 2010.

42. Miller J, Beale B: Tibiotarsal arthroscopy - Applications and long-term outcome in dogs. Veterinary and Comparative Orthopaedics and Traumatology 21:159-165, 2008.

43. Smith MM, Vasseur PB, Morgan JP: Clinical evaluation of dogs after surgical and nonsurgical management of osteochondritis dissecans of the talus. Journal of the American Veterinary Medical Association 187:31-35, 1985.

CHAPTER THREE

Comparison of Morphological and Clinical Features between Medial and Lateral Trochlear Ridge Talar Osteochondritis Dissecans in Dogs

Walter B. Dingmanse[1], Luc Duchateau[2], Henri J.J. van Bree[1], Ingrid M.V.L. Gielen[1]

[1] Department of Medical Imaging and Small Animal Orthopaedics, Ghent University, 9820 Merelbeke, Belgium
[2] Department of Comparative Physiology and Biometrics, Ghent University, 9820 Merelbeke, Belgium

Adapted from:

W. Dingemanse, I. Gielen, L. Duchateau, H. van Bree. Comparison of morphological and clinical features between medial and lateral trochlear ridge talar osteochondritis dissecans in dogs. Veterinary Surgery 42 (2013). 340-345.

ABSTRACT

Background: Osteochondrosis of the canine tarsocrural joint can occur on the lateral and medial trochlear ridge. The aim of this study was to evaluate clinical and subchondral bone lesion differences between medial (MTRT-OC) and lateral trochlear ridge tarsocrural osteochondrosis (LTRT-OC).

Methods: Retrospective case series of dogs (n = 66) with with MTRT-OC or LTRT-OC. Medical records **(**1997 – 2010) of dogs with MTRT-OC or LTRT-OC were reviewed. Clinical data (breed, age, gender, weight, duration of clinical signs) were retrieved. Computed tomographic (CT) examinations of the tarsocrural joints were performed. Length, width, and depth of the subchondral bone lesions on the CT images, and surface and volume of the lesions were estimated. The location of the OC lesion on the trochlear ridge (proximal, dorsal, or distal) was determined. Data collected from dogs with MTRT-OC (n = 56) was compared with data from dogs with LTRT-OC (10).

Results: Length, width, depth, surface, and volume of LTRT-OC lesions were significantly ($P < .01$) larger than those of MTRT-OC lesions. Dogs with LTRT-OC were significantly younger at the time of diagnosis ($P < .01$).

Conclusions: Osteochondrosis lesions on the lateral trochlear ridge are significantly larger than those on the medial trochlear ridge. Dogs with lesions on the lateral trochlear ridge are significantly younger at the time of diagnosis, and tend to have a shorter duration of lameness before presentation.

BACKGROUND

Osteochondrosis (OC) has been reported in dogs, horses, pigs, and people [1-3]. In dogs, although it is considered a multifactorial disease, the exact cause is unknown [4,5]. After the elbow and shoulder joint, the tarsocrural joint is the third most commonly affected joint in dogs, representing 4 - 9% of OC cases [6-8]. Tarsocrural OC can be further divided into medial trochlear ridge tarsocrural osteochondrosis (MTRT-OC) and lateral trochlear ridge tarsocrural osteochondrosis (LTRT-OC), depending on the affected trochlear ridge. The lateral trochlear ridge is affected in approximately 20% of tarsocrural OC [6,7,9].

Approximately 50% of tarsocrural OC are bilateral [7,10], although only ~30-50% of these dogs have bilateral lameness [11-13]. In bilaterally affected dogs, MTRT-OC lesions associated with clinical lameness are significantly larger than MTRT-OC lesions without clinical signs [13]. The Labrador Retriever and the Bull Terrier are often affected bilaterally[14]. Lesions on the lateral trochlear ridge more often seen in Rottweilers [11,15-17].

Although radiographic images are often used in the diagnosis of tarsocrural OC [7,17], computed tomography (CT) may allow a definitive diagnosis when the radiographic examination is inconclusive [18-20]. The use of CT avoids the superimposition of bony structures and provides a better view of the subchondral bone lesions, enabling the exact location, size and number of fragments to be determined [19,20].

One difference between MTRT-OC and LTRT-OC is the location on the trochlear ridge. The trochlear ridge of the talus can be divided in a proximal, dorsal, and distal part (Figure 1). In LTRT-OC, the dorsal, dorsoproximal, or proximal part can be affected [11,17,21], whereas in MTRT-OC, lesions occur mostly in the proximal part [7,15,19,22].

Our purpose was to evaluate whether significant differences exist between MTRT-OC and LTRT-OC with respect to clinical features of the affected dogs (breed, age,

gender, weight, and duration of signs) and subchondral bone lesion variables (morphologic data) of the lesions obtained by CT (size, location, number of fragments). Although it has been reported that LTRT-OC lesions tend to be larger [11], we are unaware of studies comparing subchondral bone lesion variables between MTRT-OC and LTRT-OC.

MATERIALS AND METHODS

Dogs

Medical records (1997 – 2010) of dogs diagnosed with osteochondrosis of the tarsocrural joint were reviewed. Inclusion criteria were adequately documented clinical records and a complete CT examination of both tarsocrural joints at the time of diagnosis. Clinical data (breed, age, gender, weight, duration of clinical signs) were retrieved.

CT Examination

Dogs were positioned in ventral recumbency on the CT-scanning table with the tarsal joints in extension. Lateral and dorsoplantar scout-views were acquired to confirm correct positioning and to prescribe the scan volume. Contiguous 1.25 mm collimated transverse images (120 kVp, 300 mAs) were made, using a bone reconstruction algorithm, from 2 cm proximal to the calcaneus to the tarsometatarsal joint.

Evaluation of CT Images

After acquisition of the transverse CT images, sagittal and dorsal reformatted images of the tarsocrural joint were made, using commercially available software (eFilm Workstation 3.1, Merge Healthcare, Chicago, Illinois). CT images were reviewed using a bone window (WW = 3500 HU; WL = 500 HU) and the final diagnosis of tarsocrural OC was based on identification of a subchondral defect or a mineralized fragment associated with the medial or lateral trochlear ridge.

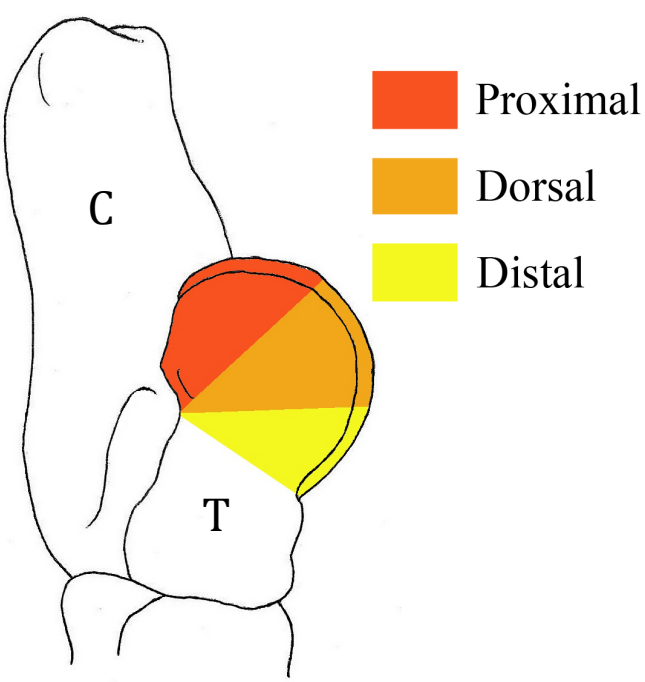

Figure 1. Location of OC lesions on the trochlear ridges of the talus (Adapted from Gielen et al., 2002) [21]. Calcaneus (C) and talus (T) are indicated.

Lesions were classified as proximal, dorsal, or distal (Figure 1) [19] and the number of fragments was recorded. Using a previously described protocol [13], the length (L), width (W), and depth (D) of all subchondral bone lesions was estimated (Figure 2) at the level they appeared to be largest. Length was estimated on the transverse (axial) images and sagittal reformatted images and mean length was calculated. A similar method was used for estimating the width on the transverse (axial) and dorsal reformatted images. For the estimation of depth, the sagittal and dorsal reconstructions were viewed, and measurements were performed in the center of the defect, from the bottom to the level where the joint surface was to be expected. These measurements resulted in the subchondral lesion size for each lesion. The subchondral bone lesion surface area was estimated by multiplying lesion length and width. The volume of a subchondral bone lesion was estimated by multiplying lesion length, width, and depth.

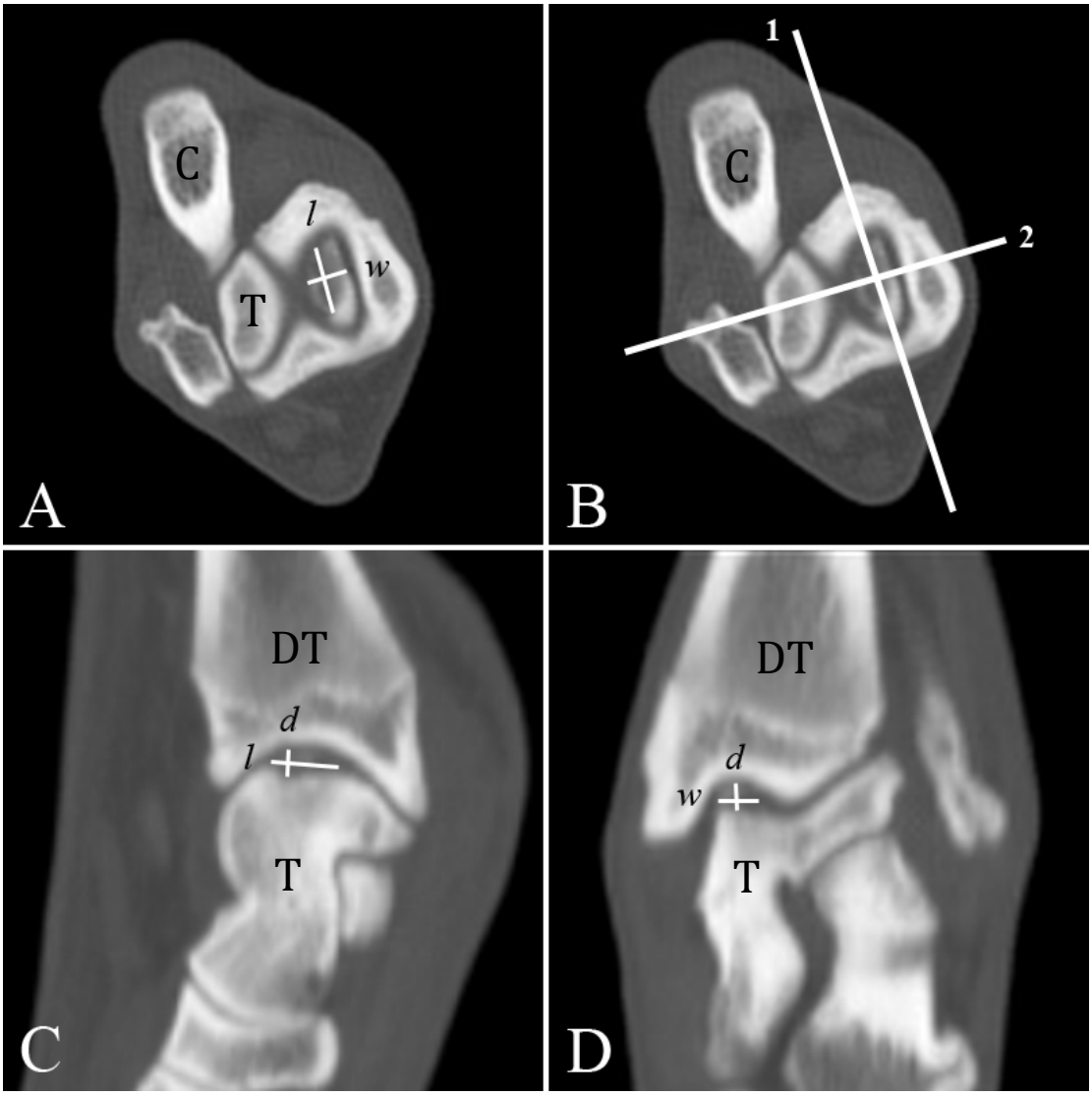

Figure 2. A: Transverse CT image showing measurements for length (l) and width (w). B: The level of the sagittal (1) and dorsal (2) reformatted images displayed on the transverse CT image. C: Sagittal CT reformatted image showing the measurements for length (l) and depth (d). D: Dorsal CT reformatted image showing the measurements for width (w) and depth (d). Talus (T), calcaneus (C), and distal tibia (DT) are indicated.

Similar to a method used in people [23] and in a previous study [24] all measurements were related to the cross section of the talus (measurement divided by the cross section of the talus and multiplied by 100), just below the trochlear ridges (Figure 3), to allow comparison of dogs with various body weights and sizes. This new set of data is referred to as relative length, relative width, relative depth, relative surface, and relative volume.

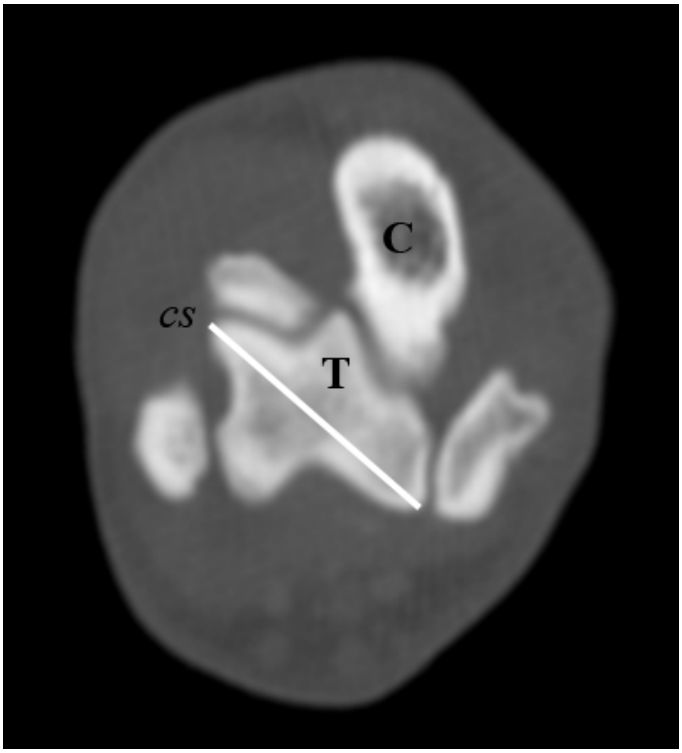

Figure 3. Transverse CT image displaying the measurement of the cross-section (cs) of the talus, just below the trochlear ridges. Talus (T) and calcaneus (C) are indicated.

Statistical Analysis

A t-test was used to compare the continuous variables for lateral and medial trochlear ridge lesions. For the categorical variables, a Wilcoxon rank sum test was used. The level of significance was set at $P < .05$.

Table 1. Breed and sex distribution of 66 dogs with tarsocrural osteochondrosis.

MTRT-OC n=56 Breed	Male	Female
Labrador Retriever	7	14
Rottweiler	5	4
Bullmastiff	1	4
Bull Terrier	2	2
Staffordshire Bull Terrier	2	1
Golden Retriever	1	1
Cross breed	-	2
Beagle	1	-
Pitbull Terrier	1	-
Giant Poodle	1	-
Belgian Shepherd	1	-
Border Collie	-	1
Boerboel	1	-
Cane Corso	1	-
Bouvier des Flandres	-	1
American Bulldog	-	1
Irish Wolfhound	-	1

LTRT-OC n=10 Breed	Male	Female
Golden Retriever	-	4
Rottweiler	1	1
Neapolitan Mastiff	-	1
Chow Chow	1	-
Irish Wolfhound	1	-
Alaskan Malamute	-	1

MTRT-OC, Medial trochlear ridge tarsocrural osteochondrosis;
LTRT-OC, Lateral trochlear ridge tarsocrural osteochondrosis.

RESULTS

Clinical and Pathologic Findings

There were 28 male and 38 female dogs (Table 1); bilateral OC was diagnosed in 14 dogs, yielding 80 lesions studied. Breeds affected bilaterally were Rottweiler, Labrador Retriever, Golden Retriever, Pit-bull Terrier, Staffordshire Terrier, Bullmastiff, Cane Corso, and Bullterrier. MTRT-OC lesions occurred in 56 dogs (67 joints) and LTRT-OC lesions in 10 dogs (13 joints). Bodyweight ranged from 11 - 72 kg (mean, 33 kg) with no significant age difference between dogs with MTRT-OC and LTRT-OC (Table 2). Mean age at diagnosis was 20 months (range, 5 - 106 months); 36 dogs were >12 months. Duration of lameness at diagnosis ranged from 1 - 40 months (mean, 6 months; Table 2).

Table 2. Summary statistics for 56 dogs with osteochondrosis lesions on the medial trochlear ridge (MTRT-OC) and 10 dogs with lesions on the lateral trochlear ridge (LTRT-OC).

	Mean (± SD)		
Variable	MTRT-OC (n = 56)	LTRT-OC (n = 10)	*P*-Value
Age (months)	22.5 (± 20.2)	8.85 (± 2.61)	0.02
Bodyweight (kg)	33.7 (± 12.8)	30.0 (± 10.9)	0.37
Duration of lameness (months)	6.6 (± 6.8)	3.2 (± 1.7)	0.08

Dogs with LTRT-OC were significantly younger ($P < .01$) than dogs with MTRT-OC lesions. There was a trend for dogs with LTRT-OC to have a shorter period of lameness before presentation ($P = .08$).

CT Localization and Number of Fragments

MTRT-OC lesions were identified on the proximal (n = 52) and dorsal (15) part of the trochlear ridge. LTRT-OC lesions were located on the proximal (11), dorsal (1), and distal (1) part of the trochlear ridge. More fragments were observed for medial than for lateral lesions, but this difference was not significant (*P* = .23; Table 3).

Table 3. Number of fragments associated with medial trochlear ridge tarsocrural osteochondrosis (MTRT-OC) and lateral trochlear ridge tarsocrural osteochondrosis (LTRT-OC).

Number of fragments	0	1	2	3
MTRT-OC lesions	21 (31.4 %)	25 (37.3 %)	10 (14.9 %)	11 (16.4 %)
LTRT-OC lesions		8 (61.5 %)	5 (38.5 %)	

CT Subchondral Bone Lesion Variables

Estimated length, width, depth, surface, and volume of the LTRT-OC subchondral bone lesions were significantly larger (*P* < .01) than for MTRT-OC lesions (Table 4). This was also true for the relative values of the length, width, depth, surface, and volume.

Table 4. Summary statistics of subchondral bone lesion variables for 67 osteochondrosis lesions on the medial trochlear ridge (MTRT-OC) and 13 lesions on the lateral trochlear ridge (LTRT-OC).

Variable	Mean (± SD)		*P*-Value
	MTRT-OC (n = 67)	LTRT-OC (n = 13)	
Length (L) (mm)	7.0 (± 2.8)	12.2 (± 5,5)	< .01
Width (W) (mm)	3.6 (± 1.3)	5.6 (± 1.4)	< .01
Depth (D) (mm)	3.2 (± 1.6)	7.6 (± 2.3)	< .01
Surface (L*W) (mm^2)	28.0 (± 18.2)	74.2 (± 43.3)	< .01
Volume (L*W*D) (mm^3)	100.1 (± 101.9)	614.2 (± 455.0)	< .01
Relative Length (%)	32.04 (± 11,81)	54.20 (± 21.06)	< .01
Relative Depth (%)	16.74 (± 5.61)	25.99 (± 6.13)	< .01
Relative Width (%)	14.76 (± 8.03)	34.81 (± 9.84)	< .01
Relative Surface (%)	126.21 (± 75.48)	328.22 (± 170.27)	< .01
Relative Volume (%)	452.13 (± 428.68)	2707.59 (± 1823.78)	< .01

DISCUSSION

We found significant differences in both clinical and morphologic features of MTRT-OC and LTRT-OC lesions, with LTRT-OC lesions having greater length, depth, width, and consequently surface and volume compared with MTRT-OC lesions. Lesion size has previously been reported to be an important factor in the evaluation of OC lesions in the tibiotarsal joint in both dogs and people. In dogs with bilateral MTRT-OC lesions and unilateral lameness, clinical lesions (i.e. those associated with visible lameness) are significantly larger than lesions not associated with clinical signs [13]. In people, a strong correlation exists between length and width of OC lesions of the talus and the outcome after arthroscopic treatment. A cut-off point for the surface of lesions of 150 mm^2 seems to exist below which a good outcome is more likely [25]. The influence of these findings in dogs on the long-term outcome after treatment warrants further research.

LTRT-OC lesions also have a larger variation in size than MTRT-OC lesions. Although shape itself was not evaluated in our study, a variation in shape has been reported in people, where lateral lesions are more wafer-shaped, and medial lesions are more cup-shaped [26]. A variation in location of the LTRT-OC lesions was thought to be suggestive of a different cause for LTRT-OC, because OC is usually very topographically consistent [27]. Our study has not shown a large variation in location of LTRT-OC lesions, as reported by others [27].

We found that dogs with LTRT-OC lesions are younger than those with MTRT-OC lesions and tend to have a shorter duration of lameness before presentation. Because LTRT-OC lesions are larger, they are likely to be associated with more severe lameness, leading to an earlier presentation. More persistent symptoms are also reported for LTRT-OC lesions in people [26], and might be an explanation for the shorter duration of lameness before presentation we found in dogs with LTRT-OC.

Bilateral lesions were found in 21% of dogs (14/66), which is less than other reports [7,10]. Lateral lesions were found in 15% of the dogs (10/66), which is consistent with

previous reports [6,9]. Although in most reports of LTRT-OC the Rottweiler is affected [11,15,27], in our study the Golden Retriever is the most affected breed. This might be explained by local differences in dog breed population. Some other breeds included in our report, like Irish Wolfhound and Alaskan Malamute, have not previously been reported with LTRT-OC.

The morphologic and clinical differences we found might support previous suggestions of a different cause for MTRT and LTRT-OC lesions [13,27,28]. In people, medial lesions are caused by inversion with the ankle joint in dorsiflexion and can be either traumatic or atraumatic in origin, whereas lateral lesions are caused by inversion of the ankle in a plantar flexed position and are most likely all associated with trauma [26,29]. In dogs, trauma and avulsion fractures of the lateral trochlear ridge have been suggested as a cause for fragments originating from the lateral trochlear ridge [16,28]. However, a correlation between LTRT-OC and avulsion fractures in the dorsal and distal part of the lateral trochlear ridge is unlikely, because the short lateral collateral ligaments do not attach here [20].

A mismatch in the biomechanical properties of the articulating surfaces and repetitive microtrauma might contribute to the development of OC lesions, as suggested in people [29,30]. These factors are closely associated with the joint biomechanics. Biomechanical differences in joint function could explain breed predispositions for certain orthopedic conditions [31,32], and applied to tarsocrural OC, tarsal joint angle could play a role. In horses, tarsal joint angle has been associated with tarsal joint pathology [33,34]. Joint biomechanics, biomechanical properties of articular surfaces, repetitive microtrauma, and trauma are all important factors to consider in the causes of OC. As in people, the larger LTRT-OC lesions might be traumatic, transchondral fractures, whereas MTRT-OC lesions are more likely to be true OC lesions, where repetitive microtrauma is an important factor. As previously suggested, microtrauma at the level of the chondro-osseous junction can disrupt the cartilage canal vessels, which may initiate the formation of osteochondrosis lesions during a specific time period [5]. Biomechanical research is necessary to elucidate the role of joint biomechanics in the development of tarsocrural OC.

There are some potential limitations to our study. The method of measuring the lesion depth might not be 100% accurate, because the definition of the top of the defect had to be estimated because of the missing actual subchondral bone surface. The surface and volume were estimated by calculating the surface of the encasing rectangle and the volume of the encasing rectangular prism respectively. This most likely leads to an overestimation of the subchondral bone lesion surface and volume. Slice thickness can have an effect on the measurements, mainly on the depth estimations on the sagittal and dorsal reformatted images, leading to underestimation. However, all measurements and calculations were made using the same protocol, so we do not expect a substantial variation in the measurements influencing the comparison of the data from MTRT-OC and LTRT-OC lesions.

In our study, defects in the subchondral bone were evaluated, because CT provides visibility of (subchondral) bone, but not of cartilage. It has been reported that CT and arthroscopic findings are not always in agreement, as there can be a subchondral defect without disruption of the overlying cartilage, and defects in the cartilage only are not visible on CT [35]. Although the use of positive contrast CT arthrography might have been advantageous, this was not possible because of the retrospective nature of this study. This makes is difficult to draw conclusions about the relationship between subchondral bone lesion size and cartilage lesion size; however, the subchondral bone and overlying cartilage are viewed as a functional unit with an important mechanical function [36], and pathologic conditions like OC, affect this functional unit. The relationship between subchondral bone, cartilage, and their respective lesion size and the implications for the treatment of OC warrants further research.

We conclude that the difference and variation in size of LTRT-OC subchondral bone lesions, the younger age of dogs with LTRT-OC lesions and the tendency to a shorter period of lameness before presentation, might support existing ideas of a different cause compared to MTRT-OC [13,16,27,28] but more research is needed to elucidate this.

REFERENCES

1. Jeffcott LB: Osteochondrosis - An international problem for the horse industry. Journal of Equine Veterinary Science 16:32-37, 1996.

2. Schenck RC, Goodnight JM: Current Concept Review - Osteochondritis Dissecans. The Journal of Bone and Joint Surgery 78:439-456, 1998.

3. Ytrehus B, Carlson CS, Lundeheim N, et al: Vascularisation and osteochondrosis of the epiphyseal growth cartilage of the distal femur in pigs - development with age, growth rate, weight and joint shape. Bone 34:454-465, 2004.

4. Richardson DC, Zentek J: Nutrition and osteochondrosis. Veterinary Clinics of North America-Small Animal Practice 28:115-135, 1998.

5. Ytrehus B, Carlson CS, Ekman S: Etiology and pathogenesis of osteochondrosis. Veterinary Pathology 44:429-448, 2007.

6. Denny HR, Gibbs C: Osteochondritis dissecans of the canine stifle joint. Journal of Small Animal Practice 21:317-322, 1980.

7. Montgomery RD, Hathcock JT, Milton JL, et al: Osteochondritis dissecans of the canine tarsal joint. Compendium on Continuing Education for the Practicing Veterinarian 16:835-845, 1994.

8. Necas A, Dvorak M, Zatloukal J: Incidence of osteochondrosis in dogs and its late diagnosis. Acta Veterinaria Brno 68:131-139, 1999.

9. Fitch RB, Beale BS: Osteochondrosis of the canine tibiotarsal joint. Veterinary Clinics of North America-Small Animal Practice 28:95-102, 1998.

10. Weinstein MJ, Mongil CM, Rhodes WH, et al: Orthopedic Conditions of the Rottweiler .2. Compendium on Continuing Education for the Practicing Veterinarian 17:925-933, 1995.

11. Wisner ER, Berry CR, Morgan JP, et al: Osteochondrosis of the Lateral Trochlear Ridge of the Talus in 7 Rottweiler Dogs. Veterinary Surgery 19:435-439, 1990.

12. Beale BS, Goring RL, Herrington J, et al: A prospective evaluation of 4 surgical approaches to the talus of the dog used in the treatment of osteochondritis dissecans. Journal of the American Animal Hospital Association 27:221-229, 1991.

13. Gielen I, Van Ryssen B, Coopman F, et al: Comparison of subchondral lesion size between clinical and non-clinical medial trochlear ridge talar osteochondritis dissecans in dogs. Veterinary and Comparative Orthopaedics and Traumatology 20:8-11, 2007.

14. Breur GJ, Spaulding KA, Braden TD: Osteochondritis dissecans of the medial trochlear ridge of the talus in the dog. Veterinary and Comparative Orthopaedics and Traumatology:168-176, 1989.

15. Robins GM, Read RA, Carlisle CH, et al: Osteochondritis dissecans of the lateral trochlear ridge of the tibial tarsal bone in the dog. Journal of Small Animal Practice 24:675-685, 1983.

16. Aron DN, Mahaffey MB, Rowland GN: Free Chondral Fragment Involving the Lateral Trochlear Ridge of the Talus in a Dog. Journal of the American Veterinary Medical Association 186:1095-1096, 1985.

17. Carlisle CH, Robins GM, Reynolds KM: Radiographic signs of osteochondritis-dissecans of the lateral ridge of the trochlea tali in the dog. Journal of Small Animal Practice 31:280-286, 1990.

18. Zinman C, Reis ND: Osteochondritis dissecans of the talus - use of the high-resolution computed-tomography scanner. Acta Orthopaedica Scandinavica 53:697-700, 1982.

19. Gielen I, van Bree H, Van Ryssen B, et al: Radiographic, computed tomographic and arthroscopic findings in 23 dogs with osteochondrosis of the tarsocrural joint. Veterinary Record 150:442-447, 2002.

20. Gielen I, van Ryssen B, van Bree H: Computerized tomography compared with radiography in the diagnosis of lateral trochlear ridge talar osteochondritis dissecans in dogs. Veterinary and Comparative Orthopaedics and Traumatology 18:77-82, 2005.

21. Vanryssen B, Vanbree H: Arhtoscopic evaluation of osteochondrosis lesions in the canine hock joint – a review of 2 cases. Journal of the American Animal Hospital Association 28:295-299, 1992.

22. Johnson KA, Howlett CR, Pettit GD: Osteochondrosis in the hock joint in dogs. Journal of the American Animal Hospital Association 16:103-113, 1980.

23. Lotke PA, Ecker ML: Osteonecrosis of the Knee. Journal of Bone and Joint Surgery-American Volume 70A:470-473, 1988.

24. Vanbree H: Evaluation of Subchondral Lesion Size in Osteochondrosis of the Scapulohumeral Joint in Dogs. Journal of the American Veterinary Medical Association 204:1472-1474, 1994.

25. Choi WJ, Park KK, Kim BS, et al: Osteochondral Lesion of the Talus Is There a Critical Defect Size for Poor Outcome? American Journal of Sports Medicine 37:1974-1980, 2009.

26. Canale ST, Belding RH: Osteochondral lesions of the talus. Journal of Bone and Joint Surgery-American Volume 62:97-102, 1980.

27. van Ee RT, Gibson K, Roberts ED: Osteochondritis dissecans of the lateral ridge of the talus in a dog. Journal of the American Veterinary Medical Association 193:1284-1286, 1988.

28. Sjostrom L, Hakanson N: Traumatic Injuries Associated with the Short Lateral Collateral Ligaments of the Talocrural Joint of the Dog. Journal of Small Animal Practice 35:163-168, 1994.

29. Schenck RC, Goodnight JM: Osteochondritis dissecans. Journal of Bone and Joint Surgery-American Volume 78A:439-456, 1996.

30. Athanasiou KA, Niederauer GG, Schenck RC: Biomechanical Topography of Human Ankle Cartilage. Annals of Biomedical Engineering 23:697-704, 1995.

31. Grondalen T: Osteochondrosis and Arthrosis in Pigs .7. Relationship to Joint Shape and Exterior Conformation. Acta Veterinaria Scandinavica:1-32, 1974.

32. Colborne GR, Innes JF, Comerford EJ, et al: Distribution of power across the hind limb joints in Labrador Retrievers and Greyhounds. American Journal of Veterinary Research 66:1563-1571, 2005.

33. Dolvik NI, Klemetsdal G: Conformational traits of Norwegian cold-blooded trotters: Heritability and the relationship with performance. Acta Agriculturae Scandinavica Section a-Animal Science 49:156-162, 1999.

34. Gnagey L, Clayton HM, Lanovaz JL: Effect of standing tarsal angle on joint kinematics and kinetics. Equine Veterinary Journal 38:628-633, 2006.

35. Moores AP, Benigni L, Lamb CR: Computed tomography versus arthroscopy for detection of canine elbow dysplasia lesions. Veterinary Surgery 37:390-398, 2008.

36. Madry H, van Dijk CN, Mueller-Gerbl M: The basic science of the subchondral bone. Knee Surgery Sports Traumatology Arthroscopy 18:419-433, 2010.

CHAPTER FOUR

Scientific Aims

SCIENTIFIC AIMS

Although the pathogenesis of osteochondrosis has been explored in different species, the exact etiology remains unclear. Also in dogs, different factors including hereditary, dietary and other environmental factors are likely to play a role, in the onset and progression of this multifactorial disease.

One environmental factor that is likely to play a role in the development of osteochondrosis is biomechanical loading. The lesions associated with osteochondrosis are found at specific locations within the joint. This suggests that local biomechanical loading and the associated tensile and compressive stresses and strains are likely negatively influencing the physiology and biochemical constitution of the cartilage and subchondral bone. This may lead to a disruption of the normal endochondral ossification process at the onset of the disease process. More specifically, a disruption of the cartilage canal vessels, leading to avascular necrosis of the growth-cartilage is likely to be the initiating event leading to osteochondrosis.

This PhD will focus on the tarsocrural joint and the reasons for this are threefold. Firstly, concomitant orthopaedic conditions in the tarsocrural joint, besides trauma, are rare, therefore OC is likely to be induced by the native mechanical environment in the joint. In the elbow joint for instance, OC can occur in the presence of joint incongruity and fragmented coronoid process, making the evaluation of OC in this joint even more complex. Secondly, the tarsocrural joint is relatively restricted in terms of the degrees of freedom, with its motion merely being limited to flexion and extension. And the last reason is the difference in clinical and morphological parameters in lesions on the medial and lateral trochlear ridge, possibly indicating a difference in etiology. Detailed research might help to elucidate a different mechanism of disease for the lateral and medial trochlear ridge lesions.

The general aim of this PhD is to gain more insight in the role of biomechanical loading in the development of osteochondrosis in dogs, with a focus on the tarsocrural joint.

Because it is very difficult, even almost impossible, to evaluate biomechanical loading *in vivo*, two complementary indirect methods will be used to evaluate joint loading and its effect on the tissue constitution in the tarsocrural joint.

Non-invasive *in vivo* evaluation of the subchondral bone density distribution, using computed tomographic osteoabsorptiometry (CTOAM), will be combined with advanced biomechanical modelling techniques, more specifically image-based musculoskeletal modeling, dynamic motion analysis and finite element analysis.

The CTOAM will show the morphological consequences of the long-term joint loading in terms of subchondral bone density. The musculoskeletal modeling will yield estimations of joint contact forces, serving as input for the finite element analysis. The latter provides the ability to relate the tissue level response, demonstrated with CTOAM, to the local mechanical environment to which the tissue is being exposed during locomotion.

These techniques will be applied to the Labrador Retriever, a breed that is often affected with OC lesions in different joints.

The central hypothesis of this PhD states that if biomechanical loading plays a central role in the onset of OC, a strong correlation will be found between a high, experimentally determined subchondral bone density, high model-based strains during locomotion, and the location of OC lesions.

Different intermediate aims have been formulated, and form the base of this PhD:

1. To evaluate the subchondral bone density distribution and strength distribution in the talus of healthy Labrador Retrievers (**Chapter 5 and 6**).

2. To evaluate the effect of age on the subchondral bone density distribution in the tarsal joint of healthy Labrador Retrievers (**Chapter 7**).

3. To describe the density changes at the level of the subchondral bone in dogs with tarsocrural osteochondrosis (**Chapter 8**).

4. To describe differences in subchondral bone density distribution between different breeds and different *Canidae* species (**Chapter 9**).

5. To evaluate local loading condition in the tarsocrural joint in terms of joint kinematics, and kinetics, estimate muscle forces and joint contact forces in healthy Labrador Retrievers using a breed-specific musculoskeletal model (**Chapter 10**).

6. To evaluate the stress and strain distribution in the cartilage and subchondral bone of the talus in the Labrador Retriever by means of a breed-specific finite element model of the tarsocrural joint (**Chapter 11**).

In the general discussion (**Chapter 12**), subchondral bone density distribution and the stress and strain distribution in the subchondral bone plate will be related to the location of the OC lesions in the tarsocrural joint.

CHAPTER FIVE

Subchondral Bone Density Distribution of the Talus in Clinically Normal Labrador Retrievers

W. Dingemanse [1], M. Müller-Gerbl [2], I. Jonkers [3], J. Vander Sloten [4], H. van Bree [1], I. Gielen [1]

[1] Department of Medical Imaging of Domestic Animals and Orthopaedics of Small Animals, Faculty of Veterinary Medicine, Ghent University. Merelbeke, Belgium

[2] Institute of Anatomy, Basel University. Basel, Switzerland

[3] Human Movement Biomechanics Research Group, Faculty of Kinesiology and Rehabilitation Sciences, KU Leuven. Leuven, Belgium

[4] Biomechanics Section, Faculty of Engineering Science, KU Leuven. Leuven, Belgium

Adapted from: W. Dingemanse, M. Müller-Gerbl, I. Jonkers, J. Vander Sloten, H. van Bree, I. Gielen. Subchondral bone density distribution of the talus in clinically normal Labrador Retrievers. BMC Veterinary Research 12 (2016) 56.

ABSTRACT

Background: Bones continually adapt their morphology to their load bearing function. At the level of the subchondral bone, the density distribution is highly correlated with the loading distribution of the joint. Therefore, subchondral bone density distribution can be used to study joint biomechanics non-invasively. In addition, physiological and pathological joint loadin are important aspects of orthopaedic disease, and research focusing on joint biomechanics will benefit veterinary orthopaedics. This study was conducted to evaluate density distribution in the subchondral bone of the canine talus, as a parameter reflecting the long-term joint loading in the tarsocrural joint.

Methods: Subchondral bone density distribution was evaluated based on CT images and computer tomographic osteoabsorptiometry (CTOAM). The location of the density maxima was quantified using a standardised grid overlay and the size of the density maximum was expressed as the maximum area ratio (MAR).

Results: Two main density maxima were found, one proximally on the medial trochlear ridge and one distally on the lateral trochlear ridge. All joints showed very similar density distribution patterns and no significant differences were found in the localisation of the density maxima between left and right limbs and between dogs.

Conclusions: Based on the density distribution, the lateral trochlear ridge is most likely subjected to highest loads within the tarsocrural joint. The joint loading distribution is very similar between dogs of the same breed. In addition, the joint loading distribution supports previous suggestions of the important role of biomechanics in the development of OC lesions in the tarsus. Important benefits of computed tomographic osteoabsorptiometry (CTOAM), i.e. the possibility of *in vivo* imaging and temporal evaluation, make this technique a valuable addition to the field of veterinary orthopaedic research.

CHAPTER 5

BACKGROUND

Joint loading, including tensile and compressive stresses, is an important factor in cartilage and subchondral bone physiology and pathology [1-3]. Changes in loading and biomechanical properties of these important load-bearing structures, play a key-role in the development and progression of orthopaedic disease [4].

In recent years, different methods have been applied to study joint biomechanics both *in vitro* and *in vivo*. The initial studies presented detailed anatomical descriptions of joint structures [5,6], followed by studies describing pressure distributions and contact areas [7,8]. These studies were often done on cadaveric specimens and required a certain degree of dissection, thus altering joint kinematics. *In vivo* biomechanics are often limited to kinetic and kinematic research using marker data and pressure plates [4]. Actual joint loading cannot easily be assessed non-invasively *in vivo*, since it requires intra-articular insertion of pressure films [9] making it difficult to apply in studies using larger populations and patient populations. Subchondral bone density is directly influenced by joint biomechanics and limb function and can be used to evaluate joint biomechanics.

The stresses acting on the joint surface induce modeling and remodeling of the bony tissue, depending on whether the local strains either exceed the modeling threshold or stay below the remodeling threshold. Because of that, increased joint loading leads to increased local strains and bone modeling ensures an increase in subchondral bone density to withstand the increased loading [1,3]. In addition, altered joint biomechanics lead to altered joint loading distribution, leading in turn to alterations in the subchondral bone density distribution [10,11].

The subchondral bone density in joints is highly correlated with joint loading and reflects the loading history of the joint [3,11-13]. Using computer tomographic osteoabsorptiometry (CTOAM), the density distribution of the subchondral bone can be visualised and evaluated [3,11-13]. In order to evaluate subchondral bone density and

changes associated with orthopaedic conditions, the normal, physiological subchondral bone density distribution needs to be described first.

In addition, this type of biomechanical research can help to elucidate the role of joint biomechanics in the development of osteochondrosis (OC) [14]. Osteochondrosis is an orthopaedic condition in dogs that is considered to be multifactorial, with hereditary, dietary and environmental factors playing a role [15]. An environmental factor likely to influence the occurrence of OC is joint biomechanics, since OC lesions are often found in specific locations within the joint [16-19]. In the tarsocrural joint, lesions can be found medially (medial trochlear ridge tarsocrural osteochondrosis (MTRT-OC)) and laterally (lateral trochlear ridge tarsocrural osteochondrosis (LTRT-OC)) [14,20,21]. The specific joint anatomy likely affects the location of the OC lesions, and this study can aid in the understanding of the pathophysiology of this condition.

This study was conducted to describe the subchondral bone density distribution of the talus of healthy Labrador Retrievers non-invasively, as a parameter reflecting long-term joint loading in the tarsocrural joint, using CTOAM. The authors hypothesise an inhomogeneous distribution of the density of the subchondral bone.

MATERIAL AND METHODS

Study population

A total of 20 tarsal joints (10 left and 10 right) from 10 adult (age 24-28 months) Labrador Retrievers, submitted for computer tomographic (CT) examination of the elbow joint for the screening of elbow dysplasia, were included in this study. The study was approved by the ethical committee of the Faculty of Veterinary Medicine, Ghent University (approval nr. EC2011/193) and informed, written owner consent was obtained in each case. Inclusion criteria for this study were no abnormalities on orthopaedic examination and lameness evaluation and no abnormalities on radiographs of hips, elbows and tarsal joints. After CT examination of the elbow joint, the tarsal joints were scanned as well.

Image acquisition

Under general anaesthesia the dog was positioned in ventral recumbency and CT images were acquired from the tarsal joints using a 4 slice helical CT scanner (Lightspeed Qx/i, General Electric Medical Systems, Milwaukee, WI, USA). The CT parameters were 120 kVp and 300 mAs. Contiguous, 1,25 mm collimated, transverse images were obtained in a soft tissue reconstruction algorithm. Left and right tarsal joints were scanned simultaneously, with the tarsal joints in extension, according to patient protocol [21]. Acquisition time was approximately five minutes, including repositioning after CT examination of the elbow joints.

Image analysis

The CT images were exported in DICOM format to commercially available software (Analyze 11.0, Biomedical Imaging Resource, Mayo Foundation, Rochester, MN, USA), used to complete the CTOAM workflow (Figure 1). The technique is described in detail in Chapter 1.

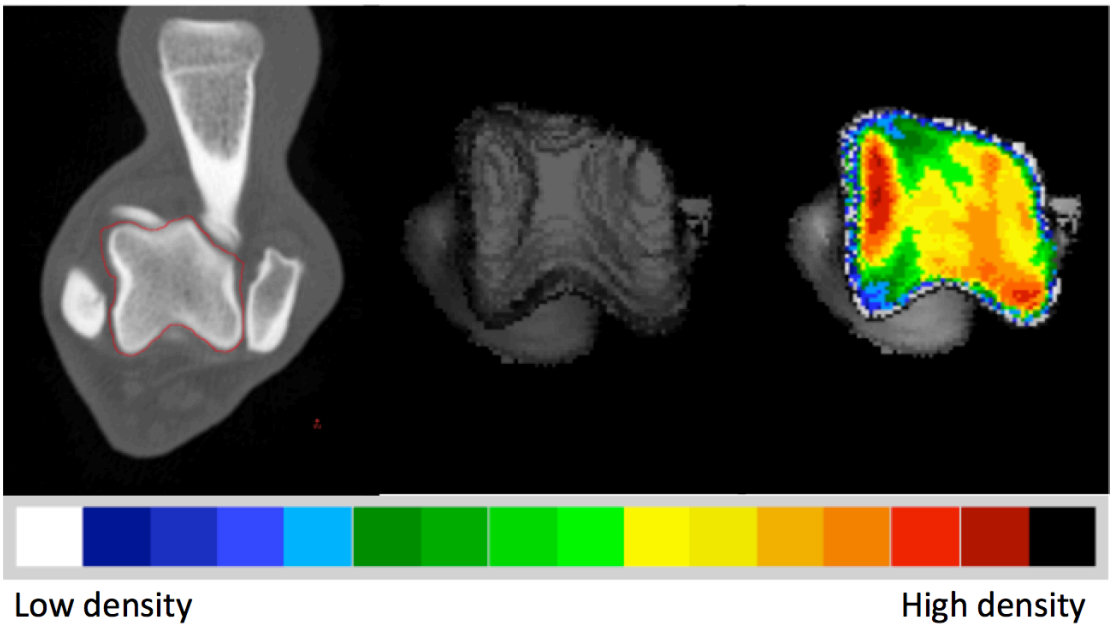

Figure 1: CTOAM workflow in Analyze. From left to right: segmentation of the talus; 3D rendering of the proximal view; overlay of the false-colour map of the subchondral bone density distribution.

For quantification purposes, the density values (in HU) were converted to 8-bit values, i.e. 256 density values, which were split equally over 8 bins, according to literature [22]. Thus, each bin contains a range of 32 density values. A density maximum was defined as an area with density values in the two highest density bins of the densitogram. To allow the comparison of the individual subchondral bone density distributions, a 30 x 30 unit grid was projected over the densitogram of the proximal and dorsal view of the trochlear ridges. The grid edges were positioned thus the entire joint surface could fit within. The number of units in each grid was kept the same, to standardize the coordinates of the density maxima. The x- and y-coordinates (Figure 2) were used to describe the location of the density maxima on the joint surface.

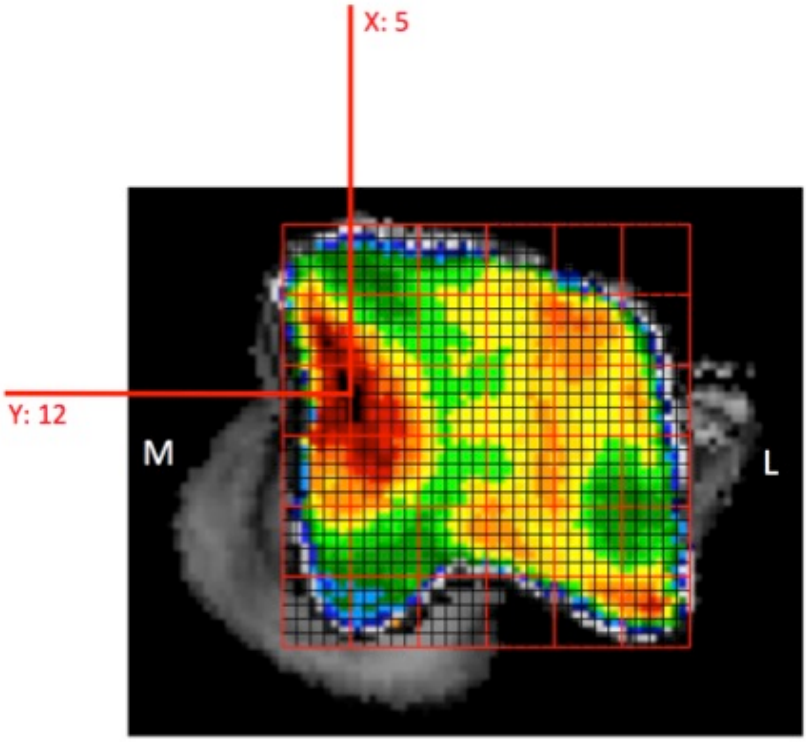

Figure 2: Positioning of the grid on a proximal view of the talus and description of the subchondral bone density maximum by x- and y-coordinates.

In addition, the size of the maximum was described as a ratio of the area of the density maximum and the joint surface area of the proximal and distal view respectively, and defined as the maximum area ratio (MAR).

$$\text{MAR} = \frac{\text{number of pixels of the density maximum}}{\text{number of pixels of the total joint surface}}$$

The use of MAR allows a relative comparison between individuals, and accounts for size-differences.

Statistics

Using commercially available software (SPSS Statistics 22), the location of the density maxima and the MAR were compared between left and right and between dogs. Data was evaluated using a Student's T-test and ANOVA (with Bonferroni post-hoc) and significance was set at $P < .05$.

RESULTS

1. Regional variation of subchondral bone density

The proximal and distal reconstructions provided full visualization of the subchondral bone, with a small visual overlap in the transitional area (proximodorsal area) (Figure 3). The subchondral bone density distribution showed considerable regional differences in both the medial and the lateral trochlear ridge. Hounsfield Units generally ranged from 200-1200, although in some dogs (n=2) the upper range was limited to around 1000 HU.

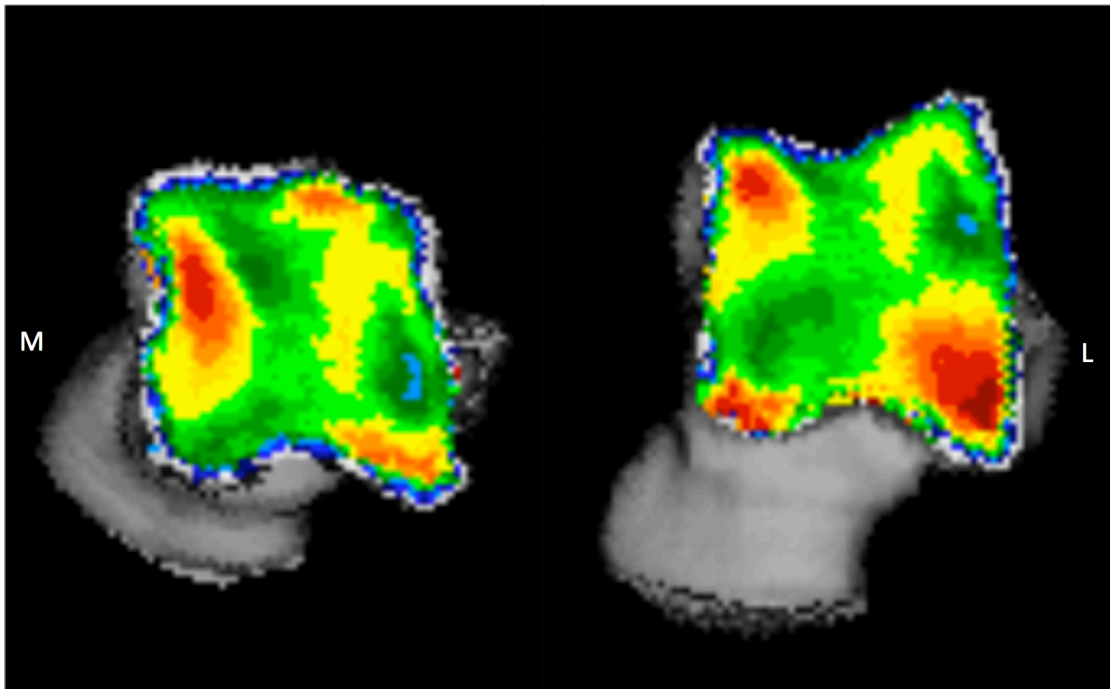

Figure 3: Typical subchondral bone density distribution of the talus of a Labrador Retriever. Left talus in a proximal (left) and distal (right) view, medial (M) and lateral (L) side are indicated.

2. Differences in subchondral bone density distribution between medial and lateral trochlear ridge

In general, the lateral trochlear ridge had a higher apparent density in comparison to the medial trochlear ridge, as illustrated by the colour map (Figure 3). The medial and lateral trochlear ridges showed a distinctly different density pattern.

The medial trochlear ridge had a density maximum in its proximal part. More distally, density values were lower. In 80% of the joints (n=16), a focal additional density maximum was present at the most distal part of the medial trochlear ridge.

On the lateral trochlear ridge, the density maximum was found at the distal part of the trochlear ridge at the level where the medial trochlear ridge shows an area of low density. This density maximum was larger (Table 1) and showed a larger variety in shape than the maximum on the medial trochlear ridge. The density maxima on medial and lateral trochlear ridges were located adjacent to the medial and lateral border of the ridge respectively.

Table 1. Results summary.

		Left	Right	P-value
Proximal view	Total # pixels	2254.8 (482.1)	2226.4 (494.9)	.909
	Area max # pixels	737.9 (212.4)	716.5 (218.0)	.845
	MAR	32.4 (4.3)	31.6 (3.9)	.720
Distal view	Total # pixels	2348.1 (404.2)	2288.8 (366.4)	.763
	Area max # pixels	919.9 (184.4)	944.4 (208.5)	.807
	MAR	39.5 (5.0)	41.5 (6.6)	.495

Total number of pixels, number of pixels of the density maximum and MAR. Values displayed as mean (SD).

3. Quantification of density maxima

The location of the density maxima on the standardized grid is displayed in a summary view for both views of the talus (Figure 5). The density maxima clearly display a very similar distribution in all dogs. No significant differences in the coordinates were found between left and right joints (p-values .607 and .540) and between different dogs (p values .755 and .367).

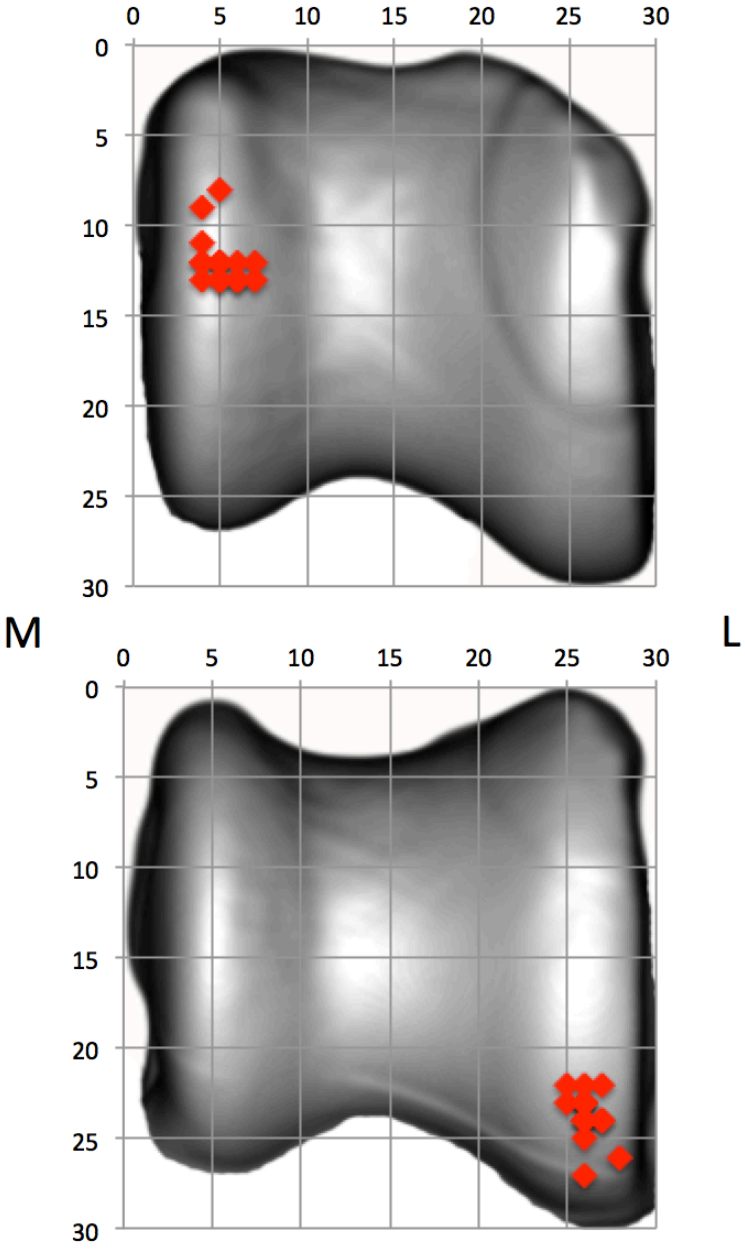

Figure 5: Summation view of the density maxima coordinates. Proximal (top) and distal (bottom) view, right coordinates were mirrored to left.

4. Comparison of MAR

There was no significant difference in the MAR between left and right (Table 1). Between dogs, there was no significant difference for the MAR in the proximal view (p-value .505), but a significant difference was found in the distal view (p-value .003).

CHAPTER 5

DISCUSSION

This study describes the subchondral bone density distribution of the talus in a group of healthy Labrador Retrievers, using conventional CT data and CTOAM. The densitograms provide a visual representation of the subchondral bone density distribution. Additionally the density maxima were described using a standardised grid overlay and the maximum area ratio (MAR) was calculated.

Previous studies in humans have shown regional subchondral bone density variations in many different joints [11,12,23], but studies in dogs have been limited to the elbow and stifle joint [24-26]. In this study, considerable regional differences of subchondral bone density were found in the convex surface of the talus, articulating with the distal tibia.

The density distribution of the trochlear ridges of the proximal talus is characterized by two density maxima. One is located at the proximal part of the medial trochlear ridge and the other one is located more distally on the lateral trochlear ridge. In addition, the apparent density of the lateral trochlear ridge is higher than the apparent density of the medial trochlear ridge. A possible explanation for this is the fact that the lateral trochlear ridge in the dog is more pronounced and is more likely to endure increased loads during gait. Geometry plays a major role in the development of subchondral bone density patterns, as it determines the magnitude and direction of the dynamic loads, which in turn will guide the modeling process, leading to morphological adaptations [3,27], which is in this case an increase in apparent density.

Both the location of the density maxima and the MAR showed no significant differences between left and right limbs. A recent study described asymmetry in limb and joint mechanics in orthopedically sound Labrador Retrievers [28]. Mechanical dominance has been described in various species, and in dogs right hind limb dominance appears to be most common [29]. These conclusions are based on the calculation of the total support moment of the limbs, and showed that the tarsal

joint moment was significantly larger on the dominant side. Mechanical dominance was not evaluated using gait analysis in the dogs used in this study. Based on our findings, we assume that the dogs used in this study have symmetrical gait, or that the differences in case of asymmetry due to hind limb dominance, did not significantly effect subchondral bone density distribution. Whether or not hind limb dominance in dogs has an influence on subchondral bone density is a very interesting topic, and is subject of further research.

On the proximal view there was no significant difference found for the MAR between dogs, whereas on the distal view there was a significant difference for the MAR. As mentioned above, the maximum on the lateral trochlear ridge was located distally, so it was visualised best on the distal view, and showed more variety in shape compared to the maximum on the medial trochlear ridge. This explains the difference in MAR between dogs in the distal view. A possible explanation is that the proximal part of the medial trochlear ridge is subjected to more homogeneous loading. Another possibility, that is likely to play a simultaneous role, is that the force-transmitting area of the medial trochlear ridge is much more constant between dogs, whereas for the lateral trochlear ridge this can vary more between dogs.

Possible drawback of CTOAM for the evaluation of subchondral bone density is that the density distribution of a 3D volume (the voxels) is displayed in 2D (pixels). Because the density is evaluated over the thickness of the subchondral bone plate, perpendicular to the line of sight on the joint surface, this will cause no problems on flat articular surfaces. On more curved articular surfaces, the use of multiple views is necessary to evaluate the subchondral bone density distribution.

Differences in the size of the area of maximum density can be caused by absolute size differences (i.e. larger or smaller talus) but in this study this effect will be very minimal since all dogs were Labrador Retrievers of approximately the same size, weight, and age. Another reason is differences in scanning parameters, specifically the size of the field of view (FOV). Pixel size depends on the size of the scanned

object and FOV used for the scan. Since we used consistently a FOV of 512x512, this effect will be minimal due to a standardised position of the joint, and minimal size differences between the dogs used in this study. The use of the MAR allows a relative comparison of the area of maximum density, accounting for the above confounders when using absolute size values.

When considering joint loading and joint congruency, another important factor is the joint cartilage. Joint cartilage has the important biomechanical role to provide an even distribution of the joint loading on the articular surface [30]. Thicker cartilage is found in places with higher biomechanical loads. A study by Brunnberg et al. supports our conclusion that the lateral trochlear ridge is most likely subjected to higher loads. The cartilage of the lateral trochlear ridge is significantly thicker than the cartilage of the medial trochlear ridge [31].

The location of the density maximum on the medial trochlear ridge is the same location where the majority of MTRT-OC lesions are found [14]. Repetitive loading above the bone modeling threshold, can cause accumulation of microdamage to the bone [32]. Areas with increased subchondral bone density, and thus increased loading conditions, are more likely to be subjected to loading causing microdamage as well. On the talus, these areas subjected to high loading coincide with the location of MTRT-OC lesions. Thus, this study supports previous suggestions that repetitive microdamage [33] is an important factor in the development of OC, although more research is necessary to elucidate the exact pathophysiology.

Lesions on the lateral trochlear ridge (LTRT-OC lesions), are larger than MTRT-OC lesions and have a larger variation in size [14]. Interestingly, the subchondral bone density maximum on the lateral trochlear ridge is larger and shows more variation compared to the medial trochlear ridge, and similar distribution as the OC lesions.

Untill now, it is not known whether changes in subchondral bone density are the cause or the effect of OC lesions. A local increase in subchondral bone density, as is the case at the level of a subchondral bone density maximum, may increase the

discrepancy between the biomechanical properties of two articulating surfaces. In humans, this mismatch has been suggested to contribute to the development of OC lesions [33,34].

CONCLUSION

This study shows a distinct pattern of subchondral bone density in the talus of healthy, adult Labrador Retrievers. This pattern, or density distribution, provides more information on the biomechanical aspects of the tarsocrural joint and the morphological adaptations under normal joint loading conditions. The influence of altered joint kinematics, bone geometry and leg conformation on the subchondral bone density distribution remains subject of further research.

Although the evaluation of the subchondral bone density distribution pattern supports previous suggestions on the role of joint biomechanics in the development of tarsocrural OC, more research is needed to determine cause and effect. Therefore, research should focus on early stages of OC lesions and systematically review all factors contributing to the biomechanical joint loading.

In the field of veterinary biomechanics, CTOAM could provide new insights in physiological joint loading distribution, and alterations in pathological conditions. The technique can be used *in vivo*, in patient populations, and to evaluate temporal changes, for instance following orthopaedic surgery. This implies significant advantages compared to more traditional and invasive techniques used to evaluate joint loading.

REFERENCES

1. Burton NJ, Ellis JR, Burton KJ, et al: An ex vivo investigation of the effect of the TATE canine elbow arthroplasty system on kinematics of the elbow. Journal of Small Animal Practice 54:240-247, 2013.

2. Turner CH: Three rules for bone adaptation to mechanical stimuli. Bone 23:399-407, 1998.

3. Frost HM: The Utah paradigm of skeletal physiology: an overview of its insights for bone, cartilage and collagenous tissue organs. Journal of Bone and Mineral Metabolism 18:305-316, 2000.

4. Colborne GR: Bringing canine biomechanics research out of the dark ages. Veterinary Journal 173:469-470, 2007.

5. Barone R: Anatomie Comparèe des mammifères domestiques. Tome 2: Arthrologie et myologie. Paris, 2000.

6. Aron DN, Purinton PT: Collateral ligaments of the tarsocrural joint - an anatomic and functional study. Veterinary Surgery 14:173-177, 1985.

7. Mason DR, Schulz KS, Fujita Y, et al: Measurement of humeroradial and humeroulnar transarticular joint forces in the canine elbow joint after humeral wedge and humeral slide osteotomies. Veterinary Surgery 37:63-70, 2008.

8. Preston CA, Schulz KS, Kass PH: In vitro determination of contact areas in the normal elbow joint of dogs. American Journal of Veterinary Research 61:1315-1321, 2000.

9. Coughlin KM, Peura GD, Fleming BC, et al: In vivo loads in the medial compartment of the rabbit knee. Clinical Biomechanics 20:1007-1009, 2005.

10. Giunta RE, Krimmer H, Krapohl B, et al: Patterns of subchondral bone mineralization in the wrist after midcarpal fusion. Journal of Hand Surgery-American Volume:138-147, 1999.

11. Müller-Gerbl M, Putz R, Hodapp N, et al: Computed-tomography-osteoabsorptiometry - A method of assessing the mechanical condition of major joint in a living subject. Clinical Biomechanics 5:193-198, 1990.

12. Müller-Gerbl M, Putz R, Kenn R: Demonstation of subchondral bone density patterns by three-dimensional CT osteoabsorptiometry as a noninvasive method for in vivo assessment of individual long-term stresses in joints. Journal of Bone and Mineral Research 7:411-418, 1992.

13. Eckstein F, Jacobs CR, Merz BR: Mechanobiological adaptation of subchondral bone as a function of joint incongruity and loading. Medical Engineering & Physics 19:720-728, 1997.

14. Dingemanse W, Gielen I, Duchateau L, et al: Comparison of morphological and clinical features between medial and lateral trochlear ridge talar osteochondrosis dissecans in dogs. Veterinary Surgery:340-345, 2013.

15. Ytrehus B, Carlson CS, Ekman S: Etiology and pathogenesis of osteochondrosis. Veterinary Pathology 44:429-448, 2007.

16. Dammrich K: Relationship between nutrition and bone-growth in large and giant dogs. Journal of Nutrition 121:S114-S121, 1991.

17. van Ee RT, Gibson K, Roberts ED: Osteochondritis dissecans of the lateral ridge of the talus in a dog. Journal of the American Veterinary Medical Association 193:1284-1286, 1988.

18. Dingemanse W, Gielen I, van Bree H: Diagnosis and treatment of tarsocrural osteochondrosis in the dog. Vlaams Diergeneeskundig Tijdschrift 80:223-232, 2011.

19. Kuroki K, Cook JL, Stoker AM, et al: Characterizing osteochondrosis in the dog: potential roles for matrix metalloproteinases and mechanical load in pathogenesis and disease progression. Osteoarthritis and Cartilage 13:225-234, 2005.

20. Montgomery RD, Hathcock JT, Milton JL, et al: Osteochondritis dissecans of the canine tarsal joint. Compendium on Continuing Education for the Practicing Veterinarian 16:835-845, 1994.

21. Gielen I, van Bree H, Van Ryssen B, et al: Radiographic, computed tomographic and arthroscopic findings in 23 dogs with osteochondrosis of the tarsocrural joint. Veterinary Record 150:442-447, 2002.

22. Patel BA, Carlson KJ: Habitual use of the primate forelimb is reflected in the material properties of subchondral bone in the distal radius. Journal of Anatomy:659-670, 2006.

23. Kraljevic M, Zumstein V, Hugli R, et al: A comparison of subchondral bone mineralization between the glenoid cavity and the humeral head on 57 cadaverous shoulder joints. Surgical and Radiologic Anatomy:295-300, 2013.

24. Bottcher P, Zeissler M, Grevel V, et al: Mapping Subchondral Bone Density of Selected Donor and Recipient Sites for Autologous Osteochondral Transplantation in the Canine Stifle Joint Using Computed Tomographic Osteoabsorptiometry. Veterinary Surgery 39:496-503, 2010.

25. Samii VF, Les CM, Schulz KS, et al: Computed tomographic osteoabsorptiometry of the elbow joint in clinically normal dogs. American Journal of Veterinary Research 63:1159-1166, 2002.

26. Dickomeit MJ, Bottcher P, Hecht S, et al: Topographic and age-dependent distribution of subchondral bone density in the elbow joints of clinically normal dogs. American Journal of Veterinary Research 72:491-499, 2011.

27. Madry H, van Dijk CN, Mueller-Gerbl M: The basic science of the subchondral bone. Knee Surgery Sports Traumatology Arthroscopy 18:419-433, 2010.

28. Colborne GR, Good L, Cozens LE, et al: Symmetry of hind limb mechanics in orthopedically normal trotting Labrador Retrievers. American Journal of Veterinary Research 72:336-344, 2011.

29. Colborne GR: Are sound dogs mechanically symmetric at trot? No, actually. Veterinary and Comparative Orthopaedics and Traumatology 21:294-301, 2008.

30. Ebel CMI, Prodinger PM, Muhlhofer H, et al: Morphological adaptation of the tarso-metatarsal joints onto load transmission in the foot. Surgical and Radiologic Anatomy 32:107-113, 2010.

31. Brunnberg MM, Engelke E, Gielen IM, et al: Cartilage thickness of the trochlea of the talus, with emphasis on sites predisposed to osteochondrosis dissecans, in clinically normal juvenile and adult dogs. American Journal of Veterinary Research 72:1318-1324, 2011.

32. Frost HM: A 2003 update of bone physiology and Wolff's Law for clinicians. Angle Orthodontist 74:3-15, 2004.

33. Schenck RC, Goodnight JM: Current Concept Review - Osteochondritis Dissecans. The Journal of Bone and Joint Surgery 78:439-456, 1998.

34. Athanasiou KA, Niederauer GG, Schenck RC: Biomechanical Topography of Human Ankle Cartilage. Annals of Biomedical Engineering 23:697-704, 1995. 2010.

CHAPTER SIX

Density and Strength Distribution of the Subchondral Bone Plate of the Canine Talus

W. Dingemanse [1], M. Müller-Gerbl [2], I. Jonkers [3], J. Vander Sloten [4], B. Van Ryssen [1]
H. van Bree [1], I. Gielen [1]

[1] Department of Medical Imaging of Domestic Animals and Orthopaedics of Small Animals Faculty of Veterinary Medicine, Ghent University. Merelbeke, Belgium

[2] Institute of Anatomy, Basel University. Basel, Switzerland

[3] Human Movement Biomechanics Research Group, Faculty of Kinesiology and Rehabilitation Sciences, KU Leuven. Leuven, Belgium

[4] Biomechanics Section, Faculty of Engineering Science, KU Leuven. Leuven, Belgium

Adapted from: W. Dingemanse, M. Müller-Gerbl, I. Jonkers, J. Vander Sloten, B. Van Ryssen, H. van Bree, I. Gielen. Density and strength distribution of the subchondral bone plate of the canine talus. Submitted.

ABSTRACT

Background: The subchondral bone plate plays an important role in the load transfer across joints. The subchoncdral bone density distribution is a reflection of the loading history of the joint, and the heterogeneous density distribution expected to be reflected in the subchondral bone material properties. The goal of this study was to evaluate the strength of the subchondral bone plate of the canine talus and to correlate it to the subchondral bone density.

Methods: On twenty, paired, cadaver tali of different large breed dogs, test points were defined on the subchondral bone plate. At these points the mechanical strength was determined by indentation testing, registering the maximum penetration force, and the density was measured by means of computer tomographic osteoabsorptiometry (CTOAM).

Results: Neither the density nor the strength were distributed homogeneously over the surface of the subchondral bone plate. In all specimens, a high correlation was found between the subchondral bone density and the mechanical strength. The location of the density maxima matched the location of maximal mechanical strength.

Conclusion: The use of CTOAM provides a non-invasive opportunity to not only assess the density of the subchondral bone plate but also the mechanical strength, and to perform longitudinal studies on subchondral bone density and strength in dogs.

BACKGROUND

In all vertebrates, bones provide a solid structure, a place for muscles to attach, and ensure protection of the most vital organs. Bones are also made of living cells that function like an organ, whose structure continually changes, and adapts to current needs. At the level of the joints, these needs are predominantly the transduction of (compressive) forces from the proximal to the distal bones forming a specific joint [1,2]. These forces give rise to local strains and stresses and induce modeling and remodeling of the subchondral bone, depending on whether the local strains either stay below the remodeling threshold or exceed the modeling threshold [3]. Increased joint loading leads to increased local strains and bone modeling ensures an increase in subchondral bone density to withstand the increased loading [3,4]. In addition, altered joint biomechanics lead to altered joint loading distribution, leading in turn to alterations in the subchondral bone density distribution [5,6]. It is this process of mechanotransduction, that allows us to evaluate joint loading based on the subchondral bone density.

The subchondral bone density can be evaluated non-invasively using computer tomographic osteoabsorptiometry (CTOAM) [1,6,7]. The application of CTOAM in the canine tarsocrural joint has shown a distinct pattern of subchondral bone density in the talus of healthy, adult Labrador Retrievers [7]. In dogs, the trochlear ridges are one of the predilection locations for osteochondrosis (OC) lesions, and it is likely that joint loading plays an important role in the development of these lesions [8,9]. However, little is known about the biomechanical properties of canine subchondral bone and the relation to subchondral bone density.

The aim of the present study is to evaluate the penetration strength of the subchondral bone plate of the canine talus and to compare the results to the mineral density distribution, evaluated by CTOAM.

MATERIALS AND METHODS

Specimens

Twenty paired canine cadaver tali, obtained from the Department of Morphology, Faculty of Veterinary Medicine (Ghent University, Belgium), were included in this study (Table 1). The bones originated from different large breed dogs (all > 25 kg, Table 1), to ensure a large enough testing surface for the indentation testing. All soft tissues were removed, and the bones were frozen until the day before testing. Exclusion criteria included macroscopic cartilage damage or degenerative changes, or any signs of osteoarthrosis on the CT images prior to testing.

Depending on the size of the specimen, 3 or 4 rows of test points were drawn onto the articular surface (Figure 1). Spacing was done using a calliper. All test points were kept a minimum of 7 mm apart, to avoid interference during testing. Test points were located on the medial and lateral trochlear ridge, and in the trochlea tali. In some cases, an additional fourth row was added on the sloped medial surface of the lateral trochlear ridge.

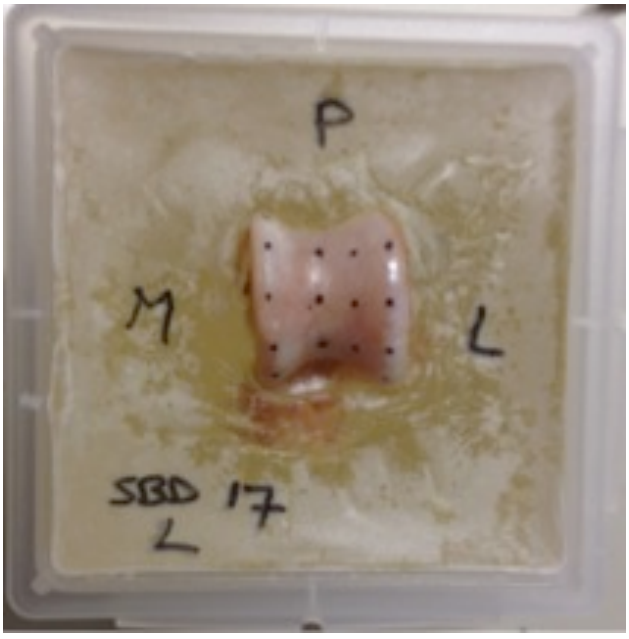

Figure 1. Specimen prepared for testing. The talus is fixed in polymethylmethacrylate (PMMA) and the testing grid is drawn onto the surface of the subcondral bone. The letters P, M, and L indicate posterior, medial and lateral respectively, to maintain an overview of the location of the different testing points.

Image acquisition and analysis

Image data was acquired using a 16-slice CT scanner (Somatom Sensation, Siemens, Erlangen, Germany). Scans were performed before and after indentation testing, to check full penetration of the subchondral bone plate and to register the exact points of indentation to compare with the CTOAM images.

The CT images were exported in DICOM format to commercially available software (Analyze 11.0, Biomedical Imaging Resource, Mayo Foundation, Rochester, MN, USA), used to complete the CTOAM workflow, which has been described in detail in previous publications [6] and in Chapter 1.

Optimal visualisation of the subchondral bone density distribution is accomplished by a view perpendicular to the test point. Therefore multiple reconstructions and matching MIPs (average n=6, range 5-8) were made in order to visualise all test points.

Indentation testing

All ligaments and other soft tissue structures were removed from the talus. The articular cartilage, covering the subchondral bone plate, was removed manually. This was done using a scalpel blade positioned almost parallel to the subchondral bone surface, taking care not to damage the subchondral bone. Prior to testing, the talus was cemented in polymethylmethacrylate (PMMA) to facilitate the positioning during testing. During testing, the PMMA blocks were fixed in a custom-made, screw-on frame, attached to a ball-joint (see Figure 2). The ball joint allowed the indentation test point to be positioned with the needle perpendicular to the surface, and the ball-joint was locked in place.

The indentation testing was performed using a materials testing machine (Figure 2) (Synergie 100, MTS systems, Eden Prairie, MN), with custom written software. This software registers the reactive force of the indentation needle in Newton (N), while a constant speed of 1 mm/sec was maintained. The steel needle (ø 2 mm) created a standardized hole at every testing point.

This resulted in a time-force curve (Figure 3) for each testing point. This curve shows the increase of resistant force measured by the testing machine until it reaches a maximum and the needle fully penetrated the subchondral bone plate (Figure 4). The maximum force (penetration force) was recorded in Newton (N) and registered into a standardized grid.

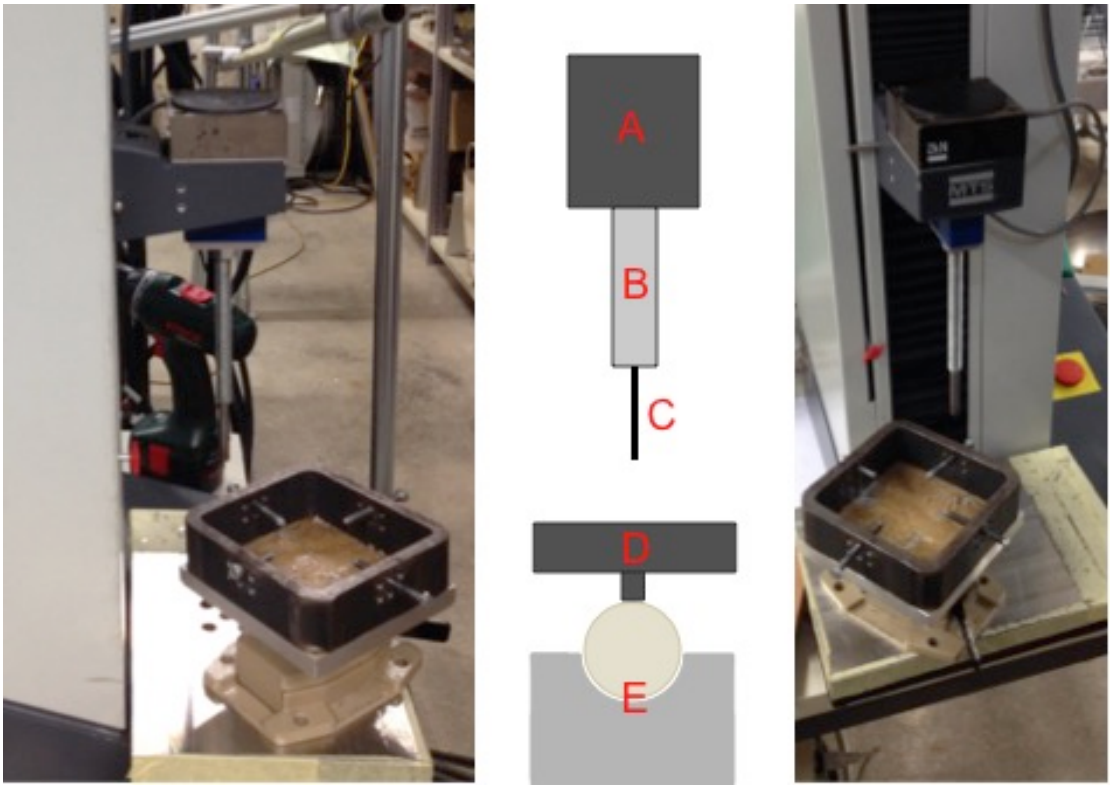

Figure 2. An overview of the materials testing machine used in this study. Left: lateral view; middle: schematic view; right: frontal view. Schematic view denotes the different parts of the testing set-up. A: Force registration module; B: Testing needle attachment; C: Testing needle; D: Positioning table for the PMMA blocks, which can be fasted with 4 screws; E: Ball-bearing joint to enable optimal positioning of the needle perpendicular to the surface of the subchondral bone plate.

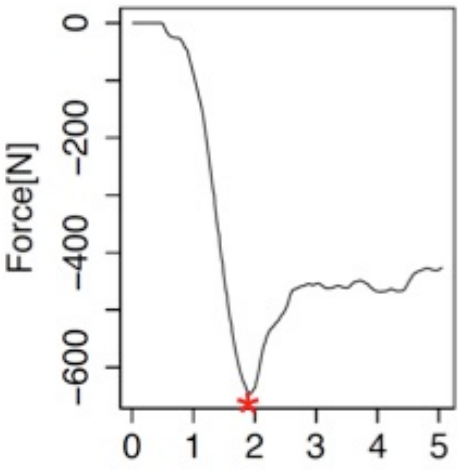

Figure 3. Force-time curve which is the result of each testing point. The curve shows an increase in resistant force (in Newton (N)), leading to a maximum (*), at which the subchondral bone plate is penetrated and the needle enters the trabecular

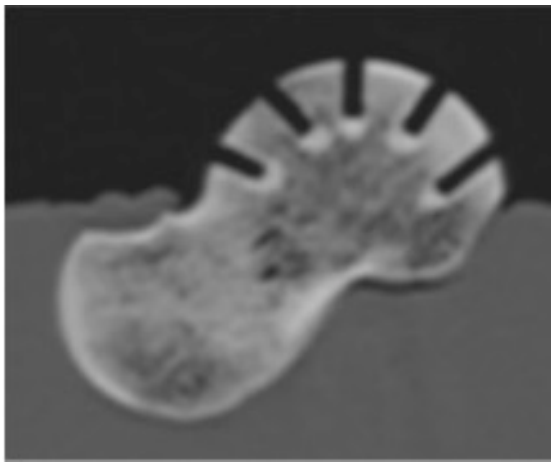

Figure 4. Sagittal reformatted CT image of a talus after testing, showing the perpendicular direction of the needle hole and full penetration of the subchondral bone plate.

Density-strength correlation

After indentation testing of the specimen a second set of CT images was made (cfr. Image acquisition and analysis) (Figure 4). For each indentation point the density was measured on the pre-testing CTOAM images, using the post-testing CTOAM images to ensure correct positioning of the region of interest (ROI).

The measured mechanical strength and subchondral bone density for all datasets were evaluated by linear regression. The Pearson product–moment correlation was determined for all the tested tali.

RESULTS

The subchondral bone density distribution was not homogeneous, and displayed one or more density maxima. The subchondral bone distribution pattern showed interindividual variation (Figure 6).

Similarly to the density distribution, the mechanical strength was also not distributed homogeneously. The pattern of the mechanical strength distribution was similar to the density distribution pattern revealed by CTOAM and also showed interindividual variation (Figure 6).

The visual comparison of the subchondral bone density distribution and strength distribution show marked similarities (Figure 6). The density maxima and maxima from the strength distribution have the same localization: there was no significant difference in the location of the density maxima and the strength maxima (p-value .512).

High correlations were found between the density values and the measured mechanical strength of all measuring point of each talus. The coefficient of determination (r^2) ranged from 0.78 to 0.96 with a mean of 0.89 and was statistically significant ($p < 0.01$) (Table 1).

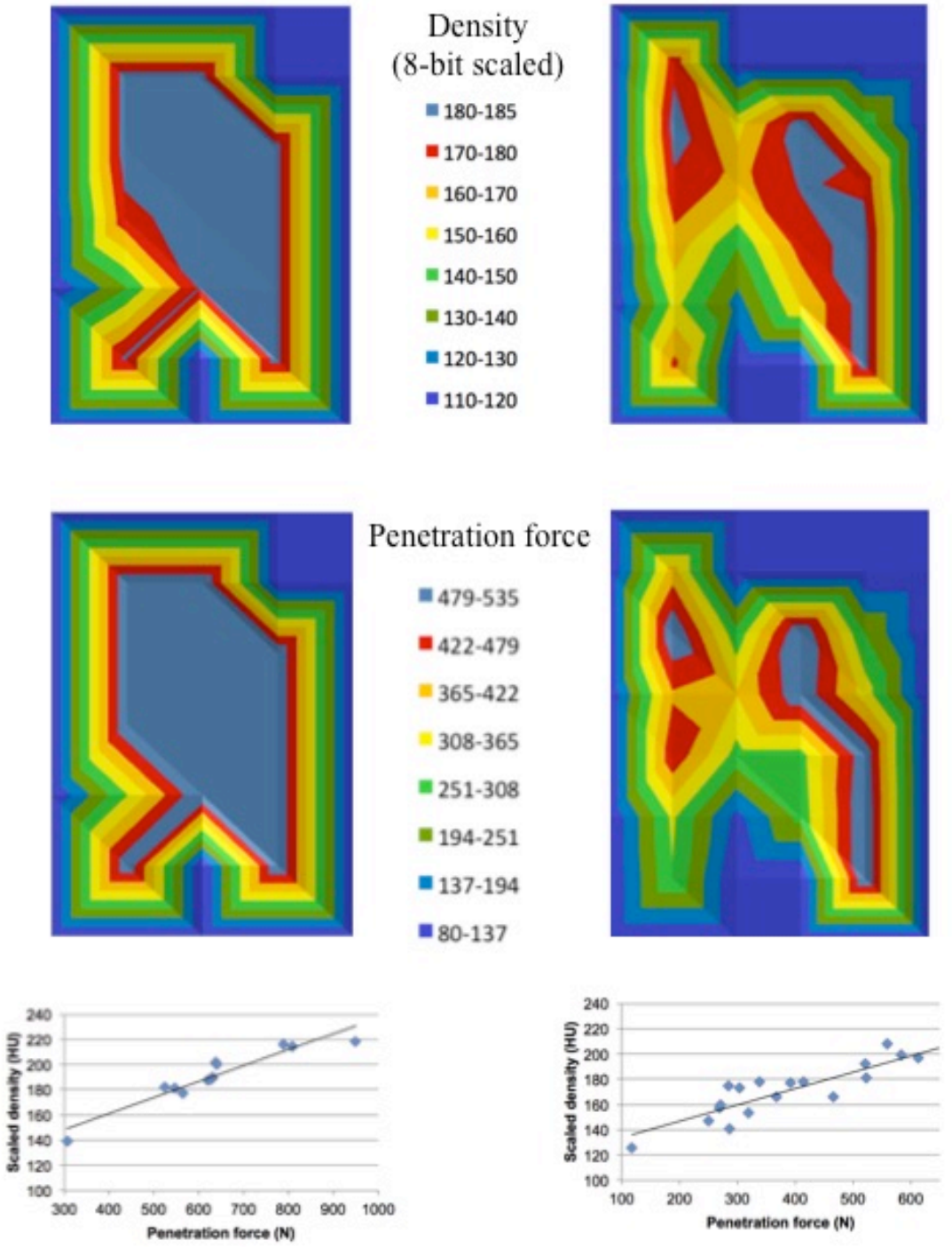

Figure 6. The results of the density and strength distribution of the talus of two different dogs (one on the right, and one on the left). Top row shows the density distribution. Middle row shows the strength distribution, which is a visual representation of the penetration force at each testing point. Bottom row shows distribution of the correlation for density values (in 8-bit scaled Hounsfield Units) and penetration force (in Newton).

Table 1. Summary of the clinical data of the specimens, including correlation results. Coefficient of determination (r^2), not available (N/A).

Specimen	Breed	Gender	Age	Side	r^2
SBD-1	German Shepherd	Male	2	Left	0.83
SBD-2				Right	0.86
SBD-3	Belgian Shepherd	Female	5	Left	0.93
SBD-4	(Mallinois)			Right	0.91
SBD-5	American Bulldog	Female	N/A	Left	0.94
SBD-6				Right	0.89
SBD-7	German Shepherd	Female	4	Left	0.96
SBD-8				Right	0.94
SBD-9	Bernese Mountain Dog	Male	6	Left	0.95
SBD-10				Right	0.91
SBD-11	Mixed breed	Male	8	Left	0.83
SBD-12				Right	0.88
SBD-13	Labrador Retriever	Female	4	Left	0.78
SBD-14				Right	0.84
SBD-15	Great Dane	Female	7	Left	0.94
SBD-16				Right	0.92
SBD-17	Poodle	Male	5	Left	0.79
SBD-18				Right	0.82
SBD-19	Mixed breed	Male	N/A	Left	0.89
SBD-20				Right	0.93

CHAPTER 6

DISCUSSION

This study evaluates the correlation between subchondral bone density and the strength of the subchondral bone plate of the canine talus. The subchondral bone density is not distributed homogeneously, but displays local variations in density and marked interindividual variation. Previous reports on subchondral bone density in dogs have reported the density distribution of the Labrador Retriever (talus) [7], or mixed breeds (the elbow joint in a sagittal plane) [10]. The interindividual variation seen in this study can be explained by the inclusion of different large breed dogs. Different breeds will most likely have differences in joint loading and the distribution of that load within the joint, leading to differences in the subchondral bone density distribution.

In humans, different patterns of subchondral bone density distribution are seen also within the same joint [11-14]. These density distributions have also been related to strength distributions in the human patella, ankle and shoulder joint [12,13,15]. A direct and high correlation between these two parameters can be seen. The results of this study show a similar correlation in dogs and CTOAM in dogs can therefore also be used to evaluate the mechanical strength of the subchondral bone plate.

The strength of the subchondral bone plate is an important functional parameter in the (patho)physiology of cartilage and subchondral bone [2,16]. In horses, material testing of the subchondral bone of the third metacarpal bone has shown significant correlations between bone mineral density, and elastic modulus and energy to failure. These parameters also varied according to anatomic location within the joint [17]. Changes in density affect these functional parameters and might play a role in the development of joint pathology such as osteoarthrosis (OA) and OC [18,19]. In the tarsocrural joint of the Labrador Retriever, the location of the density maxima is the same as the location where OC lesions are found [7]. Although there is still a lot of discussion about the exact aetiology of OC lesions, both in humans [20] and dogs [8,21,22], micro trauma or repetitive biomechanical stress is likely to play an important role [2,22,23]. These factors also influence the density of the subchondral bone plate, and

with an increase in density, the potential of regeneration and repair at the level of the subchondral bone and overlying cartilage may be impaired [24]. Although more research is necessary on the role of biomechanical loading in the development of OC lesions in dogs, current evidence supports the hypotheses on the role of joint loading in canine OC. An additional factor may be a mismatch in biomechanical characteristics of the subchondral bone and articular cartilage. Although the subchondral bone plate should be strong enough to withstand the forces during physiological joint loading, density changes may propagate (in pathological joints), or possibly even initiate (in healthy joints), different types of orthopaedic pathology including OC and OA [2].

REFERENCES

1. Eckstein F, Jacobs CR, Merz BR: Mechanobiological adaptation of subchondral bone as a function of joint incongruity and loading. Medical Engineering & Physics 19:720-728, 1997.

2. Madry H, van Dijk CN, Mueller-Gerbl M: The basic science of the subchondral bone. Knee Surgery Sports Traumatology Arthroscopy 18:419-433, 2010.

3. Frost HM: The Utah paradigm of skeletal physiology: an overview of its insights for bone, cartilage and collagenous tissue organs. Journal of Bone and Mineral Metabolism 18:305-316, 2000.

4. Burton NJ, Ellis JR, Burton KJ, et al: An ex vivo investigation of the effect of the TATE canine elbow arthroplasty system on kinematics of the elbow. Journal of Small Animal Practice 54:240-247, 2013.

5. Giunta RE, Krimmer H, Krapohl B, et al: Patterns of subchondral bone mineralization in the wrist after midcarpal fusion. Journal of Hand Surgery-American 23:138-147, 1999.

6. Müller-Gerbl M, Putz R, Hodapp N, et al: Computed-tomography-osteoabsorptiometry - A method of assessing the mechanical condition of major joint in a living subject. Clinical Biomechanics 5:193-198, 1990.

7. Dingemanse W, Muller-Gerbl M, Jonkers I, et al: Subchondral bone density distribution of the talus in clinically normal Labrador Retrievers. BMC Veterinary Research 12, 2016.

8. Dingemanse W, Gielen I, Duchateau L, et al: Comparison of morphological and clinical features between medial and lateral trochlear ridge talar osteochondrosis dissecans in dogs. Veterinary Surgery 12:340-345, 2013.

9. Gielen I, Van Ryssen B, Coopman F, et al: Comparison of subchondral lesion size between clinical and non-clinical medial trochlear ridge talar osteochondritis dissecans in dogs. Veterinary and Comparative Orthopaedics and Traumatology 20:8-11, 2007.

10. Samii VF, Les CM, Schulz KS, et al: Computed tomographic osteoabsorptiometry of the elbow joint in clinically normal dogs. American Journal of Veterinary Research 63:1159-1166, 2002.

11. Hoogbergen MM, Niessen WJ, Schuurman AH, et al: Subchondral bone mineral density patterns representing the loading history of the wrist joint. Journal of Hand Surgery-British and European Volume 27B:150-154, 2002.

12. Leumann A, Valderrabano V, Hoechel S, et al: Mineral Density and Penetration Strength of the Subchondral Bone Plate of the Talar Dome: High Correlation and Specific Distribution Patterns. Journal of Foot & Ankle Surgery 54:17-22, 2015.

13. Hoechel S, Wirz D, Muller-Gerbl M: Density and strength distribution in the human subchondral bone plate of the patella. International Orthopaedics 36:1827-1834, 2012.

14. Simon P, Gupta A, Pappou I, et al: Glenoid subchondral bone density distribution in male total shoulder arthroplasty subjects with eccentric and concentric wear. Journal of Shoulder and Elbow Surgery 24:416-424, 2015.

15. Kraljevic M, Zumstein V, Wirz D, et al: Mineralisation and mechanical strength of the glenoid cavity subchondral bone plate. International Orthopaedics 35:1813-1819, 2011.

16. Imhof H, Sulzbacher I, Grampp S, et al: Subchondral bone and cartilage disease - A rediscovered functional unit. Investigative Radiology 35:581-588, 2000.

17. Rubio-Martinez LM, Cruz AM, Gordon K, et al: Mechanical properties of subchondral bone in the distal aspect of third metacarpal bones from Thoroughbred racehorses. American Journal of Veterinary Research 69:1423-1433, 2008.

18. Kuroki K, Cook CR, Cook JL: Subchondral bone changes in three different canine models of osteoarthritis. Osteoarthritis and Cartilage 19:1142-1149, 2011.

19. Pan J, Wang B, Li W, et al: Elevated cross-talk between subchondral bone and cartilage in osteoarthritic joints. Bone 51:212-217, 2012.

20. Edmonds EW, Polousky J: A Review of Knowledge in Osteochondritis Dissecans: 123 Years of Minimal Evolution from Konig to the ROCK Study Group. Clinical Orthopaedics and Related Research 471:1118-1126, 2013.

21. Ytrehus B, Carlson CS, Ekman S: Etiology and pathogenesis of osteochondrosis. Veterinary Pathology 44:429-448, 2007.

22. Ekman S, Carlson CS: The pathophysiology of osteochondrosis. Veterinary Clinics of North America-Small Animal Practice 28:17-26, 1998.

23. Schenck RC, Goodnight JM: Current Concept Review - Osteochondritis Dissecans. The Journal of Bone and Joint Surgery 78:439-456, 1998.

24. Valderrabano V, Horisberger M, Russell I, et al: Etiology of Ankle Osteoarthritis. Clinical Orthopaedics and Related Research 467:1800-1806, 2009.

CHAPTER SEVEN

A Prospective Follow Up of Age Related Changes in the Subchondral Bone Density of the Talus of Healthy Labrador Retrievers

W. Dingemanse [1], M. Müller-Gerbl [2], I. Jonkers [3], J. Vander Sloten [4], H. van Bree [1], I. Gielen [1]

[1] Department of Medical Imaging of Domestic Animals and Orthopaedics of Small Animals. Faculty of Veterinary Medicine, Ghent University. Merelbeke, Belgium

[2] Institute of Anatomy, Basel University. Basel, Switzerland

[3] Human Movement Biomechanics Research Group, Faculty of Kinesiology and Rehabilitation Sciences, KU Leuven. Leuven, Belgium

[4] Biomechanics Section, Faculty of Engineering Science, KU Leuven. Leuven, Belgium

Adapted from:

W. Dingemanse , M. Müller-Gerbl, I. Jonkers, J. Vander Sloten, H. van Bree, I. Gielen. A prospective follow up of age related changes in the subchondral bone density of the talus of healthy Labrador Retrievers. BMC Veterinary Research 13 (2016) 57.

ABSTRACT

Background: During growth, the skeletal structures adapt to the increased loading conditions and mature to a fully-grown skeleton. Subchondral bone density reflects the effect of long-term joint loading and it is expected to change over time. The aim of this study was to describe the long-term changes in the density distribution of the subchondral bone of the talus of healthy Labrador Retrievers in a prospective study.

Methods: Healthy Labrador Retrievers (n=10) had a CT examination between 8 and 10 months of age (t_1), and between 20 and 22 months of age (t_2). Subchondral bone density distribution was evaluated using computer tomographic osteoabsorptiometry (CTOAM). The location of the density maxima was quantified using a standardised grid overlay and the size of the density maximum was expressed as the maximum area ratio (MAR).

Results: Visually, all joints showed very similar density distribution patterns. No significant differences in the topography of the density maxima were found between t_1 and t_2. The mean density, maximum density, and maximum area ratio (MAR) were significantly increased with increasing age.

Conclusions: The subchondral bone density of the talus of healthy Labrador Retrievers increases with increasing age. It is likely an adaptive response of the subchondral bone due to increased joint loading during growth.

BACKGROUND

Skeletal structures play an important role in vertebrate limb mechanics: apart from allowing locomotion, they are important for weight bearing and the associated transfer of forces through joints. In general, bones continually adapt in response to loads and these adaptive modeling and remodeling responses are guided by specific strain-related objectives [1-3]. The bone strains, induced by loads acting on the bones as a result of weight bearing and muscle action [1,4], are dedicated mechanical stimuli for bone adaptations. This adaptive process is referred to as mechano-transduction and induces geometrical adaptations of the bone as well as tissue-level adaptations [5-7]. The same principles apply to the subchondral bone, which supports the overlying joint cartilage, and transmits forces from the joint surface to the trabecular structures [8]. Although the initial skeletal anatomy is formed in utero, almost all mechanical adaptations take place after birth [4]. These adaptations are necessary for the bones to fulfill their load bearing function and to withstand the mechanical stress during locomotion [4].

At the level of the joints, it is the subchondral bone plate (SBP) that continually adapts to loading magnitude, direction and penetration depth. Indeed, the subchondral bone density in joints is highly correlated with joint loading and reflects the loading history of the joint [9-12]. Bone density can be evaluated using dual-energy x-ray absorptiometry (DEXA) or peripheral quantitative computed tomography (pQCT) [13], but they lack the regional detail required to evaluate subchondral bone density at the joint surface. Using computer tomographic osteoabsorptiometry (CTOAM), the density distribution of the subchondral bone can be visualised and evaluated in detail [9-12].

The goal of this study was to evaluate subchondral bone density, using CTOAM, in the talus of healthy Labrador Retrievers at different ages, using a longitudinal study design, in order to document the adaptation of the subchondral bone plate with increasing age. An increase in subchondral bone density with increasing age is hypothesised.

MATERIALS AND METHODS

Study population

In this study 10 healthy Labrador Retrievers were used that were included in a study on hip dysplasia and elbow dysplasia at the Faculty of Veterinary Medicine, Ghent University. The study was approved by the ethical committee of the Faculty of Veterinary Medicine, Ghent University (approval nr. EC2011/193) and verbal owner consent was obtained in each case. Inclusion criteria for this study were no abnormalities on orthopaedic examination and lameness evaluation and no abnormalities on radiographs of hips, elbows and tarsal joints. For screening of elbow dysplasia a group of Labrador Retrievers had a CT examination between 8 and 10 months of age (t_1), and between 20 and 22 months of age (t_2). After the CT examination of the elbow joint, the left and right tarsal joints were scanned as well.

Image acquisition

Under general anaesthesia, computer tomographic (CT) images were acquired from the tarsal joints using a 4 slice helical CT scanner (Lightspeed Qx/i, General Electric Medical Systems, Milwaukee, WI). The CT parameters were 120 kVp and 300 mAs. Contiguous, 1,25 mm collimated, transverse images were obtained in a soft tissue reconstruction algorithm. Dogs were positioned in ventral recumbency and left and right tarsal joints were scanned simultaneously, with the tarsal joints in extension, according to patient protocol [14]. A calibration phantom (Bone Density Calibration Phantom, QRM GmbH, Germany) was placed between the scanning table and the tarsal joints as a density reference standard. Based on the calibration phantom, the Hounsfield Units (HU) in the final measurements were converted to mg hydroxyapatite (HA)/cm^3. The use of a calibration phantom reduces the inter-scan variability [15] and can be used to convert the apparent density measures to absolute values.

Correct positioning was confirmed on the laterolateral and dorsoplantar scout view. Acquisition time was approximately five minutes, including repositioning after CT examination of the elbow joints.

Image analysis

The CT images were exported in DICOM format to commercially available software (Analyze 11.0, Biomedical Imaging Resource, Mayo Foundation, Rochester, MN, USA), used to complete the CTOAM workflow. The workflow results in an articular surface representation of the underlying subchondral bone density. The technique is described in detail in Chapter 1.

A proximal and distal view of the trochlear ridges was created (Figure 1) and for both views, the overall mean density and the maximum density were recorded at t1 and t2.

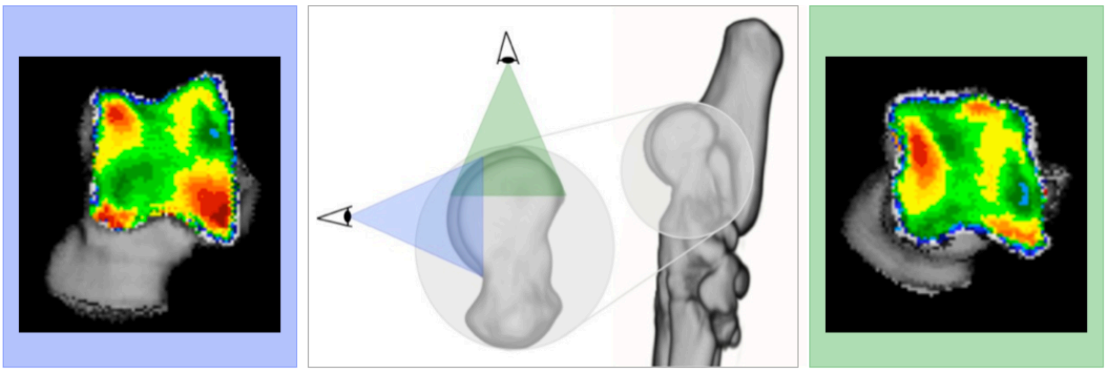

Figure 1. Three dimensional reconstruction of the tarsal and metatarsal bones of the right foot, medial view. Line of sight for the two 3D reconstructions that are reconstructed from the segmented images, proximal view (green) and dorsal view (blue). The use of these two views provides full visualisation of the trochlear ridges with the typical distribution shown for the proximal (right) and dorsal (left) view.

For quantification purposes, the density values (in HU) were converted to 8-bit values, i.e. 256 density values, which were split equally over 8 bins, according to literature [16]. Thus, each bin contains a range of 32 density values. A density maximum was defined as an area with density values in the two highest density bins of the densitogram. To quantify the density maxima, a 30 x 30 unit grid was projected onto the densitogram of the proximal and dorsal view. The grid edges were positioned to ensure that the entire joint surface could fit within. The number

of units in each grid was kept the same, to standardize the coordinates of the density maxima. The density maxima were characterized by their x- and y-coordinates (Figure 2).

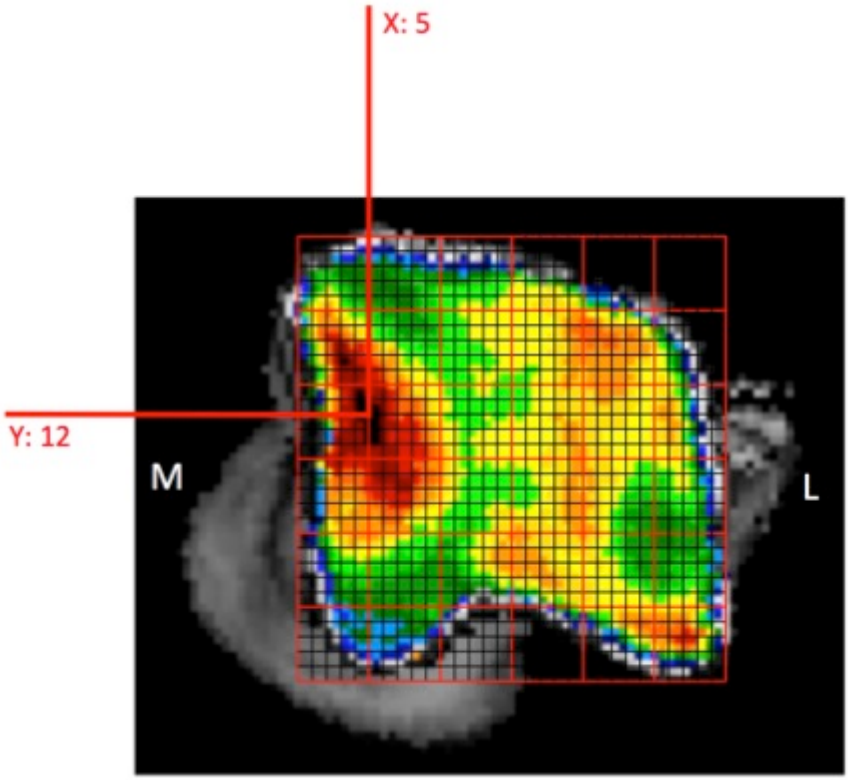

Figure 2. Positioning of the grid on a proximal view of the talus and description of the subchondral bone density maximum by x- and y-coordinates. Medial (M) and lateral (L) aspect are indicated.

In addition, the maximum was described as a ratio of the area of the density maximum and the joint surface area of the proximal or dorsal view respectively, and defined as the maximum area ratio (MAR).

$$\text{MAR} = \frac{\text{number of pixels of the density maximum}}{\text{number of pixels of the total joint surface}}$$

The use of MAR allows a relative comparison between individuals, and accounts for size-differences.

Statistics

Using commercially available software (SPSS Statistics 22), the location of the density maxima, the mean density, the maximum density, and the MAR was compared between t1 and t2. In addition mean density and maximum density were compared. Data was checked for normality with Shapiro-Wilk test and was further evaluated using a paired Student's T-test. Significance was set at $P < .05$.

RESULTS

1. Study population

Ten Labrador Retrievers had a CT scan at two different time points. Six were male, 4 were female, age at t1 was 8.7 (SD 0.8, range 8-10) months, age at t2 was 20.8 (SD 0.75, range 19-22) months and time between scans was 12.1 (1.0) months, mean weight increase was 21% (range 17-28%).

2. Qualitative interpretation of the subchondral bone density distribution

Based on the false colour scale, the overall density increased between t1 and t2 over the entire joint contact area. The density maximum on the medial trochlear ridge was located proximally, whereas the maximum on the lateral trochlear ridge was located more distally (Figure 3). The distribution pattern remained unchanged with increasing age.

3. Quantitative comparison of the subchondral bone density distribution

The overall mean density was significantly higher at t2 compared to t1 on both the proximal and the dorsal view. The maximum density was also significantly higher at t2 compared to t1 on both the proximal and the dorsal view (Table 1). There was no significant difference in the location of the density maxima (x- and y-coordinates) between t1 and t2 on the proximal (p-value .752) and dorsal view (p-value .111) (Figure 4). The MAR increased significantly with age, for both the proximal and dorsal view (Table 1).

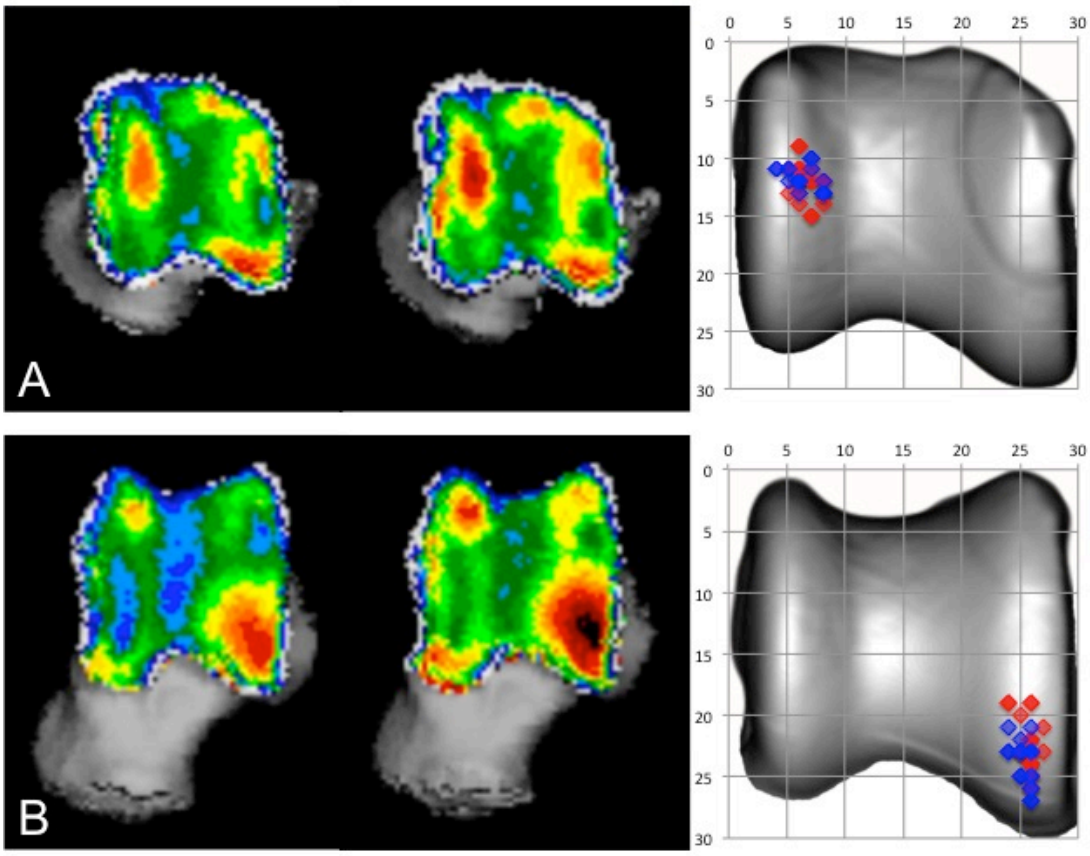

Figure 4. Summation picture of the location of the subchondral bone density maximum on a proximal (A) and dorsal (B) view of the talus. Values at t1 are displayed in blue, values at t2 are displayed in red.

Table 1. Results summary.

		t_1	t_2	p-value
Overall density	Proximal view	664.5 (51.1)	736.0 (46.3)	.001
(mg HA/cm^3)	Dorsal view	696.1 (47.3)	761.5 (36.9)	.001
Maximum density	Proximal view	1049.5 (68.7)	1122.2 (77.9)	.01
(mg HA/cm^3)	Dorsal view	1094.2 (78.0)	1186.6 (78.0)	.01
MAR	Proximal view	12.0 (5.2)	19.0 (6.6)	.002
	Dorsal view	18.9 (5.7)	26.8 (3.9)	.000

Overall density (in mg hydroxyapatite/cm^3), maximum density and maximum area ratio (MAR) for both time points (t_1 and t_2). Values displayed as mean (SD).

DISCUSSION

For the first time in bone density research in dogs, CTOAM data from a longitudinal study, using follow-up of the same individuals is presented. Other studies have used cross-sectional study designs with the classification of the study population into age groups [17], with a comparison between three different groups and an age range from 2 months to 17 years. Although in this study only 2 groups are compared and the age ranges from 8 to 22 months, the authors feel these data provide a valuable addition to the field of veterinary orthopaedic research, because of the longitudinal study design. In this study, 10 Labrador Retrievers had a CT scan of the tarsal joint at two different time points (8-10 months and 20-22 months) and subsequent evaluation of the subchondral bone density of the talus, using CTOAM. The use of a calibration phantom with known densities allowed a comparison of different scans with minimal inter-scan variability. In addition, absolute density values could be calculated, facilitating future comparisons in subchondral bone density research.

The subchondral bone adapts to loading conditions and undergoes important remodeling during skeletal maturation [4,13,18]. The age range in this study is the range in which the dogs still grow. Mean weight increase in this study was 21%, and significant changes in subchondral bone density can be expected.

For all dogs, there was an increase in overall density and maximum density of the subchondral bone between t1 and t2. An increase in loading will cause an increase in subchondral bone density, which is commonly seen during growth or increased exercise [1,4]. The mechano-biological adaptations are a life-long process. For instance in dogs, the bone mineral content of femurs increases, with increasing age [13]. A similar process is likely to take place in all load-bearing bones, including the subchondral bone underlying the joint surface. The increased density is most likely due to increased loading of the limbs due to an increase in body weight and an increase in physical activity. The dogs used in this study were guide dogs in training, and the level and amount of training increases towards the end of their training period.

In humans, an increased adaptive response in bones is seen in the peripubertal years and is linked to the number and functional competence of estrogen receptor α in bones [19,20]. This age-dependent response to bone strain may also be present in dogs. In growing horses, the mineral density of the bone matrix increased with age. These changes can be purely age-related, i.e. maturation of the bone matrix, or linked to weight gain (21% in this study). It was noted that these effects could not be evaluated separately due to the non-linear character of the growth curve in a growing individual [18]. The same applies to our results and the increase in subchondral bone density is most likely due to a combined effect of increased loading and bone maturation. The adaptive response to bone strains by osteoblasts has different pathways which have been described in detail elsewhere [21].

Interestingly, the location of the density maxima did not differ significantly between t_1 and t_2. This implies that the loading pattern, i.e. the distribution of the load over the articular surface and the cartilage-subchondral bone interface, remains similar during growth. The major adaptations in density distribution itself take place in the early post-natal months [4,18]. So, the joint loading distribution at 8 months of age is very similar to the final joint loading distribution at 20 months.

The alterations described in this study will likely be a response to an increase in loads. This increase in load also explains the increased MAR, as the area of maximum density increases to accommodate the increasing biomechanical needs of the subchondral bone plate. The use of a ratio (MAR) allowed controlling for differences in size. These differences can be caused by absolute size differences (i.e. larger or smaller talus), although in this study this effect will be very minimal since all dogs were Labrador Retrievers of approximately the same size, weight and age. The second reason is differences in the size of the field of view (FOV). The FOV was always 512x512, so pixel size depends on the size of the scanned object and FOV for the scan. Again, the effect will be minimal due to a standardised position of the joint, and minimal size differences between the dogs used in this study.

Of course, the statements above are only true in healthy individuals without orthopaedic disease, as orthopaedic pathology can alter joint loading distribution and thus alter the subchondral bone density distribution [8,10]. Indeed, altered joint biomechanics can also lead to orthopaedic disease, e.g. the development of osteochondrosis (OC). It is important to remember that changes in loading and biomechanical properties of bones, play a key-role in the development and progression of orthopaedic disease [22].

A possible drawback of using CTOAM for the evaluation of subchondral bone density is the representation of a 3D volume (voxels of the subchondral bone plate) in a 2D densitogram. Data from dogs younger than 8 months old, might provide additional information on the development of the subchondral bone density distribution pattern. However, this was not possible in the current study.

CONCLUSION

This study reports on the evolution of the subchondral bone density distribution of the talus in healthy Labrador Retrievers during an important phase of skeletal maturation. Based on current findings, the physiological joint loading distribution does not change significantly during this period, but the subchondral bone density increased, at least for most part, in response to increased joint loading, consistent with increased weight. The morphological and pathological consequences of a non-physiological joint loading distribution remain subject to further research. The strength of CTOAM is that is allows the evaluation of temporal changes and the morphological consequences of (altered) joint loading and changes over time. This makes CTOAM a valuable addition to veterinary orthopaedic research.

REFERENCES

1. Lanyon LE: Control of Bone Architecture by Functional Load Bearing. Journal of Bone and Mineral Research 7:S369-S375, 1992.

2. Boskey AL, Coleman R: Aging and Bone. Journal of Dental Research 89:1333-1348, 2010.

3. Lanyon LE, Goodship AE, Pye CJ, et al: Mechanically Adaptive Bone Remodeling. Journal of Biomechanics 15:141-154, 1982.

4. Frost HM: A 2003 update of bone physiology and Wolff's Law for clinicians. Angle Orthodontist 74:3-15, 2004.

5. Gefen A, Seliktar R: Comparison of the trabecular architecture and the isostatic stress flow in the human calcaneus. Medical Engineering & Physics 26:119-129, 2004.

6. Main RP, Biewener AA: In vivo bone strain and ontogenetic growth patterns in relation to life-history strategies and performance in two vertebrate taxa: Goats and emu. Physiological and Biochemical Zoology 79:57-72, 2006.

7. Polk JD, Blumenfeld J, Ahluwalia D: Knee posture predicted from subchondral apparent density in the distal femur: An experimental validation. Anatomical Record-Advances in Integrative Anatomy and Evolutionary Biology 291:293-302, 2008.

8. Madry H, van Dijk CN, Mueller-Gerbl M: The basic science of the subchondral bone. Knee Surgery Sports Traumatology Arthroscopy 18:419-433, 2010.

9. Frost HM: The Utah paradigm of skeletal physiology: an overview of its insights for bone, cartilage and collagenous tissue organs. Journal of Bone and Mineral Metabolism 18:305-316, 2000.

10. Müller-Gerbl M, Putz R, Hodapp N, et al: Computed-tomography-osteoabsorptiometry - A method of assessing the mechanical condition of major joint in a living subject. Clinical Biomechanics 5:193-198, 1990.

11. Müller-Gerbl M, Putz R, Kenn R: Demonstation of subchondral bone density patterns by three-dimensional CT osteoabsorptiometry as a noninvasive method for in vivo assessment of individual long-term stresses in joints. Journal of Bone and Mineral Research 7:411-418, 1992.

12. Eckstein F, Jacobs CR, Merz BR: Mechanobiological adaptation of subchondral bone as a function of joint incongruity and loading. Medical Engineering & Physics 19:720-728, 1997.

13. Schneider S, Breit SM, Grampp S, et al: Comparative assessment of bone mineral measurements obtained by use of dual-energy x-ray absorptiometry, peripheral quantitative computed tomography, and chemical-physical analyses in femurs of juvenile and adult dogs. American Journal of Veterinary Research 65:891-900, 2004.

14. Gielen I, van Bree H, Van Ryssen B, et al: Radiographic, computed tomographic and arthroscopic findings in 23 dogs with osteochondrosis of the tarsocrural joint. Veterinary Record 150:442-447, 2002.

15. Cann CE: Quantitative Ct for Determination of Bone-Mineral Density - a Review. Radiology 166:509-522, 1988.

16. Patel BA, Carlson KJ: Habitual use of the primate forelimb is reflected in the material properties of subchondral bone in the distal radius. Journal of Anatomy:659-670, 2006.

17. Dickomeit MJ, Bottcher P, Hecht S, et al: Topographic and age-dependent distribution of subchondral bone density in the elbow joints of clinically normal dogs. American Journal of Veterinary Research 72:491-499, 2011.

18. Holopainen JT, Brama PAJ, Halmesmaki E, et al: Changes in subchondral bone mineral density and collagen matrix organization in growing horses. Bone 43:1108-1114, 2008.

19. Bass SL, Saxon L, Daly RM, et al: The effect of mechanical loading on the size and shape of bone in pre-, peri-, and postpubertal girls: A study in tennis players. Journal of Bone and Mineral Research 17:2274-2280, 2002.

20. Lee KCL, Lanyon LE: Mechanical loading influences bone mass through estrogen receptor alpha. Exercise and Sport Sciences Reviews 32:64-68, 2004.

21. Ehrlich PJ, Lanyon LE: Mechanical strain and bone cell function: A review. Osteoporosis International 13:688-700, 2002.

22. Colborne GR: Bringing canine biomechanics research out of the dark ages. Veterinary Journal 173:469-470, 2007.

CHAPTER EIGHT

Subchondral Bone Density Changes of the Talus in Dogs with Tarsocrural Osteochondrosis

W. Dingemanse [1], M. Müller-Gerbl [2], C. Crijns [3], I. Jonkers [4], J. Vander Sloten [5], B. Van Ryssen [1], H. van Bree [1], I. Gielen [1]

[1] Department of Medical Imaging of Domestic Animals and Orthopaedics of Small Animals Faculty of Veterinary Medicine, Ghent University. Merelbeke, Belgium

[2] Institute of Anatomy, Basel University. Basel, Switzerland

[3] Dierenartsenpraktijk Bodegraven B.V., Bodegraven, the Netherlands

[4] Human Movement Biomechanics Research Group, Faculty of Kinesiology and Rehabilitation Sciences, KU Leuven. Leuven, Belgium

[5] Biomechanics Section, Faculty of Engineering Science, KU Leuven. Leuven, Belgium

Adapted from: W. Dingemanse, M. Müller-Gerbl, C. Crijns, I. Jonkers, J. Vander Sloten, B. Van Ryssen, H. van Bree, I. Gielen. Subchondral bone density changes of the talus in dogs with tarsocrural osteochondrosis. In preparation.

ABSTRACT

Background: Osteochondrosis is an orthopaedic condition that occurs in specific areas within a joint. Damage to the cartilage canals, leading to avascular necroses has been hypothesised to be the initiating step, eventually leading to a subchondral bone defect and cartilage flap or loose fragment (osteochondrosis dissecans).
The aim of this study was to describe the changes in the density distribution of the subchondral bone of the talus of Labrador Retrievers with tarsocrural osteochondrosis in a retrospective study.

Methods: In this retrospective study, dogs with MTRT-OC (n=8) or LTRT-OC (n=3) and a CT examination at time of diagnosis were included. Subchondral bone density distribution was evaluated using computer tomographic osteoabsorptiometry (CTOAM).

Results: All MTRT-OC lesions were hypodens, with a high-density rim surrounding it. The contralateral joint displayed a significantly higher mean apparent density compared to the affected joint. The LTRT-OC lesions showed a different density distribution, with a low-density rim, and a normal to high density in the central part of the lesion.

Conclusions: The subchondral bone density of the talus of Labrador Retrievers with tarsocrural osteochondrosis shows severe changes in both the ipsi- and contra-lateral joint. The changes in the contra-lateral joint are likely an adaptive response to the weightshift associated with lameness. The differences observed between MTRT-OC and LTRT-OC lesions support previous suggestions on a different aetiology for both lesions.

BACKGROUND

Pathophysiology of osteochondrosis

The disruption of the complex process of enchondral ossification is generally accepted as the main pathogenesis of canine osteochondrosis (OC) [1-3]. This failure in the ossification process is focal and a specific area of growth cartilage is not converted to bone, due to failure of matrix calcification and vascular invasion [4]. More specifically, the primary event is most likely a local disruption of the epiphyseal cartilage canals during growth, leading to ischemic necrosis of the growth cartilage [3]. These cartilage canals harbour microscopic vessels that invade the epiphyseal growth cartilage. Cartilage canals regress naturally during growth, a process called chondrification, as the growth cartilage is replaced with bone [3,5].

Joint loading and the associated tensile and compressive stresses play an important role in subchondral bone physiology and pathology in general [6,7]. The morphological characteristics of canine osteochondrosis lesions, with their location being constant within a joint, has led to the hypothesis that joint loading plays an important role in the development of canine osteochondrosis. Similar to humans, a mismatch in biomechanical properties can be the start of a cascade leading to the development of osteochondrosis lesions [8,9]. In pigs it has been found that the location of cartilage canal necrosis is at the cartilage-bone interface. This region that is most likely to suffer from differences in biomechanical properties, and this might lead to damage to the cartilage canal and cartilage canal necrosis [5,10]. The damage of cartilage canals due to micro trauma also explains the site specificity of osteochondrosis lesions, as areas that undergo higher loads are more likely to suffer from micro trauma [3].

The exact role of diet, genetics and biomechanics in the development of OC lesions is still under debate, although the consensus is that OC is a multifactorial condition [3,11]. The disruption of the enchondral ossification process leads to thickening of the articular cartilage, making it more prone to damage due to biomechanical stress. This can cause fissures, leading to a cartilage flap or a loose fragment (joint mouse) [1]. In this stage, the condition is called osteochondrosis dissecans (OCD) [4].

Joint loading and subchondral bone density

The evaluation of actual joint loading is very difficult *in vivo*, since it requires the use of intra-articular pressure films [12]. Invasive (*in vitro*) methods to study joint loading include the description of pressure distribution and contact areas on cadavers [13,14]. However, these techniques require a certain degree of dissection, which will ultimately alter the joint kinematics. As demonstrated in humans, the subchondral bone density distribution is highly correlated with joint loading and reflects the loading history of the joint [15-17]. The density at any given time is the result of the bone functional adaptation, mentioned above, and provides an opportunity for non-invasive research of joint loading [15,18]. The subchondral bone density distribution can be visualized and quantified using computer tomographic osteoabsorptiometry (CTOAM) [16,17,19].

The biomechanical properties of the underlying subchondral bone are characterized by mineral density, collagen content, and ash fraction [20]. These biomechanical properties can change through modeling and remodeling of the articulating bones, guided by local strains [21,22]. These strains result from the biomechanical loading conditions the joint is subjected to. This ability to adapt is summarized in the term 'bone functional adaptation'. Although bone mineral density is an important aspect of the subchondral bone biomechanical properties, little is known about subchondral bone density in dogs. In the elbow joint, both the normal and age-related changes of subchondral bone density distribution have been described [23,24]. More recently the normal and age-related subchondral bone changes in the talus of healthy Labrador Retrievers were reported [19].

The evaluation of the subchondral bone density distribution can be used to study joint loading *in vivo*, and non-invasively. The available data in literature allows the evaluation of pathological subchondral bone changes, and the comparison to normal, healthy joint. The aim of this study was to describe the subchondral bone density changes in Labrador Retrievers with tarsocrural osteochondrosis.

MATERIALS AND METHODS

Study population

In this retrospective study 8 Labrador Retrievers were included that were diagnosed with unilateral tarsocrural osteochondrosis of the medial trochlear ridge (MTRT-OC) at the Faculty of Veterinary Medicine, Ghent University. Inclusion criteria for this study were complete orthopaedic examination and a computer tomographic (CT) examination of both tarsal joints.

For two dogs, a follow-up CT was available at 11 and 14 months after arthroscopic treatment of the lesion. These data are also included in the study, as they provided the opportunity to evaluate of density distribution changes after arthroscopic treatment of tarsocrural OC lesions.

Image acquisition

All CT examinations were done under general anaesthesia, and CT images were acquired from the tarsal joints using a 4 slice helical CT scanner (Lightspeed Qx/i, General Electric Medical Systems, Milwaukee, WI). The CT parameters were 120 kVp and 300 mAs. Contiguous, 1,25 mm collimated, transverse images were obtained in both a bone and a soft tissue reconstruction algorithm.

Dogs were positioned in ventral recumbency and left and right tarsal joints were scanned simultaneously, with the tarsal joints in extension, according to patient protocol and previous publications [19,25]. Correct positioning was confirmed on the laterolateral and dorsoplantar scout view. Acquisition time was approximately five minutes, including positioning. A calibration phantom (Bone Density Calibration Phantom, QRM GmbH, Germany) was placed between the scanning table and the tarsal joints as a density reference standard. Based on the calibration phantom, the Hounsfield Units (HU) in the final measurements were converted to mg hydroxyapatite (HA)/cm^3. The use of a calibration phantom reduces the inter-scan variability [26] and can be used to convert the apparent density measures to absolute values.

Image analysis

The CT images were exported in DICOM format to commercially available software (Analyze 11.0, Biomedical Imaging Resource, Mayo Foundation, Rochester, MN, USA), used to complete the CTOAM workflow (Figure 2). The workflow results in an articular surface representation of the underlying subchondral bone density, and has been described in detail in Chapter 1.

This resulted in two visual representations (Figure 2) of the density distribution (densitogram) of each joint, which was further evaluated. For both views, the overall mean density and the maximum density were recorded.

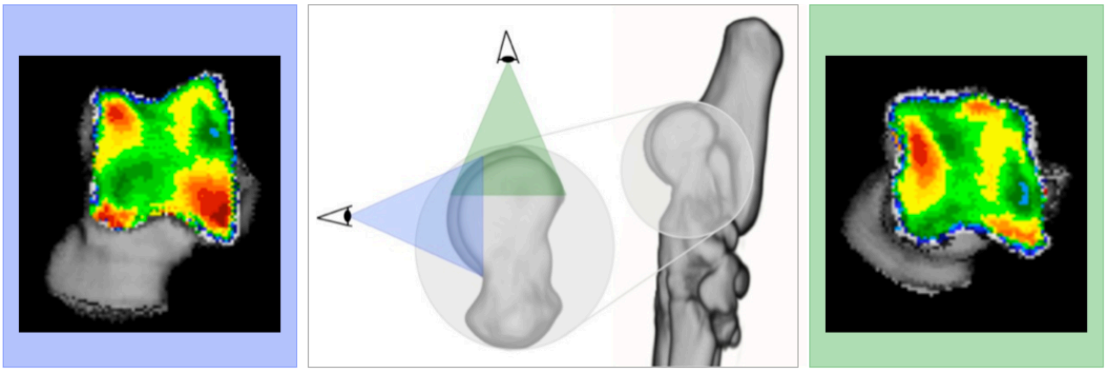

Figure 2. Three dimensional reconstruction of the tarsal and metatarsal bones of the right foot, medial view. Line of sight for the two 3D reconstructions that are reconstructed from the segmented images, proximal view (green) and dorsal view (blue). The use of these two views provides full visualisation of the trochlear ridges with the typical distribution shown for the proximal (right) and dorsal (left) view.

It is likely that joint loading, and thus the subchondral bone density distribution, in the contralateral joint is also changed, even though the OC lesion is unilateral. Therefore two densitograms were made for each joint, of both the affected and the contralateral joint.

For the dogs with follow-up CT studies, the mean density and maximum density were compared on both the affected and contralateral joint at both time points.

Statistics

Using commercially available software (SPSS Statistics 22), the mean density and maximum density, was compared between the affected and contralateral joint. Data was checked for normality with Shapiro-Wilk test and was further evaluated using a paired Student's T-test. Significance was set at $P < .05$.

RESULTS

1. Study population

Eleven dogs had a CT scan at the time of diagnosis. Age at the time of diagnosis ranged from 8 to 21 months (mean 13 months). There were 7 male dogs and 4 females. Eight dogs were diagnosed with MTRT-OC and three with LTRT-OC. For two dogs with MTRT-OC a follow-up CT was available at 11 and 14 months after arthroscopic treatment of the lesion (for reasons unrelated to this study). These data are also included in the study, as they provided the opportunity to evaluate the density distribution changes after arthroscopic treatment of tarsocrural OC lesions.

2. Subchondral bone density distribution in the affected joint

For the dogs with MTRT-OC, all affected joints showed a lower density at the location of the OC lesion at the level of the medial trochlear ridge. This area of lower density is surrounded by a ring of increased density (Figure 3). Because the lesions are located on the proximal aspect of the medial trochlear ridge, they are best visualized on the proximal view. The mean and maximal subchondral bone density was significantly lower, compared to the contra-lateral joint (p-value of 0.01) (Table 1).

In dogs with LTRT-OC, the densitogram looked very different compared to dogs with MTRT-OC. The lesions were large, and the periphery of the lesions was a ring of very low density, with an area of normal to high density in the central part of the lesion (Figure 4 and 5). In one dog, an area of increased density was seen immediately medial to the lesion, in the trochlea of the talus (Figure 5).

As displayed in Table 2, the density of the lesions differed significantly to the average normal density of that area, based on healthy reference joints. This diference was more pronounced in dogs with MTRT-OC, in line with the visual differences described above.

Table 1. Results summary overall density.

		Affected	Contralateral	p-value
Mean density	Proximal view	729.2 (67.4)	819.4 (56.9)	.001
(mg HA/cm^3)	Dorsal view	757.4 (51.1)	911.8 (44.7)	.001
Maximum density	Proximal view	1112.3 (73.2)	1154. (61.5)	.01
(mg HA/cm^3)	Dorsal view	1161.8 (67.4)	1205.2 (57.6)	.01

Mean density (in mg hydroxyapatite/cm^3). Values displayed as mean (SD).

Table 2. Results summary lesion density.

		Lesion	Normal (healthy reference)	p-value
Mean density	MTRT-OC	612.6 (88.4)	780.7 (39.8)	.00
(mg HA/cm^3)	LTRT-OC	703.8 (112.7)	745.2 (88.4)	.01

Mean density (in mg hydroxyapatite/cm^3). Values displayed as mean (SD).

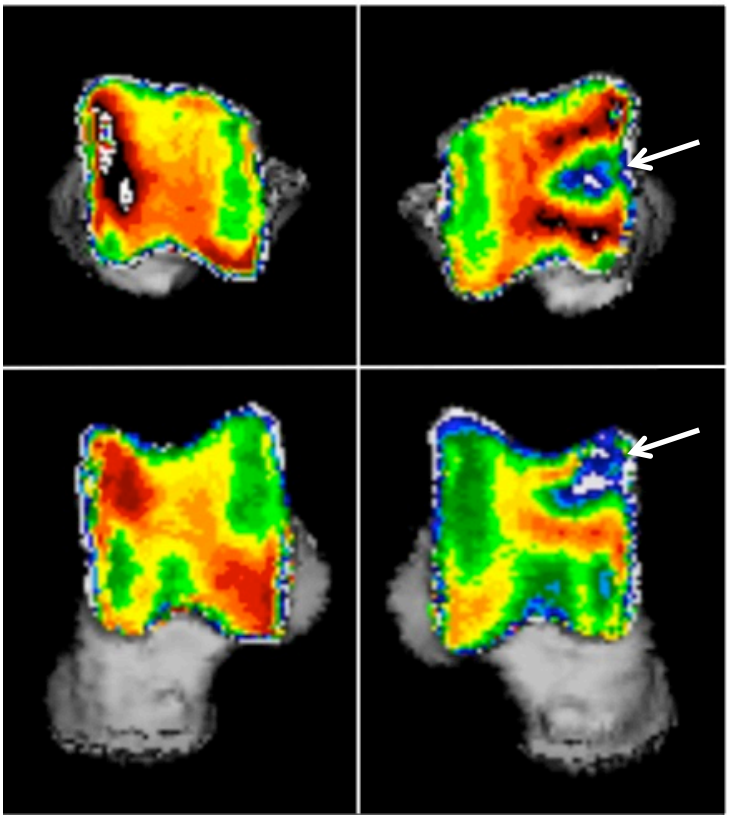

Figure 3. Densitograms of the right and left talus of a Labrador Retriever with MTRT-OC on the left side. Note the appearance of the OC lesion and the overall difference in density between the affected and the contralateral joint.

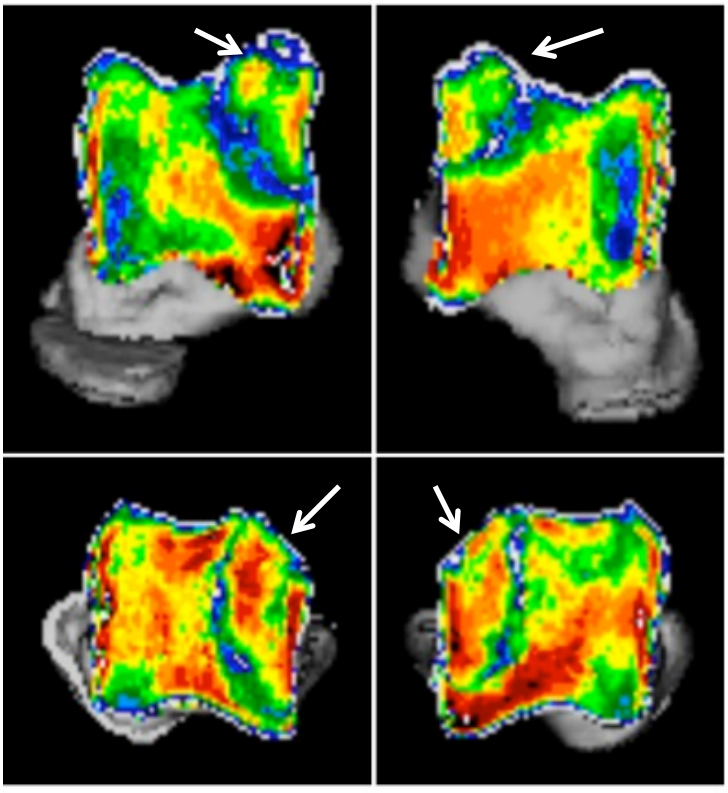

Figure 4. Densitograms of the right and left talus of an Alaskan Malamute with bilateral LTRT-OC lesions. Note the appearance of the OC lesion and the difference with the MTRT-OC lesion in Figure 3.

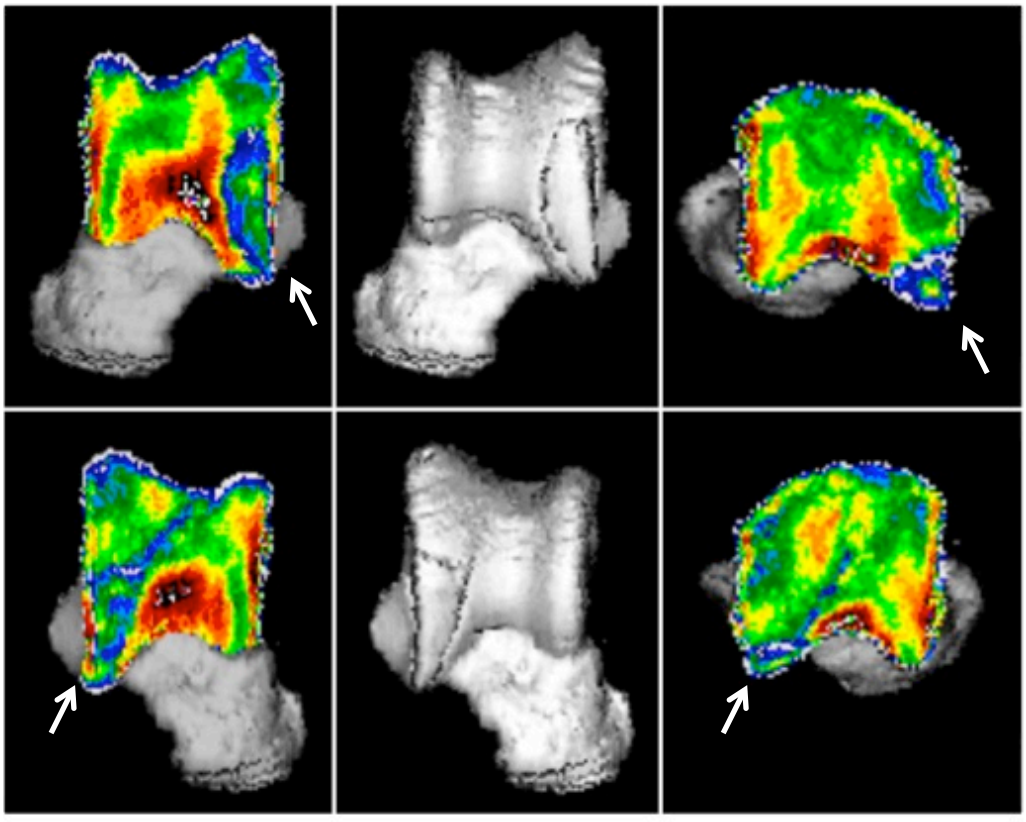

Figure 5. Densitograms of the right and left talus of a mixed breed dog with bilateral LTRT-OC lesions. Note the difference in location of the lesion in comparison with Figure 4.

3. Subchondral bone density distribution in the contra-lateral joint

For the Labradors with MTRT-OC, the overall density distribution shows two density maxima at the level of the proximal medial trochlear ridge and distal lateral trochlear ridge respectively. The mean subchondral bone density was significantly higher, compared to the affected joint (p-value of 0.01).

The dogs with LTRT-OC lesions all had bilateral lesions, so differences in both density distribution and maximum density values could not be evaluated.

4. Subchondral bone density distribution after arthroscopic treatment

The subchondral bone density distribution showed differences between the two time points. At the level of the subchondral bone defect, the difference between the low-density defect and the high-density area surrounding the defect, decreased. One

dog showed a decrease in mean subchondral bone density in the affected joint (Figure 6), while the other dog showed an increase. In both dogs, the contralateral limb showed an increase in mean and maximum density (Figure 7).

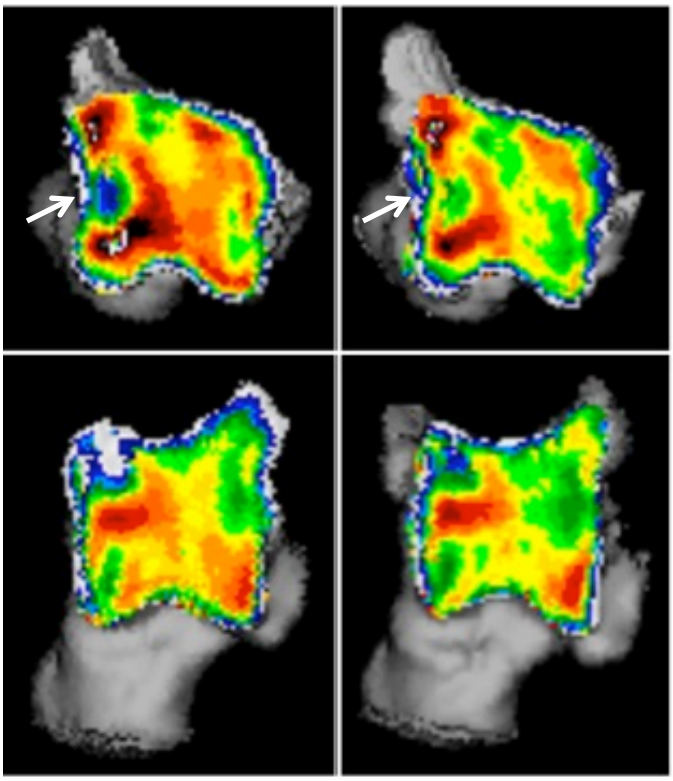

Figure 6. Densitogram of the talus of a Labrador with MTRT-OC. On the left the subchondral bone density distribution at the time of diagnosis, on the right 14 months post-operatively.

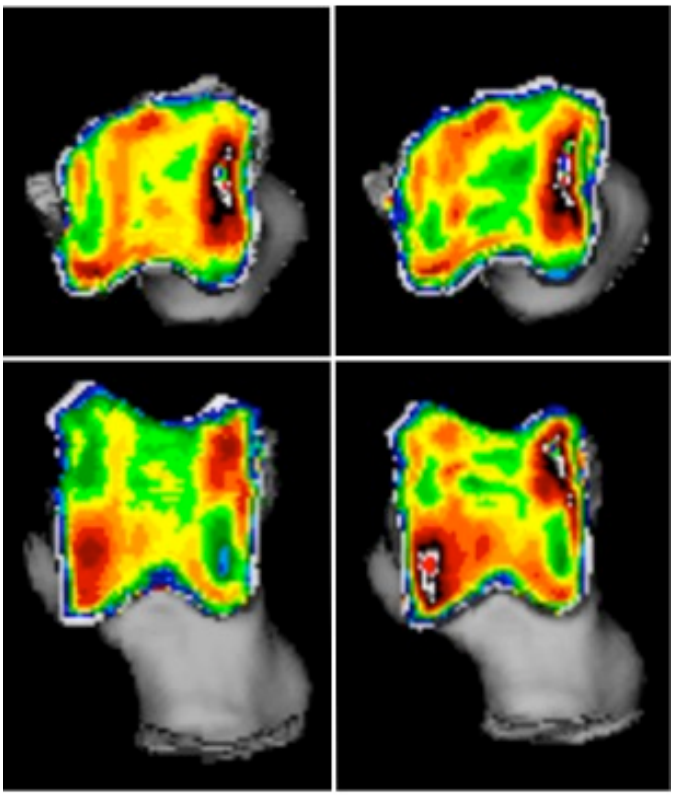

Figure 7. Densitogram of the contralateral talus of a Labrador with MTRT-OC. On the left the subchondral bone density distribution at the time of diagnosis, on the right 14 months post-operatively.

DISCUSSION

In this study, CTOAM is used to evaluate the subchondral bone density distribution in dogs with tarsocrural osteochondrosis. A total of 11 dogs were included in this study with an age range of 8 to 21 months of age.

In dogs with MTRT-OC a region with a low apparent density, surrounded by a high-density area was the common finding in all affected joints. Osteochondrosis is characterized by a subchondral bone defect, that is visible in severe cases even on radiography [25,27], which is consistent with the findings of this study. Similarly, *in vitro* experiments in bovine knees have shown a rim shaped contact area that increases with increasing defect size [28].

In dogs with LTRT-OC, the density distribution at the level of the lesion was different compared to MTRT-OC lesions. The periphery of the lesion showed a very low density, whilst the central part of the lesion showed an average to high density. A high-density area was found adjacent to the lesion, medially at the level of the trochlea talus.

The different densitograms of MTRT-OC and LTRT-OC lesions support previous suggestions of a different etiology for both lesions [29]. The appearance of LTRT-OC lesions is more a transchondral fracture of a part of the lateral trochlear ridge, whilst the MTRT-OC lesions show an actual subchondral bone defect. In humans both osteochondrosis lesions and transchondral fractures are subsets of osteochondral lesions of the talus (OLT) [30,31]. A similar categorisation of joint pathology may be appropriate in dogs as well. However, more research into the exact mechanism of pathology or injury for these type of lesions is necessary before such categories can be applied.

Interestingly, changes in the subchondral bone density distribution are not limited to the affected joint. In the contralateral tarsocrural joint of dogs with MTRT-OC, the maximum density and mean density increased and was significantly higher than the

affected joint. Tarsocrural osteochondrosis causes lameness located in the hind limbs, and thus alters joint kinematics and joint loading. Changes in the joint loading conditions cause adaptation of the subchondral bone through modeling and remodeling [15,32].

In general lameness is characterised by a shorter stance phase of the affected limb, and thus a longer stance phase and increased loading of the contralateral leg. Although these 'mechanics' of lameness are common knowledge, these data show the morphological consequences at the level of the subchondral bone plate. These alterations in the contralateral joint were less obvious in dogs with LTRT-OC. A possible explanation is that dogs with LTRT-OC usually have a shorter duration of lameness at the time of diagnosis [29], and altered joint kinematics have not yet influenced the subchondral bone density. Additionally, the lesions were bilateral, masking the lameness effect.

The exact time frame of subchondral bone density adaptations due to changed joint kinematics in dogs remains subject to further research, as it is currently unknown how quickly subchondral bone adaptations become visible after altered joint loading.

Although the high-density area, in the follow-up scans of MTRT-OC lesions, surrounding the OC lesion was slightly decreased in density in the follow-up scans, the high-density area still remains. An increased density may influence the regeneration potential at the level of the subchondral bone and articular cartilage, as it prevents the invasion of mesenchymal stem cells, and likely has a negative influence on the repair process [13,28]. The effect of subchondral bone density changes on the improvement of clinical signs and the progression of secondary osteoarthrosis is subject to further research. In the contra-lateral limb, a high-density area at the proximal aspect of the lateral trochlear ridge remains apparent, which is not seen in the joints of healthy Labrador Retrievers [19]. It is possible residual lameness is the cause for a long-term change in limb loading, reflected in the subchondral bone density distribution.

To conclude, the subchondral bone density distribution in Labrador Retrievers with MTRT-OC shows significant abnormalities associated with the OC lesion itself, and secondary changes, also present in the contralateral limb. It also highlights one of the important advantages of CTOAM in the field of canine orthopaedic research: the ability to show morphological changes over time i.e. the longitudinal evaluation of subchondral bone density. The differences between dogs with MTRT-OC and LTRT-OC support previous suggestions that MTRT-OC are true OC lesions, characterised by a subchondral bone defect, and that LTRT-OC lesions have another ethiology, and are possibly transchondral fractures, as commonly seen in humans.

The application of CTOAM in earlier stages of the disease, i.e. before the onset of clinical signs, might help to elucidate the pathophysiology of OC in dogs, and aid in the design of screening programs and preventive measures.

REFERENCES

1. Milton JL: Osteochondritis dissecans in the dog. Veterinary Clinics of North America-Small Animal Practice 13:117-134, 1983.

2. Dammrich K: Relationship between nutrition and bone-growth in large and giant dogs. Journal of Nutrition 121:S114-S121, 1991.

3. Ytrehus B, Carlson CS, Ekman S: Etiology and pathogenesis of osteochondrosis. Veterinary Pathology 44:429-448, 2007.

4. Ekman S, Carlson CS: The pathophysiology of osteochondrosis. Veterinary Clinics of North America-Small Animal Practice 28:17-32, 1998.

5. Ytrehus B, Haga HA, Mellum CN, et al: Experimental ischemia of porcine growth cartilage produces lesions of osteochondrosis. Journal of Orthopaedic Research 22:1201-1209, 2004.

6. Frost HM: The Utah paradigm of skeletal physiology: an overview of its insights for bone, cartilage and collagenous tissue organs. Journal of Bone and Mineral Metabolism 18:305-316, 2000.

7. Turner CH: Three rules for bone adaptation to mechanical stimuli. Bone 23:399-407, 1998.

8. Athanasiou KA, Niederauer GG, Schenck RC: Biomechanical Topography of Human Ankle Cartilage. Annals of Biomedical Engineering 23:697-704, 1995.

9. Schenck RC, Goodnight JM: Current Concept Review - Osteochondritis Dissecans. The Journal of Bone and Joint Surgery 78:439-456, 1998.

10. Carlson CS, Meuten DJ, Richardson DC: Ischemic Necrosis of Cartilage in Spontaneous and Experimental Lesions of Osteochondrosis. Journal of Orthopaedic Research 9:317-329, 1991.

11. Richardson DC, Zentek J: Nutrition and osteochondrosis. Veterinary Clinics of North America-Small Animal Practice 28:115-135, 1998.

12. Coughlin KM, Peura GD, Fleming BC, et al: In vivo loads in the medial compartment of the rabbit knee. Clinical Biomechanics 20:1007-1009, 2005.

13. Mason DR, Schulz KS, Fujita Y, et al: Measurement of humeroradial and humeroulnar transarticular joint forces in the canine elbow joint after humeral wedge and humeral slide osteotomies. Veterinary Surgery 37:63-70, 2008.

14. Preston CA, Schulz KS, Kass PH: In vitro determination of contact areas in the normal elbow joint of dogs. American Journal of Veterinary Research 61:1315-1321, 2000.

15. Madry H, van Dijk CN, Mueller-Gerbl M: The basic science of the subchondral bone. Knee Surgery Sports Traumatology Arthroscopy 18:419-433, 2010.

16. Müller-Gerbl M, Putz R, Hodapp N, et al: Computed-tomography-osteoabsorptiometry - A method of assessing the mechanical condition of major joint in a living subject. Clinical Biomechanics 5:193-198, 1990.

17. Müller-Gerbl M, Putz R, Kenn R: Demonstation of subchondral bone density patterns by three-dimensional CT osteoabsorptiometry as a noninvasive method for in vivo assessment of individual long-term stresses in joints. Journal of Bone and Mineral Research 7:411-418, 1992.

18. Patel BA, Carlson KJ: Habitual use of the primate forelimb is reflected in the material properties of subchondral bone in the distal radius. Journal of Anatomy:659-670, 2006.

19. Dingemanse W, Muller-Gerbl M, Jonkers I, et al: Subchondral bone density distribution of the talus in clinically normal Labrador Retrievers. BMC Veterinary Research 12, 2016.

20. van der Meulen MCH, Jepsen KJ, Mikic B: Understanding bone strength: Size isn't everything. Bone 29:101-104, 2001.

21. Rayfield EJ: Finite element analysis and understanding the biomechanics and evolution of living and fossil organisms, in Annual Review of Earth and Planetary Sciences, Vol 35. Palo Alto, Annual Reviews, 2007, pp 541-576.

22. Ruff C, Holt B, Trinkaus E: Who's afraid of the big bad wolff? "Wolff is law" and bone functional adaptation. American Journal of Physical Anthropology 129:484-498, 2006.

23. Dickomeit MJ, Bottcher P, Hecht S, et al: Topographic and age-dependent distribution of subchondral bone density in the elbow joints of clinically normal dogs. American Journal of Veterinary Research 72:491-499, 2011.

24. Samii VF, Les CM, Schulz KS, et al: Computed tomographic osteoabsorptiometry of the elbow joint in clinically normal dogs. American Journal of Veterinary Research 63:1159-1166, 2002.

25. Gielen I, van Bree H, Van Ryssen B, et al: Radiographic, computed tomographic and arthroscopic findings in 23 dogs with osteochondrosis of the tarsocrural joint. Veterinary Record 150:442-447, 2002.

26. Cann CE: Quantitative Ct for Determination of Bone-Mineral Density - a Review. Radiology 166:509-522, 1988.

27. Fitch RB, Beale BS: Osteochondrosis of the canine tibiotarsal joint. Veterinary Clinics of North America-Small Animal Practice 28:95-102, 1998.

28. Flanigan DC, Harris JD, Brockmeier PM, et al: The Effects of Lesion Size and Location on Subchondral Bone Contact in Experimental Knee Articular Cartilage Defects in a Bovine Model. Arthroscopy-the Journal of Arthroscopic and Related Surgery 26:1655-1661, 2010.

29. Dingemanse W, Gielen I, Duchateau L, et al: Comparison of morphological and clinical features between medial and lateral trochlear ridge talar osteochondrosis dissecans in dogs. Veterinary Surgery:340-345, 2013.

30. Talusan PG, Milewski MD, Toy JO, et al: Osteochondritis Dissecans of the Talus: Diagnosis and Treatment in Athletes. Clinics in Sports Medicine 33:267-277, 2014.

31. Lee M, Kwon JW, Choi WJ, et al: Comparison of Outcomes for Osteochondral Lesions of the Talus With and Without Chronic Lateral Ankle Instability. Foot & Ankle International 36:1050-1057, 2015.

32. Lanyon LE, Goodship AE, Pye CJ, et al: Mechanically Adaptive Bone Remodeling. Journal of Biomechanics 15:141-154, 1982.

CHAPTER NINE

Spatial Subchondral Bone Density Reflecting Joint Loading of the Talus in Different *Canidae*

W. Dingemanse [1], M. Lazarevic Macanovic [2], M. Müller-Gerbl [3], N. Krstic [2], H. van Bree [1], I. Gielen [1]

[1] Department of Medical Imaging of Domestic Animals and Orthopaedics of Small Animals Faculty of Veterinary Medicine, Ghent University. Merelbeke, Belgium

[2] Department of Medical Imaging, Faculty of Veterinary Medicine, University of Belgrade, Belgrade, Serbia

[3] Institute of Anatomy, Basel University. Basel, Switzerland

Adapted from: W. Dingemanse, M. Lazarevic Macanovic, M. Müller-Gerbl, N. Krstic, H. van Bree, I. Gielen. Spatial Subchondral Bone Density Reflecting Joint Loading of the Talus in Different *Canidae*. In preparation.

ABSTRACT

Background: Subchondral bone density distribution can be used to study joint biomechanics non-invasively. Differences in joint loading between related species can aid in the understanding of joint loading, and the development of certain types of orthopaedic pathology. This study was conducted to evaluate density distribution in the subchondral bone of the talus of different *Canidae* species, as a parameter reflecting the long-term joint loading in the tarsocrural joint.

Methods: The tarsal joints of cadaver dogs of different breeds were included, i.e. German Shepherd (n=5), Bouvier des Flandres (n=3) and Labrador Retriever (n=6). Additionally golden jackals (n=5) (*Canis aureus*) and wolves (n=5) (*Canis lupus*) were included. Consecutive CT slices were made and the subchondral bone density distribution was evaluated using CTOAM. Different breeds and species were visually compared.

Results: Differences were found in the subchondral bone density distribution of the talus between breeds and between species (*Canis familiaris*, *Canis lupus* and *Canis Aureus*).

Conclusions: Based on the density distribution there are differences in loading conditions of the tarsocrural joint in different species of *Canidae*. The joint loading distribution is very similar between dogs of the same breed and within the same species. Although between-breed differences can be explained by conformational differences, the between-species differences remain subject to further research.

BACKGROUND

The diversity of locomotion and limb posture can be related to different species, and the evolution of specific gait patterns [1]. In primates, different types of locomotor behaviour such as bipedalism, quadrupedalism, and suspensory locomotion have been studied to evaluate limb-loading regimes [1,2]. The joint loading has two different aspects, i.e. body weight and the forces exerted by musculotendon complexes [1]. Since the evaluation of actual joint loading is very difficult *in vivo*, most studies focus on the morphological properties of bone, as they reflect the loading history [2-5]. Using intra-articular pressure films[6] or other *in vitro* methods joint loading can be studied [7,8]. However, these techniques require a certain degree of dissection, which will ultimately alter the joint kinematics, and by definition cannot be applied to living animals.

The density distribution of the subchondral bone is the result of functional adaptation and provides an opportunity for non-invasive research of joint loading [9,10]. As demonstrated in different species, the subchondral bone density distribution is highly correlated with joint loading and reflects the loading history of the joint [5,9,11]. The main morphological properties of bones are bone porosity and bone density [10,12] and in radiographic techniques such as CT, these properties determine the output in Hounsfield Units. Therefore, the subchondral bone density distribution can be visualized and quantified using computer tomographic osteoabsorptiometry (CTOAM) [5,11,13].

All over the world, dogs (*Canis familiaris*) are represented in numerous different breeds, showing great phenotypic diversity (Figure 1). Some of the most striking differences are seen in morphology, but they also exist in, for instance, behavioural traits [14]. The breed-specific morphology is also reflected in their locomotion characteristics such as joint kinematics and dynamics [15,16]. Although the differences in joint loading between dogs of different breeds will not be as big as between bipedal and quadrupedal primate species, or even between knuckle-walk and

palmigrade primates [2,10], differences in joint loading will be reflected in the subchondral bone density pattern.

Figure 1. Different breeds showing the variation in conformation and general morphology. From left to right. Upper row: Basset Hound, Whippet, German Shepherd. Lower row: Labrador Retriever, English Bulldog, and Great Dane.

Joint loading has been linked to the development of different types of orthopaedic conditions in dogs, such as osteochondrosis, cranial cruciate ligament rupture and elbow dysplasia [13,17-20]. In many orthopaedic conditions a breed predisposition is seen [21,22]. This can be due to genetic factors within the breed [23], but can also be due to conformational traits (although these are ultimately also influenced by genetics) influencing general conformation and joint kinematics. For instance, femoral angles have been described in different breeds, and show significant differences [24]. These kind of conformational parameters are likely to influence joint loading, and thus influence subchondral bone density distribution.

Of course this morphologic diversity of different dog breeds has a genetic base, linking different dog breeds and their common ancestors [14]. The closest relative of the dog is the gray wolf (*Canis lupus*), followed by the coyote (*Canis latrans*), golden jackal (*Canis aureus*) and Ethiopian wolf (*Canis simensis*) [14]. The comparison of joint

loading between dogs and their close relatives can aid in the understanding of joint loading and joint pathology in dogs. The aim of this study was to compare the subchondral bone density distribution of the talus between different dog breeds, the gray wolf and the golden jackal. The central hypothesis is that spatial differences in subcondral bone density exist between different dog breeds and different species of *Canidae*.

MATERIALS AND METHODS

Study population

In this study cadaver dogs of different breeds were included, i.e. German Shepherd (n=5), Bouvier des Flandres (n=3) and Labrador Retriever (n=6), euthanised for reasons unrelated to this study. The tarsal joints of 5 golden jackals (*Canis aureus*) and 5 wolves (*Canis lupus*) (cadaveric specimens) were included for comparison with the different dog breeds.

Image acquisition

CT images were acquired from the tarsal joints using a 4 slice helical CT scanner (Lightspeed Qx/i, General Electric Medical Systems, Milwaukee, WI). The CT parameters were 120 kVp and 300 mAs. Contiguous, 1,25 mm collimated, transverse images were obtained in both a bone and a soft tissue reconstruction algorithm.

Left and right tarsal joints were scanned simultaneously, with the tarsal joints in extension, according to patient protocol and previous publications [13,25]. Correct positioning was confirmed on the laterolateral and dorsoplantar scout view. Acquisition time was approximately five minutes.

Image analysis

The CT images were exported in DICOM format to commercially available software (Analyze 11.0, Biomedical Imaging Resource, Mayo Foundation, Rochester, MN, USA), used to complete the CTOAM workflow. The workflow results in an articular surface representation of the underlying subchondral bone density, and has been described in detail recently [13].

Two visual representations (proximal and distal view, Figure 1) of the density distribution (densitogram) of each joint were created, which was further evaluated.

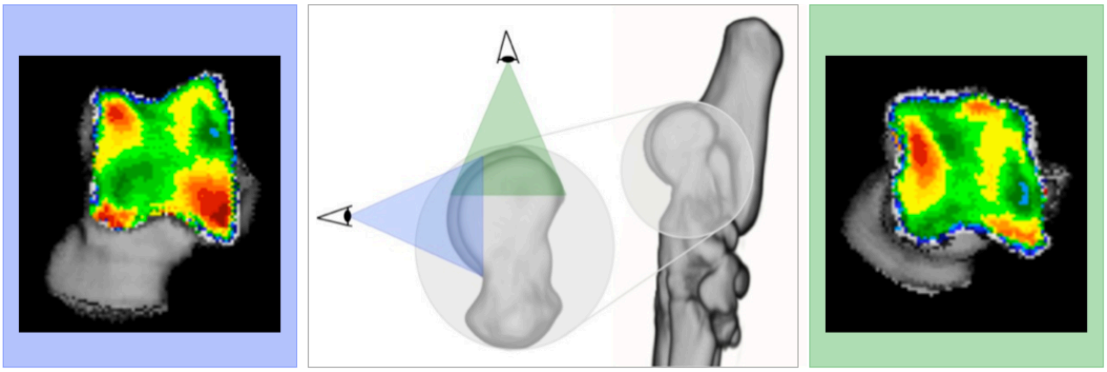

Figure 1. Three dimensional reconstruction of the tarsal and metatarsal bones of the right foot, medial view. Line of sight for the two 3D reconstructions that are reconstructed from the segmented images, proximal view (green) and dorsal view (blue). The use of these two views provides full visualisation of the trochlear ridges with the typical distribution shown for the proximal (right) and dorsal (left) view.

RESULTS

Subchondral bone density distribution of the different dog breeds

In the different breeds, different patterns of subchondral bone density were seen in the talus and these patterns were very similar between dogs of the same breed. In Figure 2, representative densitograms of the different breeds are shown.

In the Labrador Retriever, two density maxima can be seen, one proximal on the medial trochlear ridge and one distal on the lateral trochlear ridge. In the German Shepherds, also two density maxima are present, but they are located at the distal aspect of the lateral and medial trochlear ridge. The Bouviers showed a large density maximum covering almost the entire lateral trochlear ridge, slightly more pronounced at the distal aspect of the lateral trochlear ridge.

Subchondral bone density distribution of the gray wolf and golden jackal

Representative densitograms of the talus of the gray wolf, golden jackal and Labrador Retriever (for comparison) are displayed in Figure 3. At the proximal aspect of the wolf talus, two density maxima can be seen, one on the medial trochlear ridge and one on the lateral trochlear ridge. An area with increased density is also present at the distal aspect of the lateral trochlear ridge.

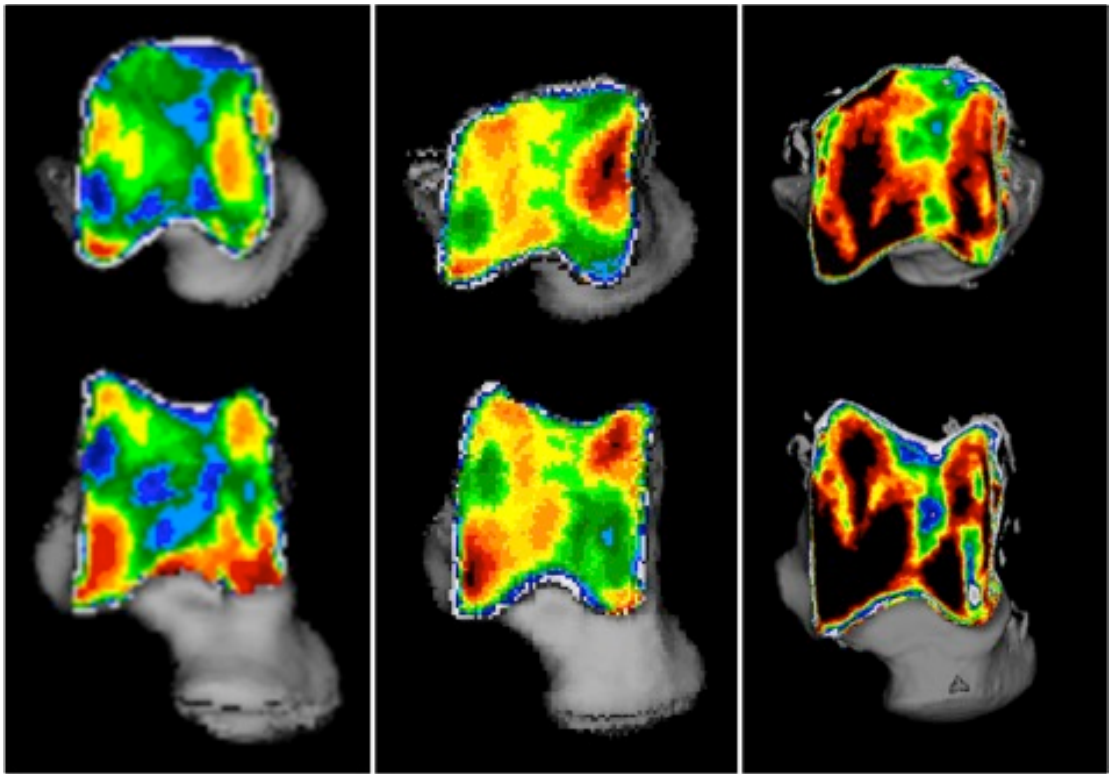

Figure 2. Representative densitograms of different dog breeds: German Shepherd (left), Labrador Retriever (middle), and Bouvier des Flandres (right).

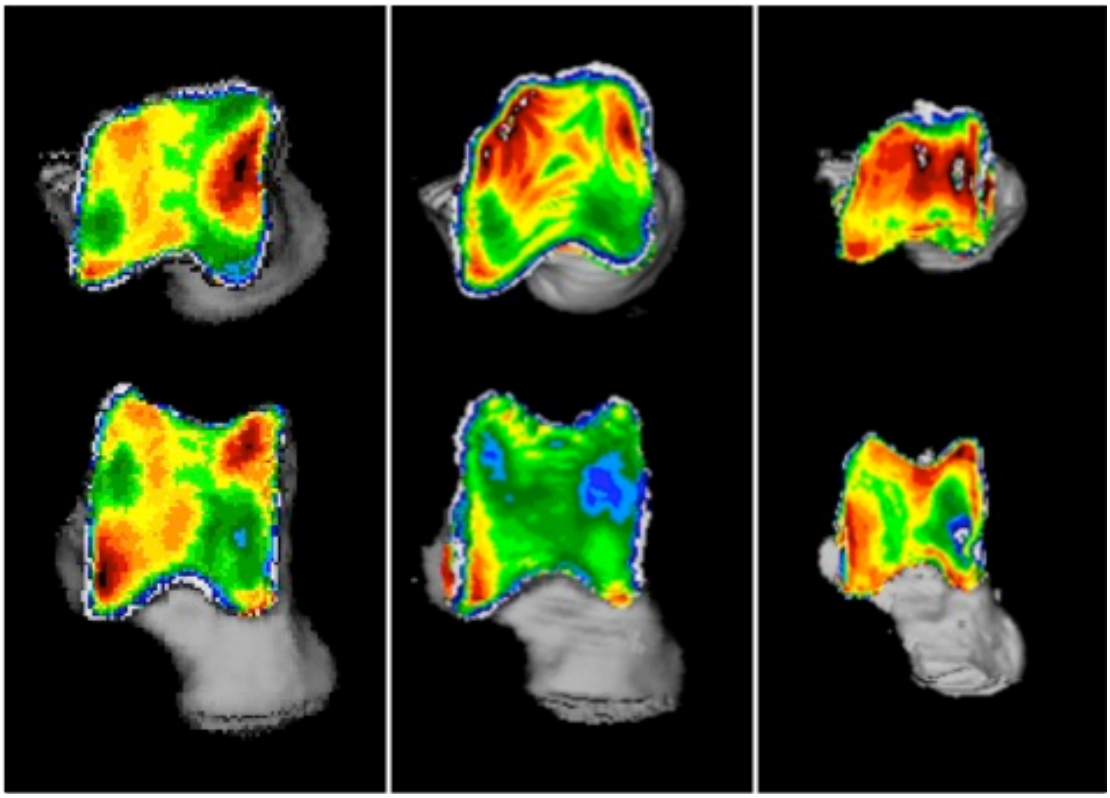

Figure 3. Representative densitograms of the Labrador Retriever (left), gray wolf (middle), and golden jackal (right).

In the golden jackals, an overall high density is seen at the proximal aspect of both trochlear ridges, with a large density maximum located on the medial trochlear ridge. The distal aspect of the lateral trochlear ridge shows an increased density, whereas the medial trochlear ridge shows an area of very low density at the same level.

Table 1. Results summary overall density of different dog breeds.

		Labrador Retriever	German Shepherd	Bouvier des Flandres
Mean density (mg HA/cm^3)	Proximal view	736.0 (46.3)	705.4 (52.7)	884.2 (48.2)
	Dorsal view	761.5 (36.9)	781.4 (49.1)	911.3 (62.8)
Maximum density (mg HA/cm^3)	Proximal view	1122.2 (77.9)	1084.4 (61.5)	1291.5 (77.3)
	Dorsal view	1186.6 (78.0)	1161.7 (47.9)	1351.7 (81.4)

Mean density and maximum density (in mg hydroxyapatite/cm^3). Values displayed as mean (SD).

Table 2. Results summary overall density of different *Canidae*.

		Labrador Retriever	Gray Wolf	Golden Jackal
Mean density (mg HA/cm^3)	Proximal view	736.0 (46.3)	757.6 (46.1)	784.9 (42.1)
	Dorsal view	761.5 (36.9)	719.4 (48.8)	745.4 (57.3)
Maximum density (mg HA/cm^3)	Proximal view	1122.2 (77.9)	1131.9 (71.4)	1189.6 (82.5)
	Dorsal view	1186.6 (78.0)	1088.4 (83.4)	1091.4 (79.7)

Mean density and maximum density (in mg hydroxyapatite/cm^3). Values displayed as mean (SD).

DISCUSSION

In this study the spatial characteristics of the subchondral bone density of the talus were compared between different dog breeds, wolves, and golden jackals. For the domestic dog (*Canis familiaris*), the density distribution differs between breeds and is very similar within the same breed. This is consistent with previous reports on the subchondral bone density distribution in the talus of healthy Labrador Retrievers [13]. The most notable difference is seen between the Labrador Retrievers and German Shepherds. In the latter, two density maxima are located at the distal aspect of the medial and lateral trochlear ridge. The breed-specific conformation of this breed, especially with regards to the hind limb angulation, can easily explain the subchondral bone density distribution described in this study (Figure 4).

Breed differences have also been reported for joint kinematics and kinetics [15,16]. Gross differences exist in the joint moments and power in the hip, stifle and hock joint between Labrador Retrievers and Greyhounds [16]. This will reflect on the muscle work done by the pelvic limb musculature, which is an important component of joint loading, in addition to the effect of bodyweight and velocity. Therefore the hypothesis of this study was a between-breed difference in joint loading at the level of the tarsocrural joint, which is reflected in the spatial characteristics of the subchondral bone density. Although only three breeds are included in this study, there are gross differences in the subchondral bone density distribution.

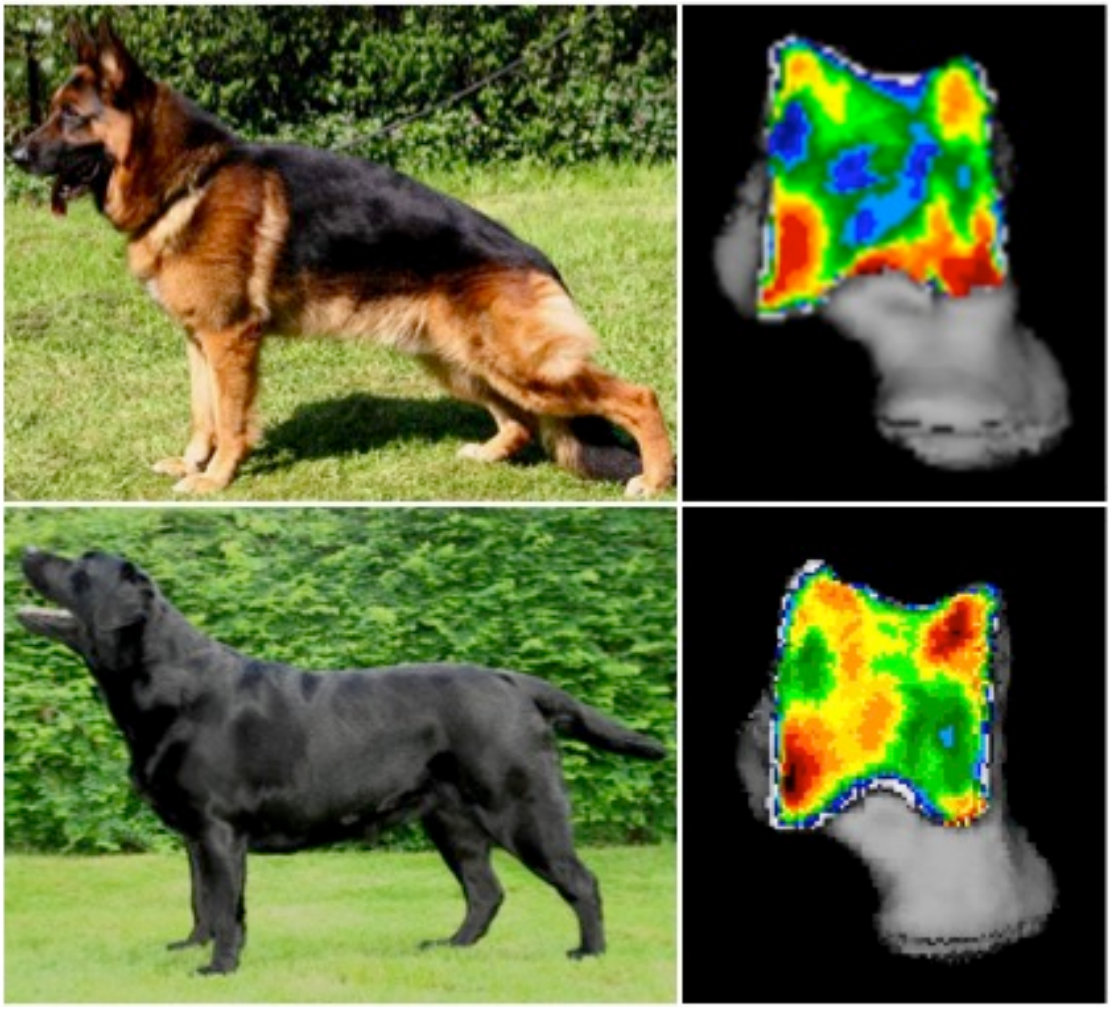

Figure 4. Comparison of the body conformation and subchondral bone density distribution of the talus between the German Shepherd (top) and Labrador Retriever (bottom). Note the extreme angulation of the tarsal joint in the German Shepherd, typical for dogs of this breed.

The subchondral bone density distribution of two of the closest relative of the domestic dog, i.e. the wolf and the golden jackal, also showed regional differences between the different *Canidae*. How these differences in subchondral bone density distribution correlate to hind limb angulation, and locomotion behaviour remains subject to further research.

The functional anatomy of joints can be used to study joint biomechanics, and to reveal differences in gait and limb use in specific species [1,2,26]. Studies on the evolutionary aspect of locomotion have used the general form-function relationship as the central mechanism in bone biology [26]. Gross differences have been described

between bipedal and quadrupedal primates [1], and between arboreal and terrestrial marsupials [26]. Although such gross differences probably will not exist between the domestic dog and *Canis lupus* and *Canis aureus*, the same underlying form-function relationship still applies. Conformational adaptations related to specific breeds will alter joint loading patterns and may in turn have an effect on the incidence of orthopaedic pathology.

The increase of studies looking at joint biomechanics and breed specific parameters highlights the need for breed-specific biomechanical data [21]. The use of CTOAM in the evaluation of subchondral bone density distribution can play a central role in canine orthopaedic research, as CT data is more readily available than specific kinematic or kinetic datasets. By looking beyond the domestic dog, joint pathology can be evaluated in the light of joint loading and the adaptations within different breeds. This will aid in our understanding of joint loading, and maybe help to explain the breed predisposition seen in many orthopaedic conditions in domestic dogs.

REFERENCES

1. Nowak MG, Carlson KJ, Patel BA: Apparent Density of the Primate Calcaneo-Cuboid Joint and Its Association With Locomotor Mode, Foot Posture, and the "Midtarsal Break". American Journal of Physical Anthropology 142:180-193, 2010.

2. Ebel CMI, Prodinger PM, Muhlhofer H, et al: Morphological adaptation of the tarso-metatarsal joints onto load transmission in the foot. Surgical and Radiologic Anatomy 32:107-113, 2010.

3. Eckstein F, Jacobs CR, Merz BR: Mechanobiological adaptation of subchondral bone as a function of joint incongruity and loading. Medical Engineering & Physics 19:720-728, 1997.

4. Frost HM: A 2003 update of bone physiology and Wolff's Law for clinicians. Angle Orthodontist 74:3-15, 2004.

5. Müller-Gerbl M, Putz R, Kenn R: Demonstation of subchondral bone density patterns by three-dimensional CT osteoabsorptiometry as a noninvasive method for in vivo assessment of individual long-term stresses in joints. Journal of Bone and Mineral Research 7:411-418, 1992.

6. Coughlin KM, Peura GD, Fleming BC, et al: In vivo loads in the medial compartment of the rabbit knee. Clinical Biomechanics 20:1007-1009, 2005.

7. Mason DR, Schulz KS, Fujita Y, et al: Measurement of humeroradial and humeroulnar transarticular joint forces in the canine elbow joint after humeral wedge and humeral slide osteotomies. Veterinary Surgery 37:63-70, 2008.

8. Preston CA, Schulz KS, Kass PH: In vitro determination of contact areas in the normal elbow joint of dogs. American Journal of Veterinary Research 61:1315-1321, 2000.

9. Madry H, van Dijk CN, Mueller-Gerbl M: The basic science of the subchondral bone. Knee Surgery Sports Traumatology Arthroscopy 18:419-433, 2010.

10. Patel BA, Carlson KJ: Habitual use of the primate forelimb is reflected in the material properties of subchondral bone in the distal radius. Journal of Anatomy:659-670, 2006.

11. Müller-Gerbl M, Putz R, Hodapp N, et al: Computed-tomography-osteoabsorptiometry - A method of assessing the mechanical condition of major joint in a living subject. Clinical Biomechanics 5:193-198, 1990.

12. van der Meulen MCH, Jepsen KJ, Mikic B: Understanding bone strength: Size isn't everything. Bone 29:101-104, 2001.

13. Dingemanse W, Muller-Gerbl M, Jonkers I, et al: Subchondral bone density distribution of the talus in clinically normal Labrador Retrievers. Bmc Veterinary Research 12, 2016.

14. Lindblad-Toh K, Wade CM, Mikkelsen TS, et al: Genome sequence, comparative analysis and haplotype structure of the domestic dog. Nature 438:803-819, 2005.

15. Agostinho FS, Rahal SC, Miqueleto NSML, et al: Kinematic analysis of Labrador Retrievers and Rottweilers trotting on a treadmill. Veterinary and Comparative Orthopaedics and Traumatology 24:185-191, 2011.

16. Colborne GR, Innes JF, Comerford EJ, et al: Distribution of power across the hind limb joints in Labrador Retrievers and Greyhounds. American Journal of Veterinary Research 66:1563-1571, 2005.

17. Cook JL: Cranial Cruciate Ligament Disease in Dogs: Biology versus Biomechanics. Veterinary Surgery 39:270-277, 2010.

18. Dickomeit MJ, Bottcher P, Hecht S, et al: Topographic and age-dependent distribution of subchondral bone density in the elbow joints of clinically normal dogs. American Journal of Veterinary Research 72:491-499, 2011.

19. Dingemanse W, Gielen I, Duchateau L, et al: Comparison of morphological and clinical features between medial and lateral trochlear ridge talar osteochondrosis dissecans in dogs. Veterinary Surgery:340-345, 2013.

20. Alves-Pimenta S, Ginja MM, Fernandes AM, et al: Computed tomography and radiographic assessment of congruity between the ulnar trochlear notch and humeral trochlea in large breed dogs. Veterinary and Comparative Orthopaedics and Traumatology 30:8-14, 2017.

21. Colborne GR: Bringing canine biomechanics research out of the dark ages. Veterinary Journal 173:469-470, 2007.

22. Griffon DJ: A Review of the Pathogenesis of Canine Cranial Cruciate Ligament Disease as a Basis for Future Preventive Strategies. Veterinary Surgery 39:399-409, 2010.

23. Coopman F, Broeckx B, Verelst E, et al: Combined prevalence of inherited skeletal disorders in dog breeds in Belgium. Veterinary and Comparative Orthopaedics and Traumatology 27:395-397, 2014.

24. Tomlinson J, Fox D, Cook JL, et al: Measurement of femoral angles in four dog breeds. Veterinary Surgery 36:593-598, 2007.

25. Gielen I, van Bree H, Van Ryssen B, et al: Radiographic, computed tomographic and arthroscopic findings in 23 dogs with osteochondrosis of the tarsocrural joint. Veterinary Record 150:442-447, 2002.

26. Carlson KJ, Jashashvili T, Houghton K, et al: Joint Loads in Marsupial Ankles Reflect Habitual Bipedalism versus Quadrupedalism. Plos One 8, 2013.

CHAPTER TEN

Quantification of Joint Loading in the Hind Limbs of the Labrador Retriever (Canis Familiaris) using a Three-Dimensional Musculoskeletal Model

W. Dingemanse [1], I. Jonkers [2], M. Wesseling [2], J. Vander Sloten [3], M. Müller-Gerbl [4], B. Van Ryssen[1], H. van Bree [1], I. Gielen [1]

[1] Department of Medical Imaging of Domestic Animals and Orthopaedics of Small Animals Faculty of Veterinary Medicine, Ghent University. Merelbeke, Belgium

[2] Human Movement Biomechanics Research Group, Faculty of Kinesiology and Rehabilitation Sciences, KU Leuven. Leuven, Belgium

[3] Biomechanics Section, Faculty of Engineering Science, KU Leuven. Leuven, Belgium

[4] Institute of Anatomy, Basel University. Basel, Switzerland

Adapted from: W. Dingemanse, I. Jonkers, M. Wesseling, J. Vander Sloten, M. Müller-Gerbl, B. Van Ryssen, H. van Bree, I. Gielen. Quantification of joint loading in the hind limbs of the Labrador Retriever (Canis familiaris) using a three-dimensional musculoskeletal model. Submitted.

ABSTRACT

Background: The use of musculoskeletal modelling in canine biomechanical research can aid in the understanding of canine locomotion and pathophysiology of orthopaedic disorders such as cranial cruciate ligament disease and osteochondrosis.

Methods: In order to apply advances in human biomechanical research to the canine biomechanical field, a breed-specific musculoskeletal model of Labrador Retriever hind limb and pelvis is presented. The model includes 7 segments and 10 degrees of freedom (DOF). Bone geometry is based on CT data, and muscle geometry of all muscles with a moment arm acting on the hip, stifle, or hock joint is included in the model. Muscles are modelled as actuators.

Results: The musculoskeletal model can be used to calculate joint angles and moments, and to estimate muscle moment arms, muscle forces, and joint contact forces.

Conclusions: The introduction of this breed-specific musculoskeletal model that allows the estimation of musculoskeletal loading provides an interesting tool for the canine biomechanical research community and contributes towards the application of musculoskeletal models in canine biomechanical research. Because of its open-source nature, the model can be improved upon as canine biomechanical research progresses and can be tailored towards specific research questions.

CHAPTER 10

BACKGROUND

Canine locomotive and biomechanical research has traditionally focused on evaluating both normal and pathological gait patterns, and the nature of these studies is mainly descriptive. The last decade, different types of gait and gait pathology have been described using kinematic analysis and the evaluation of ground reaction forces [1-4], and joint moments [5-7].

In human biomechanical research, musculoskeletal models have been used to investigate walking, jumping, climbing stairs, and numerous other day-to-day activities [8-11]. In addition to normal gait, human research has focused on underlying causes of abnormal gait [12-15], as well as understanding the effect of medical interventions [16,17].

A musculoskeletal model incorporates bone, muscle, and tendon geometry and segmental dynamic parameters. Using magnetic resonance imaging (MRI) or computed tomography (CT), these parameters can be non-invasively determined [18-20]. The model kinematics are driven by three dimensional (3D) marker data and ground reaction force data, measured experimentally. Based on these data, joint moments can be calculated using inverse dynamics analysis. When muscle force distribution algorithms are used, the joint moments can be used to calculate individual muscle forces, based on optimisation.

For both normal and abnormal gait, the use of musculoskeletal models has played an important role in the recent advances made in the field of human biomechanics and has recently been introduced in veterinary biomechanics as well. Biomechanical modelling techniques allow the calculation of musculoskeletal loading in terms of muscle forces and joint contact forces, parameters that cannot be measured non-invasively *in vivo* [21-24]. When these advances are applied to canine biomechanics, it allows researchers to evaluate parameters that are currently out of reach, such as muscle forces and joint contact forces or in a broader term joint loading.

Joint loading has been linked to a variety of canine orthopaedic conditions, but so far studies have been limited to invasive *in vitro* experiments. In dogs, osteochondrosis is an important cause of lameness, which can occurs in different joints and lesions develop in specific anatomical regions within the joint. It is considered to be a multifactorial condition in which both genetic and environmental factors play a role [25,26]. Joint biomechanics is an environmental factor that is more and more often suggested to play an important role, since OC lesions are often found in specific locations within the joint [27-31]. In addition, joint loading, more specifically the tensile and compressive stresses, are predominant local factors affecting cartilage and subchondral bone physiology and pathology [32,33].

Musculoskeletal models have the unique potential to further elucidate the role of joint loading. Kinematic and kinetic parameters vary with different gait patterns, and change in case of orthopaedic pathology [2,3,34]. But more importantly, gait patterns and ground reaction forces also vary widely with different breeds [2,35]. Bone geometry, muscle moment arms, and joint moments are also likely to vary, since they are largely dependent on breed-specific anatomy and (joint) conformation [35,36]. In addition, different orthopaedic pathologies show a breed predisposition, and general morphology and joint biomechanics are likely to make certain breeds more susceptible for specific conditions, such as osteochondrosis, or cranial cruciate ligament rupture. Therefore it is necessary to invest in research on breed specific morphological and biomechanical data, i.e. kinematic and kinetic gait parameters. Biomechanical research is a valuable tool in the understanding of different orthopaedic conditions [37].

In this paper we present a three-dimensional musculoskeletal model of the pelvis and hind limbs of a Labrador Retriever allowing the study of musculoskeletal loading. To the authors' knowledge, no breed-specific musculoskeletal model exists so far. Such a model can aid in the understanding of both normal and pathological gait patterns and the pathophysiology of orthopaedic conditions.

MATERIALS AND METHODS

General

A schematic view of the workflow used to create the musculoskeletal model and the different kinematic and kinetic analysis methods used in this study is presented in Figure 1. The study was approved by the local ethical committee of the Faculty of Veterinary Medicine, Ghent University (approval nr. EC2011/193) and informed owner consent was obtained.

The model was constructed using OpenSim, an open-source, biomechanical simulation software that was originally developed for human research [38]. All model files as well as the input data are available at www.simtk.org for other researchers. To illustrate the current possibilities of the model, the joint angles, joint moments, muscle forces, and joint reaction forces during gait will be discussed. Data was collected from 7 Labrador Retriever dogs of which a data summary is given in Table 1.

Table 1. Data summary of the dogs used for kinematic and kinetic data collection.

Dog	Sex	Weight	Age
1	Male	21	18 months
2	Male	23	18 months
3	Male	23	22 months
4	Female	21	22 months
5	Female	20	19 months
6	Male	25	22 months
7	Female	23	22 months

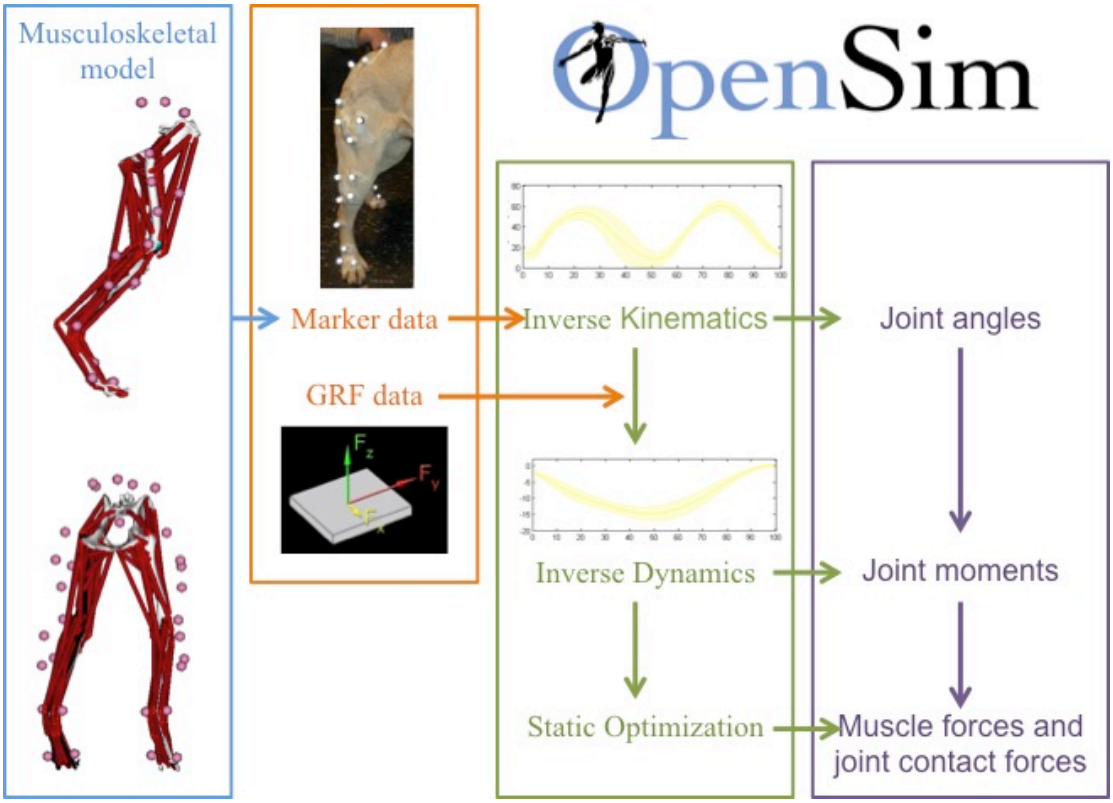

Figure 1. An overview of the workflow, from left to right: Muscuskeletal model, input from marker and ground reaction force (GRF) data, calculations for inverse kinematics (IK), inverse dynamics (ID) and static optimization (SO), resulting in jont angles, joint moments, and muscle forces respectively.

Model definition: bone geometry, segments, and joints

Bone geometry of the pelvis and hind limbs was derived from the CT scan of a healthy adult (2,5 years old, 24 kg) male Labrador Retriever. Under general anaesthesia, CT images were acquired using a 4 slice helical CT scanner (Lightspeed Qx/i, General Electric Medical Systems, Milwaukee, WI). The dog was positioned in ventral recumbency with the stifle and tarsal joints in extension and images were aquired from the fifth lumbar vertebra (L5) till the distal tip of the phalanges, to include the pelvis, femur, patella, tibia and fibula, tarsal and metatarsal bones, and the phalanges. The CT parameters were 120 kVp and 300 mAs. Contiguous, 1,25 mm collimated, transverse images were obtained in a bone and a soft tissue reconstruction algorithm. The CT images were exported as DICOM images, and these were imported to Mimics (Mimics software, Materialise, Leuven, BE). All the skeletal

elements were segmented individually using a combination of thresholding and manual segmentation, and were exported as STL (Stereolithography) files.

Functionally, the musculoskeletal model consists of a mechanical linkage of seven segments, i.e. pelvis, left and right femur, left and right tibia, and left and right foot segment. To ensure symmetrical bone geometry, the left leg was mirrored from the right leg. The model contains 10 degrees of freedom (DOF, Table 2) and local coordinate systems (LCS) for each segment were defined (Table 3 and Figure 2) according to the International Society of Biomechanics recommendations and previous publications [39].

Table 2. Degrees of freedom (DOF) of the musculoskeletal model.

Joint	# DOF	DOF
Hip	3	Flexion – extension Abduction – adduction Endorotation – exotoration
Stifle	1	Flexion – extension
Hock	1	Flexion – extension

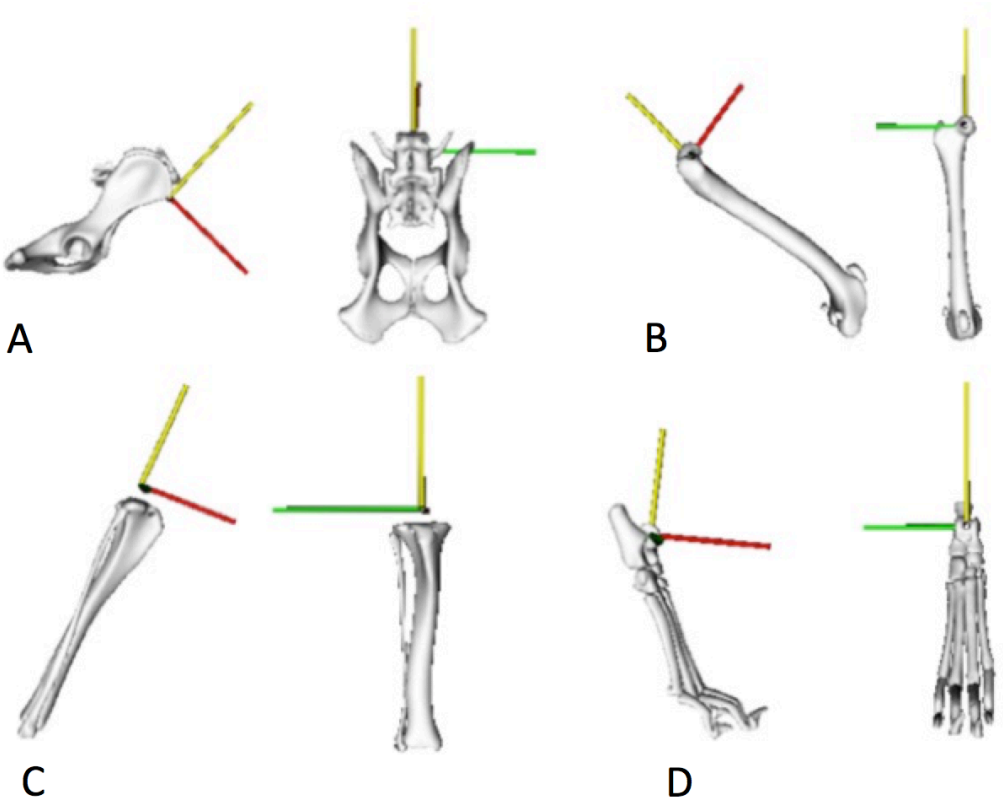

Figure 2. The local coordinate systems (LCS) for the 4 different segments, pelvis (A), femur (B), tibia (C), and foot (D). Y-axis (yellow), z-axis (green) and x-axis (red).

Joints kinematics of the hip, stifle, and hock were modelled based on the anatomical joint configurations: The hip joint was modelled as a ball and socket joint between the head of the femur and the acetabulum with the centre of rotation located at the hip joint centre. The latter was defined by fitting a sphere to the femoral head. The stifle joint was modelled as a hinge joint with one degree of freedom. The joint axis was defined as the axis connecting the centre of two spheres fitted to the lateral and medial condyle. Due to the shape of the femoral condyles, rotation around the joint axis led to interference of the femoral condyles on the tibial plateau. Therefore, the rotational movement was coupled to translational movement of the tibia relative to the femur. The translations of the tibial plateau were determined visually so that they followed the femoral condyles during flexion and extension of the stifle joint. The movement of the patella was implemented similarly, to allow the patella to transfer along the patellar groove on the femur, as a function of the stifle flexion angle.

Table 3. Bone coordinate segment definitions

Segment	Axis	Definition
Pelvis	Origin	The midpoint between the most ventral aspect of the left and right ilial wing
	x	Cross-product of the y- and z-axis
	y	The line connecting the midpoint of the centre of the left and right femoral head and the origin
	z	The line connecting the most ventral aspect of the left and right ilial wing
Femur	Origin	Centre of the femoral head
	x	Cross-product of the y- and z-axis
	y	The line through the centre of the femoral head and the midpoint between the lateral and medial femoral epicondyle
	z	Line parallel to the line connecting the lateral and medial femoral epicondyle (Flexion-Extension axis)
Tibia	Origin	The midpoint between the lateral and medial femoral epicondyle
	x	Cross-product of the y- and z-axis
	y	The line connecting the midpoint between the lateral and medial malleolus and the origin
	z	Line connecting the lateral and medial femoral epicondyle (Flexion-Extension axis)
Foot	Origin	The midpoint between the lateral and medial malleolus
	x	Cross-product of the y- and z-axis
	y	The line between the midpoint of the distal aspect of the third and fourth metatarsal bone and the origin
	z	The line between the lateral and medial malleolus (Flexion-Extension axis)

The hock joint was defined as a hinge joint with one rotational degree of freedom. The most distal point of the medial and lateral malleolus defined the hock joint axis. The tarsal, metatarsal, and phalangeal joints were locked for reasons of simplification. The left hip joint centre was defined as described for the right leg, and all coordinates were mirrored accordingly.

Although segmental inertial parameters in dogs have been described [20], the inertial parameters for the model were determined based on the CT data set in order to obtain a concise data set. Three different tissues were segmented, i.e. bone, fat, and other soft tissue (mainly muscle) for the four different segments and density values were assigned according to values based on literature (bone 1,7 g/mm^3, fat 0,9 g/mm^3, others 1.18 g/mm^3) [20]. The segmented images were exported as STL files and imported into Abaqus FEA (Dassault Systemes, Dassault Group, Vélizy-Villacoublay, France). In Abaqus all inertial parameters, i.e. mass, centre of mass, and moments of inertia, were calculated. These results were integrated into the segment parameters in OpenSim.

Muscle-tendon units

Muscle-tendon units were defined by their muscle path and their maximum force generating capacity. All muscles with a moment arm acting on the hip, stifle, or hock joint were included, leading to a total of 39 muscle-tendon units on each side represented in the model. The origin and insertion of each muscle path were based on published anatomical data [40,41] and were manually adjusted based on the CT images. Care was taken to position the origin and insertion as close to the centre of the attachment area as possible. The intrinsic muscles of the foot were not modelled because the tarso-metatarsal and metatarsal-phalangeal joints were locked in the current model.

To maintain anatomically correct muscle paths throughout the full limb range of motion, via-points were used where judged appropriate by the authors (Table 4). The definition of muscle paths is used in the calculation of muscle-tendon length and muscle moment arm, which have been described in detail previously [42]. These via points constrain the muscle path, mimicking the function of soft tissue constraints [43,44]. For instance, the tendon of the long digital extensor muscle runs through the proximal and distal extensor retinaculum. Both conditional and unconditional (fixed) via-points were used, the former being active at specified joint angles, the latter being active at all times.

Table 4. Muscles and via-points within the model.

Muscle	Unconditional via points	Conditional via points
Superficial gluteal	1	1
Middle gluteal	-	-
Deep gluteal	-	-
Piriformis	-	1
Cranial tensor fascia lata	-	-
Caudal tensor fascia lata	-	-
Sartorius cranial part	-	2
Sartorius caudal part	1	-
Rectus femoris	-	2
Biceps femoris	1	1
Caudal crural abductor	1	-
Semimembranosus	-	-
Semitendinosus	-	-
Gracilis	-	-
Adductor longus	-	-
Adductor magnus et brevis	-	-
Pectineus	-	-
Internal obturator	1	-
External obturator	-	-
Gemelli	-	-
Quadratus femoris	-	-
Articularis coxae	-	-
Iliopsoas – Iliacus	2	2
Iliopsoas – Psoas major	2	2
Vastus lateralis-intermedius	1	2
Vastus medialis	1	2
Popliteus	-	2
Gastrocnemius medialis	1	2
Gastrocnemius lateralis	1	2
Superficial digital flexor	2	1
Caudal tibial	5	-
Lateral digital flexor	3	2
Medial digital flexor	5	1
Cranial tibial	3	-
Long peroneal	2	1
Short peroneal	1	1
Long digital extensor	3	2
Lateral digital extensor	2	1
Long extensor of the first digit	3	-

The muscles were modelled as actuators with one input parameter, i.e. maximal muscle force. The maximal muscle force was based on physical cross-sectional area (PSCA) data available in literature [41], and was calculated assuming a maximum isometric muscle stress of 22 N cm^{-2} [45,46].

Collection of kinematic and kinetic data

Kinematic and kinetic data were collected simultaneously from 8 healthy, adult Labrador Retrievers at trot (informed owner consent was obtained in all cases). Kinematic data was collected using a ten camera VICON system (250 Hz), measuring the three dimensional movement of retroflective markers placed on the hind limb at different bony landmarks. Marker locations were chosen based on anatomical landmarks and placement repeatability (Figure 2), as well as previous publications [39]. For the pelvis, femur and tibia segment, an additional cluster of markers was used. This cluster consists of 3 markers in a fixed triangular configuration and provides additional kinematic data for these segments. Kinetic data, more specifically the ground reaction forces in three directions, was collected using three AMTI force plates (size 463.5 x 508 mm, type OR6-7 and OR6-6, sampling rate 1000 Hz, 1 kHz anti-aliasing filter) integrated in the walkway.

Dogs were led on lead by their own handler, back and forth over the force plate area trotting in a straight line at a self-selected speed. During measuring, care was taken to have trials with only one paw on one forceplate, dogs trotting in a straight line, and no distractions of deviations from the trotting direction.

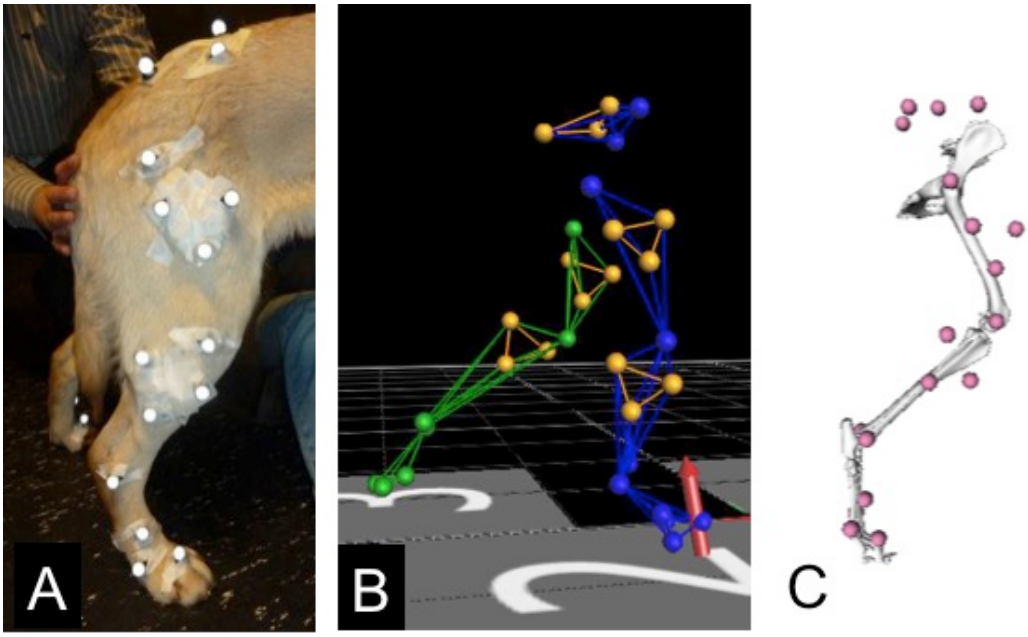

Figure 3. A – Marker placement on the dog hind limbs. Individual markers were placed on bony landmarks, and clustered markers in a triangular configuration were added to the pelvis, thigh and tibia segments. B – Marker data labelled and visualized in the VICON software. Individual markers on the left leg are labelled in green, individual markers on the right leg in blue, and clusters in yellow. C – Skeletal structure of the musculoskeletal model in OpenSim with the different markers used for the motion analysis.

Only those trials with a constant, self-selected speed (range 1.7 – 2.1 m/s, average 1,85 m/s), and no sudden deviations of the trotting direction were used for further analysis. A full gait cycle was defined as toe strike of the hind foot, till the next toe strike of that hind foot, to include the full stance phase and swing phase. The stance phase was defined as toe strike of the hind foot, till toe off of the same hind foot. Only trials with one foot in contact with a single force plate during the entire stance time were used. This resulted in 3-4 trials for each dog that were used in the remainder of the workflow.

Inverse kinematics

The inverse kinematics (IK) workflow available in OpenSim matches the model markers with the collected marker data while minimizing the sum of weighted squared errors of the markers by adjusting the different DOF of the model [47]. All IK results were time normalized to a gait cycle.

Inverse dynamics

The inverse dynamics (ID) workflow calculates the joint moments based on the markerdata and GRF data. The motion of the model is defined by the positions, velocities and accelerations that are on the left-hand side of the equation of motion (N is the number of DOF):

$$M(q)\ddot{q} + C(q,\dot{q}) + G(q) = \tau$$

$q, \dot{q}, \ddot{q} \in R^N$	vectors of the positions, velocities and accelerations
$M(q) \in R^{NxN}$	system mass matrix
$C(q,\dot{q}) \in R^N$	vector of Coriollis and centrifugal forces
$G(q) \in R^N$	vector of gravitational forces
$\tau \in R^N$	vector of generalized forces

In the ID workflow, the known motion of the model is used to solve for the unknown generalized forces (τ). Assumptions during the execution of the inverse dynamics (ID) workflow are a constant mass and length, a fixed center of mass and constant mass moments of intertia for each body segment. All ID results were time normalized to a stance phase and normalized to bodyweight.

Static optimization

The standard static optimization (SO) protocol available in OpenSim was used. Similar to the ID workflow, it uses the known motion of the model to solve the equations of motion for the unknown generalized forces (i.e. joint moments) subject to the following condition:

$$\sum_{m=1}^{n} (a_m F_m^0) r_{m,j} = \tau_j \Big|$$

while mimimizing the objective function:

$$J = \sum_{m=1}^{n} (a_m)^p \Big|$$

where a_m is the activation of muscle m at a discrete time step, $F_m^0|$ is its maximum isometric force, $r_{m,j}$ is its moment arm around the jth joint axis, $\tau_j|$ is the generalized force around the jth joint axis, and p is a user defined constant. All SO results were time normalized to a stance phase and normalized to bodyweight.

RESULTS

The results will be discussed from a functional point of view, and joint angles, joint moments and estimated muscle forces will be grouped for each joint. In the model, the neutral joint position (legs in extended position) was set to zero, so joint flexion is indicated with positive values, hyperextension with negative values.

Hip joint

The range of motion during the entire gait cycle ranges from 25 – 75 degrees flexion. The hip joint displays a gradual extension throughout the stance phase, starting at the last quarter of the swing phase. In the beginning of the swing phase, there is a rapid joint flexion (Figure 4). The first 50-80% of the stance phase there is a net extensor moment present at the level of the hip. The gluteus muscles, semimembranosus, and biceps femoris muscle are the major contributors in addition to the semitendinosus and adductor muscle. In the remaining part of the stance phase there is a small net flexor moment (Figure 5), with obturator and psoas muscles and other small hip musculature as the main contributors. The hip contact force peaks at around 2.5 times bodyweight (BW) (Figure 6).

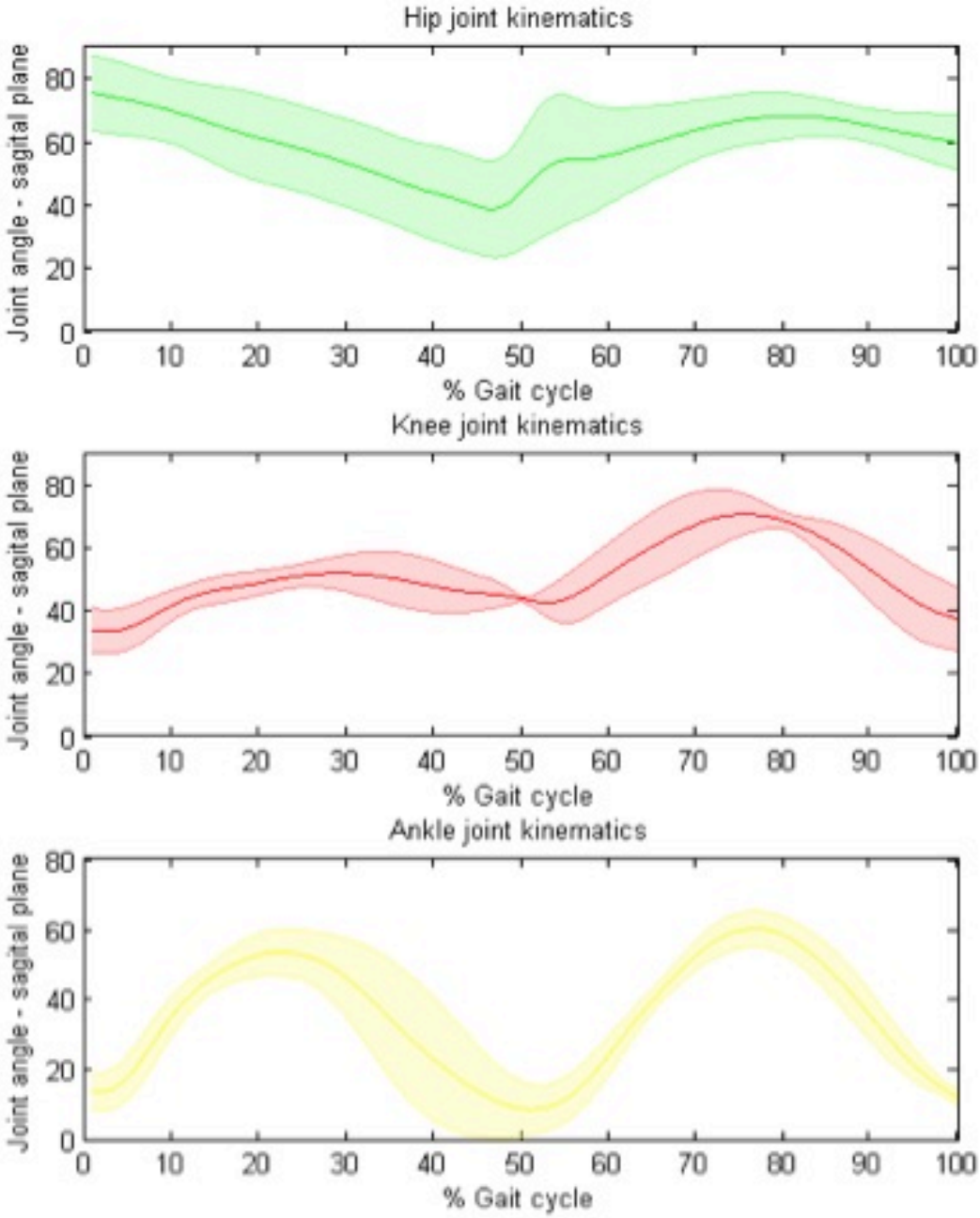

Figure 4. Joint kinematics for the hip (green), stifle (red) and hock (yellow) joint. Joint angles in the sagittal plane.

Stifle joint

During the stance phase there is joint flexion from 30 – 50 degrees of flexion, followed by an extension phase (Figure 4). Maximum joint flexion (around 80 degrees) is present in the mid-swing phase, followed by maximum extension (30 degrees) at the end of the swing phase. The flexion angle during stance phase is smaller (approximately 30 degrees difference) than the flexion angle in the swing phase.

The first 25-40% of the stance phase there is a net flexor moment (Figure 5) at the level of the stifle, as the paw hits the ground and the stifle acts as a shock absorber and decelerates the body. This phase is followed by a net extensor moment, in which the stifle extensors are activated, and the body is propelled forward, propagating to the next swing phase. The rectus femoris muscle, the lateral and the medial vastus muscles are the main stifle extensor muscles activated at this stage. The stifle joint contact force is almost twice as high as the hip or hock joint contact force at approximately 4 to 5 times BW (Figure 6).

Hock joint

The hock joint angle displays a biphasic flexion-extension motion during a full gait cycle, with the timing of maximum flexion (60 degrees) and extension (10 degrees) almost coinciding with maximum stifle flexion and extension (Figure 4). The range of motion is 10 – 60 degrees of joint flexion. In the first half of the stance phase, there is an increased flexion of the hock, followed by extension during the second half of the stance phase. At the end of the stance phase, there is an increased flexion again, followed by maximum extension at the end of the swing phase.

During the entire stance phase, the hock joint exhibits a net extensor moment, with it's peak approximately at mid-stance (40-50% stance phase) (Figure 5). The majority of muscle force during the stance phase originates from both the lateral and the medial gastrocnemius muscle, providing an active push-off. The joint reaction force peaks at around 2.5 times BW in midstance (Figure 6).

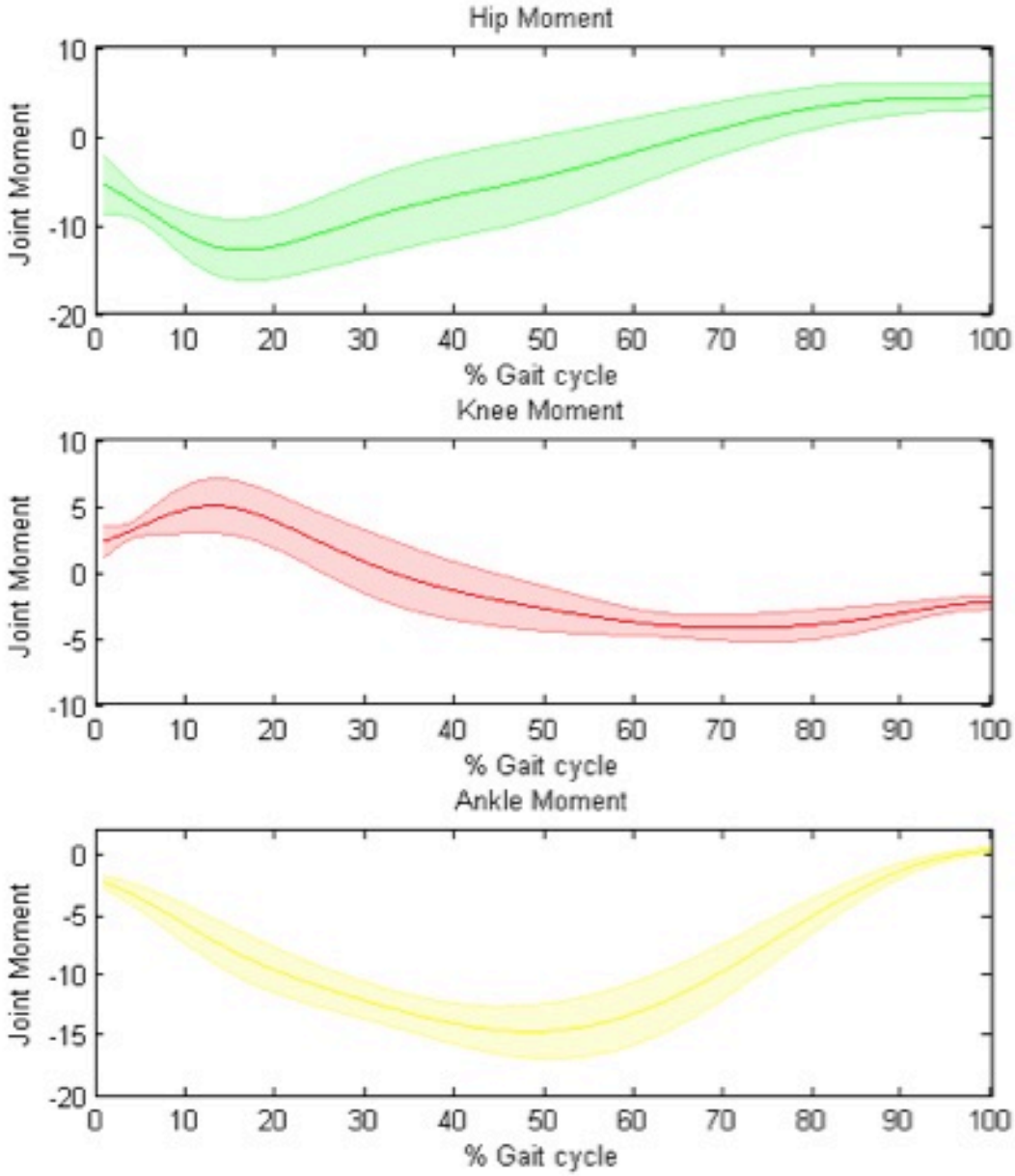

Figure 5. Joint moments for the hip (green), stifle (red) and hock (yellow) joint. Joint moments in the sagittal plane. Joint moments are reported as external joint moments.

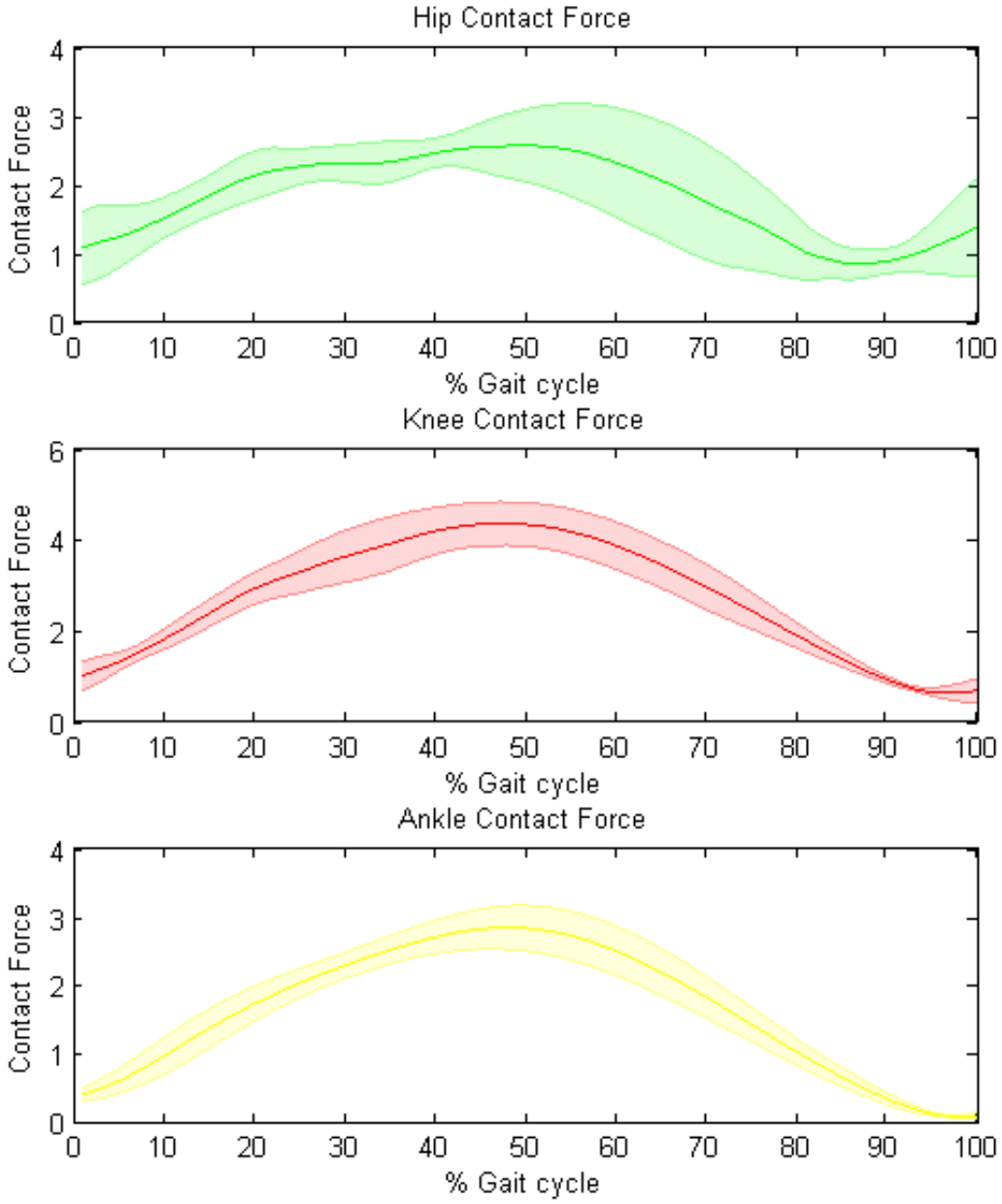

Figure 6. Joint contact forces for the hip (green), stifle (red) and hock (yellow) joint. Joint forces normalized to BW.

CHAPTER 10

DISCUSSION

This paper describes the development of the first, breed-specific, canine musculoskeletal model. The model includes left and right hind limbs, pelvis and the last two lumbar vertebrae and contains 10 DOF. The model can be used to calculate joint angles and moments, and to estimate muscle moment arms, muscle forces, and joint contact forces. These estimated parameters are very difficult or impossible to measure *in vivo*.

Results

The results from the inverse dynamics are consistent with a previous study on canine pelvic limb moments [48]. Existing differences in joint moments can be (partially) attributed to breed-specific anatomy [35], confirming the need for breed-specific musculoskeletal models.

Unfortunately, no *in vivo* experimental data is available in canine literature to validate the model. In general, mathematical models are used to estimate parameters that are difficult or impossible to measure *in vivo*, either due to ethical considerations or technical and practical difficulties [49]. In human biomechanical research, results from instrumented prostheses have been used to validate musculoskeletal models and simulations [50,51]. Electromyography (EMG) data could have been beneficial to evaluate muscle activation patterns and muscle force estimates, but was not included in the current study due to practical limitations. The advantages and challenges of EMG in animal biomechanics have recently been discussed in detail [52].

Model assumptions and limitations

Three segments, in addition to the pelvic segment, represent each hind limb. The hip joint was modelled with three DOF, the stifle joint and hock joint with one DOF, as the range of motion in the other DOF is limited. The metatarsal-phalangeal and interphalangeal joints were locked in this model, so the tarsal and foot bones are one segment. Different DOF joints at this level can be incorporated in the future.

However, it is difficult to accurately describe the motion of these individual segments, especially in dogs, because of practical limitation such as the number of markers that can be fitted. Dynamic segmental properties were calculated using CT image segmentations and assigned to each segment.

For modelling purposes, only muscles with a moment-arm acting on the hip, stifle and/or hock joint were incorporated in the model. In current literature there is no dynamic data available on moment-arms for canine pelvic muscles, so data calculated with the model could not be validated yet. The muscles were modelled as ideal actuators with their force generating capacity based on one input parameter, i.e. maximal muscle force. The use of actuators implies omitting of the force-length and force-velocity relationship. At this stage, the muscle path of the muscles was approximated by one single line segment along which forces are being applied. This approach is problematic to represent the line of action of mutipenate muscles with larger areas of origin or insertion such as the *m. gluteus medius,* in which the division into multiple muscle lines of action in the model would improve the representation of the muscle. In future research, the definition of the muscle-tendon units can be enhanced by incorporation of a Hill-type muscle model, consisting of a contractile element, with an elastic element in parallel and a second elastic element in series [53]. This will allow the use of the muscles force-length relationship in the calculation of the muscle force, but will require muscle specific parameters i.e. maximum isometric force, optimal muscle fiber length, tendon slack length, maximum contraction velocity, and pennation angle for each muscle. These parameters are currently unavailable in canine literature, and are therefore not incorporated in the current musculoskeletal model. The nature of the model and the used platform (OpenSim) allows future incorporation of more realistic muscle models based on more elaborate input parameters. Similarly, no ligaments were incorporated in the model, due to lack of available data on ligament parameters such as slack length and general biomechanical behaviour of canine ligaments.

Marker placement is a potential source of error during all types of kinematic studies. The same person (WD) applied the markers in all dogs, and individual markers were

placed on palpable anatomical landmarks. This way, marker placement errors are reduced to a minimum. Further analysis of the effects of marker placement variability was not conducted in this study. In addition to marker placement, skin motion artefacts or soft tissue artefacts (STAs) can also influence the acquired kinematic data [54]. However, joint kinematics were calculated using an inverse kinematics algorithm that uses a global minimization of the measurement error, thereby reducing the error due to STA [47].

Joint kinematics were simplified to flexion and extension at the level of the stifle and hock joint and the hip joint was modelled as a perfect ball and socket joint. Dynamic CT studies can be used to advance the current joint definitions of the model and to improve joint kinematics based on measured joint kinematics, joint anatomy and contact surface area [55,56]. In addition the model can be used in research on multi-joint coordination and dynamic coupling, i.e. the effect of neighbouring joint positions on the moment production of muscles acting on a certain joint.

Conclusions and future perspectives

As with any model, our model is based on assumptions and has some limitations as has been discussed above. At this point the model can be used to calculate joint angles and moments and to estimate muscle moments, lengths, and forces. The latter are parameters that are difficult, if not impossible to measure *in vivo*. Future improvements to the current model can be done as more input parameters become available. These improvements include muscle specific parameters leading to the incorporation of a Hill-type muscle model and joint ligaments. The use of fine wire EMG may be useful in the validation of muscle activation patterns and force estimations of this model. The main application of this model will lay in the evaluation of musculoskeletal loading during gait. In most orthopaedic conditions, joint loading plays an important role in the pathophysiology and progression of the disease. An improved understanding of joint loading and generated muscle forces, in normal and pathological conditions, will aid in the understanding of both normal and abnormal gait patterns and their causative orthopaedic conditions.

REFERENCES

1. Agostinho FS, Rahal SC, Miqueleto NSML, et al: Kinematic analysis of Labrador Retrievers and Rottweilers trotting on a treadmill. Veterinary and Comparative Orthopaedics and Traumatology 24:185-191, 2011.

2. Bertram JEA, Lee DV, Case HN, et al: Comparison of the trotting gaits of Labrador Retrievers and Greyhounds. American Journal of Veterinary Research 61:832-838, 2000.

3. Voss K, Imhof J, Kaestner S, et al: Force plate gait analysis at the walk and trot in dogs with low-grade hindlimb lameness. Veterinary and Comparative Orthopaedics and Traumatology 20:299-304, 2007.

4. Holler PJ, Brazda V, Dal-Bianco B, et al: Kinematic motion analysis of the joints of the forelimbs and hind limbs of dogs during walking exercise regimens. American Journal of Veterinary Research 71:734-740, 2010.

5. Nielsen C, Stover SM, Schulz KS, et al: Two-dimensional link-segment model of the forelimb of dogs at a walk. American Journal of Veterinary Research 64:609-617, 2003.

6. Ragetly CA, Griffon DJ, Mostafa AA, et al: Inverse Dynamics Analysis of the Pelvic Limbs in Labrador Retrievers With and Without Cranial Cruciate Ligament Disease. Veterinary Surgery 39:513-522, 2010.

7. Shahar R, Banks-Sills L: A quasi-static three-dimensional, mathematical, three-body segment model of the canine knee. Journal of Biomechanics 37:1849-1859, 2004.

8. Giarmatzis G, Jonkers I, Wesseling M, et al: Loading of Hip Measured by Hip Contact Forces at Different Speeds of Walking and Running. Journal of Bone and Mineral Research 30:1431-1440, 2015.

9. Lenaerts G, De Groote F, Demeulenaere B, et al: Subject-specific hip geometry affects predicted hip joint contact forces during gait. Journal of Biomechanics 41:1243-1252, 2008.

10. Moissenet F, Cheze L, Dumas R: A 3D lower limb musculoskeletal model for simultaneous estimation of musculo-tendon, joint contact, ligament and bone forces during gait. Journal of Biomechanics 47:50-58, 2014.

11. Erdemir A, McLean S, Herzog W, et al: Model-based estimation of muscle forces exerted during movements. Clinical Biomechanics 22:131-154, 2007.

12. Bosmans L, Jansen K, Wesseling M, et al: The role of altered proximal femoral geometry in impaired pelvis stability and hip control during CP gait: A simulation study. Gait & Posture 44:61-67, 2016.

13. Lerner ZF, Browning RC: Compressive and shear hip joint contact forces are affected by pediatric obesity during walking. Journal of Biomechanics 49:1547-1553, 2016.

14. Prinold JAI, Mazza C, Marco R, et al: A Patient-Specific Foot Model for the Estimate of Ankle Joint Forces in Patients with Juvenile Idiopathic Arthritis. Annals of Biomedical Engineering 44:247-257, 2016.

15. Baert IAC, Jonkers I, Staes F, et al: Gait characteristics and lower limb muscle strength in women with early and established knee osteoarthritis. Clinical Biomechanics 28:40-47, 2013.

16. Wesseling M, Meyer C, Corten K, et al: Does surgical approach or prosthesis type affect hip joint loading one year after surgery? Gait & Posture 44:74-82, 2016.

17. Li JY, Redmond AC, Jin ZM, et al: Hip contact forces in asymptomatic total hip replacement patients differ from normal healthy individuals: Implications for preclinical testing. Clinical Biomechanics 29:747-751, 2014.

18. Overend TJ, Cunningham DA, Paterson DH, et al: Antropometric and computed tomographic assessment of the thigh in young and old men. Canadian Journal of Applied Physiology 18:263-273, 1993.

19. Ragetly CA, Griffon DJ, Thomas JE, et al: Noninvasive determination of body segment parameters of the hind limb in Labrador Retrievers with and without cranial cruciate ligament disease. American Journal of Veterinary Research 69:1188-1196, 2008.

20. Amit T, Gomberg BR, Milgram J, et al: Segmental inertial properties in dogs determined by magnetic resonance imaging. Veterinary Journal 182:94-99, 2009.

21. Seireg A, Arkivar RJ: A mathemathical model for evaluation of forces in lower extremities of the musculo-skeletal system. Journal of Biomechanics 6:313-326, 1973.

22. Crowninshield RD, Johnston RC, Andrews JG, et al: Biomechanical investigation of the human hip. Journal of Biomechanics 11:75-85, 1978.

23. Brand RA, Crowninshield RD, Wittstock CE, et al: A model of lower-extremity muscular anatomy Journal of Biomechanical Engineering-Transactions of the Asme 104:304-310, 1982.

24. de Zee M, Hansen L, Wong C, et al: A generic detailed rigid-body lumbar spine model. Journal of Biomechanics 40:1219-1227, 2007.

25. Hazewinkel HAW, Goedegebuure SA, Poulos PW, et al: Influences of chronic calcium excess on the skeletal development of growing Great Danes. Journal of the American Animal Hospital Association 21:377-391, 1985.

26. Ytrehus B, Carlson CS, Ekman S: Etiology and pathogenesis of osteochondrosis. Veterinary Pathology 44:429-448, 2007.

27. van Ee RT, Gibson K, Roberts ED: Osteochondritis dissecans of the lateral ridge of the talus in a dog. Journal of the American Veterinary Medical Association 193:1284-1286, 1988.

28. Gielen I, van Ryssen B, van Bree H: Computerized tomography compared with radiography in the diagnosis of lateral trochlear ridge talar osteochondritis dissecans in dogs. Veterinary and Comparative Orthopaedics and Traumatology 18:77-82, 2005.

29. Kuroki K, Cook JL, Stoker AM, et al: Characterizing osteochondrosis in the dog: potential roles for matrix metalloproteinases and mechanical load in pathogenesis and disease progression. Osteoarthritis and Cartilage 13:225-234, 2005.

30. Dingemanse W, Gielen I, Duchateau L, et al: Comparison of morphological and clinical features between medial and lateral trochlear ridge talar osteochondrosis dissecans in dogs. Veterinary Surgery:340-345, 2013.

31. Dingemanse W, Muller-Gerbl M, Jonkers I, et al: Subchondral bone density distribution of the talus in clinically normal Labrador Retrievers. BMC Veterinary Research 12, 2016.

32. Frost HM: The Utah paradigm of skeletal physiology: an overview of its insights for bone, cartilage and collagenous tissue organs. Journal of Bone and Mineral Metabolism 18:305-316, 2000.

33. Turner CH: Three rules for bone adaptation to mechanical stimuli. Bone 23:399-407, 1998.

34. Madore E, Huneault L, Moreau M, et al: Comparison of trot kinetics between dogs with stifle or hip arthrosis. Veterinary and Comparative Orthopaedics and Traumatology 20:102-107, 2007.

35. Colborne GR, Innes JF, Comerford EJ, et al: Distribution of power across the hind limb joints in Labrador Retrievers and Greyhounds. American Journal of Veterinary Research 66:1563-1571, 2005.

36. Tomlinson J, Fox D, Cook JL, et al: Measurement of femoral angles in four dog breeds. Veterinary Surgery 36:593-598, 2007.

37. Colborne GR: Bringing canine biomechanics research out of the dark ages. Veterinary Journal 173:469-470, 2007.

38. Delp SL, Anderson FC, Arnold AS, et al: OpenSim: open-source software to create and analyze dynamic Simulations of movement. Ieee Transactions on Biomedical Engineering 54:1940-1950, 2007.

39. Fu YC, Torres BT, Budsberg SC: Evaluation of a three-dimensional kinematic model for canine gait analysis. American Journal of Veterinary Research 71:1118-1122, 2010.

40. Barone R: Anatomie Comparèe des mammifères domestiques. Tome 2: Arthrologie et myologie. Paris, 2000.

41. Shahar R, Milgram A: Morphometric and anatomic study of the hind limb of a dog. American Journal of Veterinary Research 62:928-933, 2001.

42. Delp SL, Loan JP: A Graphics-Based Software System to Develop and Analyze Models of Musculoskeletal Structures. Computers in Biology and Medicine 25:21-34, 1995.

43. Delp SL, Loan JP, Hoy MG, et al: An Interactive Graphics-Based Model of the Lower-Extremity to Study Orthopedic Surgical-Procedures. Ieee Transactions on Biomedical Engineering 37:757-767, 1990.

44. Delp SL, Loan JP: A computational framework for simulating and analyzing human and animal movement. Computing in Science & Engineering 2:46-55, 2000.

45. Close RI: Dynamic Properties of Mammalian Skeletal-Muscles. Physiological Reviews 52:129-&, 1972.

46. Maganaris CN, Baltzopoulos V, Ball D, et al: In vivo specific tension of human skeletal muscle. Journal of Applied Physiology 90:865-872, 2001.

47. Lu TW, O'connor JJ: Bone position estimation from skin marker co-ordinates using global optimisation with joint constraints. Journal of Biomechanics 32:129-134, 1999.

48. Headrick JF, Zhang SN, Millard RP, et al: Use of an inverse dynamics method to describe the motion of the canine pelvic limb in three dimensions. American Journal of Veterinary Research 75:544-553, 2014.

49. Brown NAT, Pandy MG, Kawcak CE, et al: Force- and moment-generating capacities of muscles in the distal forelimb of the horse. Journal of Anatomy 203:101-113, 2003.

50. Bergmann G, Deuretzbacher G, Heller M, et al: Hip contact forces and gait patterns from routine activities. Journal of Biomechanics 34:859-871, 2001.

51. Modenese L, Phillips ATM, Bull AMJ: An open source lower limb model: Hip joint validation. Journal of Biomechanics 44:2185-2193, 2011.

52. Valentin S, Zsoldos RR: Surface electromyography in animal biomechanics: A systematic review. Journal of Electromyography and Kinesiology 28:167-183, 2016.

53. Thelen DG: Adjustment of muscle mechanics model parameters to simulate dynamic contractions in older adults. Journal of Biomechanical Engineering-Transactions of the Asme 125:70-77, 2003.

54. Schwencke M, Smolders LA, Bergknut N, et al: Soft Tissue Artifact in Canine Kinematic Gait Analysis. Veterinary Surgery 41:829-837, 2012.

55. Conconi M, Castelli VP: Functional Modeling of Human Joints: A Feasibility Study for the Knee. Proceedings of the Asme International Design Engineering Technical Conferences and Computers and Information in Engineering Conference 4:12-14, 2014.

56. Conconi M, Leardini A, Parenti-Castelli V: Joint kinematics from functional adaptation: A validation on the tibio-talar articulation. Journal of Biomechanics 48:2960-2967, 2015.

CHAPTER ELEVEN

Future Perspectives:

Evaluation of Joint Loading Distribution in the Tarsocrural Joint by means of Finite Element Modeling

BACKGROUND

With finite-element analysis (FEA) the mechanical behaviour of complex biological structures can be studied. It can provide an approximation of the strains and stresses in structures with complex geometry by dividing it into smaller elements with a simple geometry [1,2]. Stress (σ) is the force per unit area (F/A), while strain (ε) is the deformation that is the result of the loading force (measured in N) and is defined as ($\Delta L/L$) [2,3]. Bones have the ability to adapt to their mechanical environment, influencing the bone material properties. Bone modeling and remodeling is guided by the loading of bones and the resulting local stresses and strains. This ability to adapt is generally summarized as 'bone functional adaptation' and implies the organisms' ability to adapt the supporting structure, i.e. bones, to environmental changes and the ability of bone cells to respond to local changes in biomechanical loading [3,4].

The bone material properties, with the most important ones being Young's modulus and Poisson's ratio), together with structural parameters, such as trabecular orientation, determine the resulting magnitude, direction and orientation of the local strains and stresses [3]. The material properties itself are influenced by bone mineral density, collagen content, and ash fraction [5].

As the relationship between structural and functional characteristics is an important aspect of musculoskeletal research [6], FEA has been applied to various different research topics in this area such as canine hip implants and equine hoof biomechanics [7,8]. It has the potential to greatly improve our understanding of the form-function relationship and mechanism of injury in for instance fracture pathology [9]. Similarly, when evaluating the role of biomechanical loading in the development of osteochondrosis, FEA can provide valuable information.

The aim of the development of a breed-specific finite element model of the canine tarsocrural joint is to evaluate the stress and strain distribution in the cartilage and

subchondral bone of the talus in the Labrador Retriever. These distributions can be related to the location of OC lesions in the tarsocrural joint.

Additionally, the effect of OC lesions on the stress and strain distribution can be evaluated, and can possibly explain the subchondral bone density distribution of the talus seen in dogs with tarsocrural OC.

FINITE ELEMENT MODEL OF THE CANINE TARSOCRURAL JOINT

Geometry

Geometry was derived from a microCT study of the distal tibia, tarsal bones and proximal metatarsal bones of a healthy Labrador Retriever cadaver, euthanized for reason unrelated to this study.

The sample was scanned in a custom built cone beam micro CT. The source object distance was 457 mm and the source detector distance was 1390 mm. The resulting voxel size was 0.065411 mm. A total of 1806 images were reconstructed with an average scanning time of 1.188 s per slice.

Images were exported as TIF-images and loaded into Mimics (Mimics software, Materialise, Leuven, BE). All the skeletal elements were segmented individually using a combination of thresholding and manual segmentation, and were exported as STL files (Figure 1).

FE mesh and material properties

The STL files were loaded into 3-Matic (Materialise 3-Matic, Materialise, Leuven, BE) to convert the STL files to a surface mesh. The articular cartilage mesh for the talus and tibia was manually created in 3-Matic using local offset parameters. The offset was determined by mapping the distance between the subchondral bone plate of the distal tibia and the trochlear ridges of the talus. The cartilage thickness (0.8 mm) was modelled with a homogeneous thickness set to 50 % of the average value of this distance.

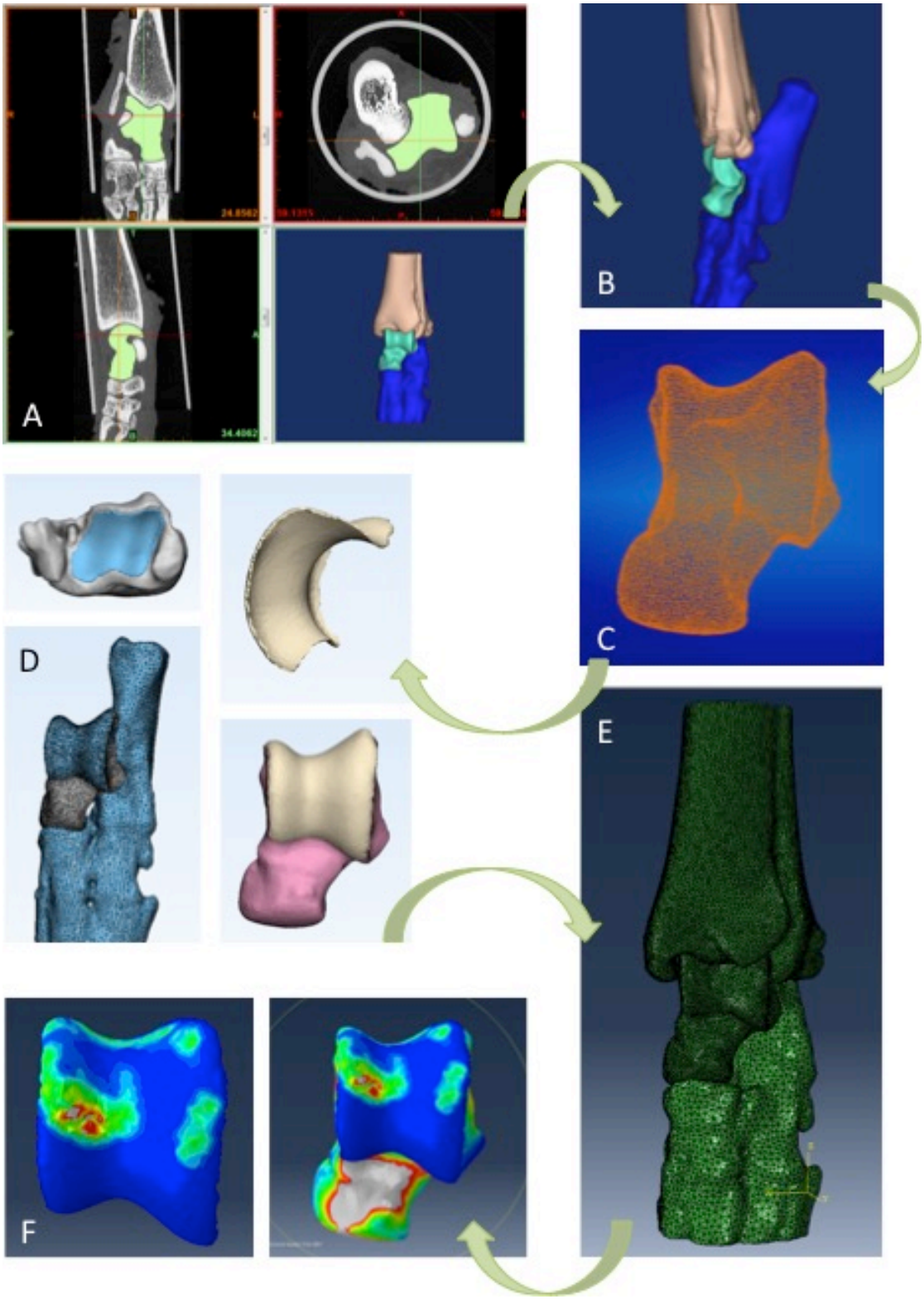

Figure 1. The workflow used in the creation of the breed-specific FE model of the tarsocrural joint. A) Segmentation of micro-CT images and creation of 3D models of the individual parts. B) Full 3D model of the tarsocrural joint. C) Creation of surface meshes from the 3D geometry. D) Creation of cartilage meshes of the talus and distal tibia. E) The final finite element model. F) Preliminary results after the application of a 600 Newton load from the distal tibia to the talus.

This resulted in 5 parts i.e. talus, talus cartilage, tibia, tibia cartilage, and tarsus. The tarsus part incudes all tarsal and metatarsal bones, except the talus. The surface mesh for all the parts except the tarsus were made with an edge length of 1 mm, for the tarsus an edge length of 3 mm was used, to reduce the amount of elements in the volume mesh.

The surface meshes were exported as neutral files and loaded into Patran (Patran, MSC Software, Newport Beach, CA, USA) to create solid volume meshes (Table 1). All meshes were generated using Tet4 elements and exported as Abaqus input files.

Table 1. Different parts of the FE model and the number of elements included.

Part	Number of elements	Type of elements
Talus	117666	Tet4
Talus cartilage	9470	Tet4
Tibia	350970	Tet4
Tibia cartilage	5087	Tet4
Tarsus	95958	Tet4

These volume meshes were imported into Abaqus (Simulia, Providence, RI, USA) where the model was assembled, consisting of all 5 parts. Bone and cartilage were each assigned specific material properties (Table 2) and were modelled as isotropic, homogeneous elastic material.

Table 2. Material properties used in the FE model.

Structure	Young's modulus	Poison's ratio
Bone	17000	0.3
Cartilage	15	0.45

Boundary conditions

The tarsus was modelled as a solid with movement restricted in all directions. The movement of the distal tibia was restricted to rotation and translation along the longitudinal axis (proximal-distal). Contact was modeled between the tibia and tibial

cartilage, the tibial and talus cartilage, the talus cartilage and talus, and the talus and tarsus, and a slave and master surface were defined for each contact set.
The contact conditions for the tibia and tibial cartilage and talus and talus cartilage were set as surface to surface contact with a tied surface. During the creation of the surface meshes, care was taken to match the surface mesh of the adjacent surfaces to get a perfectly matched surface for these surface pairs. The contact pair of the tibia and talus cartilage were adjusted for overclosure (penetration of the slave surface into the master surface) and the slave surface (tibia cartilage) was adjusted to remove any overclosure. The distal talus was tied to the opposite contact area (central tarsal bone), with an adjustment limit of 1 mm, to avoid a non-contact area, as no cartilage was modeled in this region.

The loading conditions on the hock joint can be derived from musculoskeletal models, as described in Chapter 8. Both the joint contact force and the individual muscle forces can be applied to the FE model. Since all forces are vectors, not only a magnitude but also a point of action and direction has to be incorporated. All these parameters can be derived from the musculoskeletal model.

CHAPTER 11

DISCUSSION AND FUTURE PERSPECTIVES

When completely operational, the finite element model presented here offers the opportunity to study the effect of different loading conditions on the stress and strain distribution at the level of the subchondral bone and cartilage.

However, extensive sensitivity testing of parameters such as material properties, boundary conditions and loading conditions is necessary before the model can be applied to answer the research questions it was designed for. Sensitivity analysis is aimed at identifying and quantifying the effect of parameter variation. There will always be uncertainties within the model, compared to the true biological system it is modelled after, and sensitivity analysis can show the effect of these input uncertainties on the model output [10].

Several potential sources of inaccuracy can be identified when it comes to the development of FE models, especially with the application of joint biomechanics and orthopaedic research [11].
Firstly the geometry has to be accurately represented. Geometry is generally derived from CT images and the FE mesh should accurately describe the bone geometry [12,13].
A finer mesh usually allows for more accurate mesh geometry. The mesh used in the current FE model has an average edge length of 1 mm allowing sufficient anatomical detail.

Secondly, the mechanical behaviour has to be modelled adequately [11,14]. The mechanical behaviour, reflected in the material properties, is one of the most important input parameters and is the subject of numerous research papers [14-18]. It can range from simple isotropic material properties to complex anisotropic properties, and can be modelled with regional variations [2,6,15]. The assignment of bone material properties can be done in three different ways, i.e. homogenous, cortical and trabecular bone, and heterogenous material properties [17,18]. The latter is often based on CT Hounsfield Units (HU), and expressed as a linear relationship between bone density and the elastic modulus (Young's modulus) [19]. Although such

linear relationship equations have not been described for canine bone, equations from human biomechanics can be used. In the current model, the use of HU based equations is not possible because the microCT scan output is in TIFF images, not containing the density values like the classic DICOM format from conventional CT scanners. Thus for this model, the assignment of material properties is restricted to either completely homogenous material or separation of cortical and trabecular bone.

The modeling approach when it comes to the elastic properties of the model depends on the research question. The goal here is to analyse gross patterns of deformity and therefore a relatively coarse approach is adequate. However, to progress to quantitative analysis of stress and strain data, more precise modeling is required [15].

Thirdly, the boundary conditions applied to the model have to accurately reproduce the kinematic restrictions from ligaments, and loading conditions from the joint and muscle forces [11,20]. The central application of FE modeling in biomechanical research is to evaluate the (elastic) behaviour of a structure under specific loading conditions [6]. For joints, these loading conditions include joint contact forces and muscle forces. For muscle forces, the point of application depends on the insertion area and fiber orientation of the muscle. The most accurate, yet complex approach would be to model muscle fibers and to spread the load over the entire origin and insertion [2]. However, to start, muscles can be incorporated with a point of origin and insertion, and the direction of the applied force follows the line connecting the origin and insertion of the specific muscle. These data can be derived from the musculoskeletal model (Chapter 8). Similarly the load magnitude can be divided over different muscle parts of even muscle fibers, but as a first step load magnitudes as estimated from the static optimization of the musculoskeletal model can be used as input for the FE model.

And lastly, the volume mesh and the shape of the elements have to allow the numerical solution to the FE problem [10,11,21]. For the current model, the meshing and modeling of contact-pairs has proven to be challenging, especially at the cartilage-cartilage interface between the distal tibia and proximal talus. All volume meshes in the model are constructed with four node tetrahedron (tet4) elements. However, the current contact definitions do not prevent the development of unfavorable, distorted element configurations leading to a disturbance in the numerical accuracy of the model [11,21]. Material properties of the cartilage will also play an important role in the contact behaviour at this level so systematic sensitivity testing is indicated here.

REFERENCES

1. Marinescu R, Daegling DJ, Rapoff AJ: Finite-element modeling of the anthropoid mandible: The effects of altered boundary conditions. Anatomical Record Part A-Discoveries in Molecular Cellular and Evolutionary Biology 283A:300-309, 2005.

2. Richmond BG, Wright BW, Grosse L, et al: Finite element analysis in functional morphology. Anatomical Record Part a-Discoveries in Molecular Cellular and Evolutionary Biology 283A:259-274, 2005.

3. Rayfield EJ: Finite element analysis and understanding the biomechanics and evolution of living and fossil organisms, in Annual Review of Earth and Planetary Sciences, Vol 35. Palo Alto, Annual Reviews, 2007, pp 541-576.

4. Ruff C, Holt B, Trinkaus E: Who's afraid of the big bad wolff? "Wolff is law" and bone functional adaptation. American Journal of Physical Anthropology 129:484-498, 2006.

5. van der Meulen MCH, Jepsen KJ, Mikic B: Understanding bone strength: Size isn't everything. Bone 29:101-104, 2001.

6. Ross CF: Finite element analysis in vertebrate biomechanics. Anatomical Record Part a-Discoveries in Molecular Cellular and Evolutionary Biology 283A:253-258, 2005.

7. Panagiotopoulou O, Rankin JW, Gatesy SM, et al: A preliminary case study of the effect of shoe-wearing on the biomechanics of a horse's foot. Peerj 4, 2016.

8. Shahar R, Banks-Sills L, Eliasy R: Mechanics of the canine femur with two types of hip replacement stems - Finite element analysis. Veterinary and Comparative Orthopaedics and Traumatology 16:145-152, 2003.

9. Harrison SM, Whitton RC, Kawcak CE, et al: Evaluation of a subject-specific finite-element model of the equine metacarpophalangeal joint under physiological load. Journal of Biomechanics 47:65-73, 2014.

10. Viceconti M, Olsen S, Nolte LP, et al: Extracting clinically relevant data from finite element simulations. Clinical Biomechanics 20:1010-1010, 2005.

11. Viceconti M, Davinelli M, Taddei F, et al: Automatic generation of accurate subject-specific bone finite element models to be used in clinical studies. Journal of Biomechanics 37:1597-1605, 2004.

12. Prevrhal S, Engelke K, Kalender WA: Accuracy limits for the determination of cortical width and density: the influence of object size and CT imaging parameters. Physics in Medicine and Biology 44:751-764, 1999.

13. Gelaude F, Sloten JV, Lauwers B: Accuracy assessment of CT-based outer surface femur meshes. Computer Aided Surgery 13:188-199, 2008.

14. Kopperdahl DL, Morgan EF, Keaveny TM: Quantitative computed tomography estimates of the mechanical properties of human vertebral trabecular bone. Journal of Orthopaedic Research 20:801-805, 2002.

15. Strait DS, Wang Q, Dechow PC, et al: Modeling elastic properties in finite element analysis: How much precision is needed to produce an accurate model? Anatomical Record Part a-Discoveries in Molecular Cellular and Evolutionary Biology 283A:275-287, 2005.

16. Cheung JTM, Zhang M, Leung AKL, et al: Three-dimensional finite element analysis of the foot during standing - a material sensitivity study. Journal of Biomechanics 38:1045-1054, 2005.

17. Taddei F, Cristofolini L, Martelli S, et al: Subject-specific finite element models of long bones: An in vitro evaluation of the overall accuracy. Journal of Biomechanics 39:2457-2467, 2006.

18. Schileo E, Dall'Ara E, Taddei F, et al: An accurate estimation of bone density improves the accuracy of subject-specific finite element models. Journal of Biomechanics 41:2483-2491, 2008.

19. Xin PF, Nie PL, Jiang B, et al: Material Assignment in Finite Element Modeling: Heterogeneous Properties of the Mandibular Bone. Journal of Craniofacial Surgery 24:405-410, 2013.

20. Stolk J, Verdonschot N, Huiskes R: Hip-joint and abductor-muscle forces adequately represent in vivo loading of a cemented total hip reconstruction. Journal of Biomechanics 34:917-926, 2001.

21. Polgar K, Viceconti M, O'Connor JJ: A comparison between automatically generated linear and parabolic tetrahedra when used to mesh a human femur. Proceedings of the Institution of Mechanical Engineers Part H-Journal of Engineering in Medicine 215:85-94, 2001.

CHAPTER TWELVE

General Discussion

GENERAL DISCUSSION

The general aim of this PhD is to gain more insight in the role of biomechanical loading in the development of osteochondrosis in dogs. Due to feasibility reasons, the majority of this work focuses on the tarsocrural joint. Two complementary methods were used to evaluate joint loading in the tarsocrural joint: 1) an indirect method through the evaluation of subchondral bone density distribution using CTOAM, and 2) a direct method through the evaluation of joint loading and joint loading distribution using musculoskeletal modeling, dynamic motion analysis, and finite element analysis (**Chapter 4**).

The central hypothesis states that biomechanical loading plays a central role in the onset of OC, therefore a strong correlation will be found between a high, experimentally determined subchondral bone density, high model-based strains during locomotion, and the location of OC lesions.

A disruption in the enchondral ossification is considered to be the main pathogenesis of canine OC [1-3]. The primary event is most likely a local disruption of the epiphyseal cartilage canals during growth, leading to ischemic necrosis of the growth cartilage [1]. In pigs it has been found that the location of cartilage canal necrosis is at the cartilage-bone interface. It is in this region, where the cartilage canals cross the enchondral ossification front, that the cartilage canals vessels are most vulnerable, and this might lead to damage of the cartilage canal vessels and subsequent cartilage canal necrosis [4-6].

The local disruption and subsequent ischemic necrosis also explains the site specificity of osteochondrosis lesions [1]. This site specificity is also seen within the canine tarsocrural joint, where OC lesions can be divided in medial trochlear ridge tarsocrural osteochondrosis (MTRT-OC) and lateral trochlear ridge tarsocrural osteochondrosis (LTRT-OC). Although both MTRT-OC and LTRT-OC are considered to be osteochondral lesions, there are several clinical and morphological differences. Most important is the difference in size (length, depth, and width), where LTRT-OC

lesions are larger compared to MTRT-OC lesions, in addition to a larger variation in size seen in LTRT-OC lesions (**Chapter 3**).

The focal nature and site-specific lesions indicate that joint specific parameters such as joint conformation and joint biomechanics likely play a role in the pathogenesis of canine OC. However, *in vivo* evaluation of joint biomechanics is very difficult and studies addressing this subject in canine veterinary literature are scarce. The use of CTOAM can aid in the understanding of local joint biomechanics, as the subchondral bone density distribution is highly correlated with the joint loading distribution [7]. The identification of areas that undergo higher loading, will aid in the understanding of the site-specificity of canine osteochondrosis. Repeated bone strains can cause microscopic damage: if the strains exceed the repair threshold, the damage can no longer be repaired by remodeling, and starts to accumulate [8]. Thus micro damage or micro trauma is more likely to occur in areas that undergo higher loads, as these have a higher chance of exceeding the repair threshold. Secondly, the site specificity of osteochondral lesions can, in part, be attributed to the morphology and development of cartilage canals in young animals [6]. In foals and piglets, the deep parts of the epiphyseal cartilage are most susceptible to necrosis, as the superficial cartilage canals show normal chondrification even after transection [5,6].

The application of CTOAM to the tarsocrural joint of healthy Labrador Retrievers shows regional differences in subchondral bone density distribution on the articular surface of the talus, consistent between different dogs of the same breed. Two density maxima, one at the proximal part of the medial trochlear ridge, and one more distally on the lateral trochlear ridge characterise the density distribution of the talus. In addition, the apparent density of the lateral trochlear ridge is higher than the apparent density of the medial trochlear ridge (**Chapter 5**). This difference is most likely due to joint anatomy and the increased loads on the lateral trochlear ridge, which is more pronounced in dogs. Although mechanical limb dominance has been described [9], the subchondral bone density distribution of the talus is symmetrical between left and right joints.

It is important to note that these spatial variations are reflected in the mechanical characteristics of the subchondral bone plate. Indentation testing demonstrates similar regional variations and a high correlation (mean coefficient of variation of 0.89) between the density values and the measured mechanical strength at the indentation points (**Chapter 6**). Between breeds different patterns of subchondral bone density distribution and mechanical strength distribution are seen, most likely due to breed-related differences in joint loading [10].

As changes in density affect the functional properties of the subchondral bone plate, this might play a role in the development of joint pathology such as OC. More specifically, a mismatch in functional properties between the underlying subchondral bone plate and overlying articular cartilage may increase the chance of lesions to the cartilage canals at the chondro-osseous junction, as their response to joint loading will differ. A second way subchondral bone changes can play a role in the development of osteochondrosis is in the progression of subclinical osteochondral lesions to clinical *osteochondrosis dissecans* lesions. This progression is due to rupture of the overlying joint cartilage and the formation of a cartilage flap or loose fragment, and is more likely when the articular cartilage is more vulnerable to loading due to subchondral bone changes [11].

Another clinical characteristic of osteochondrosis is the time frame of 6 to 12 months of age, in which symptoms usually occur [12,13]. Although the initial lesions most likely develop at an earlier age, it is important to note that the lesions occur in a limited time window. This time window coincides with the time that the growth cartilage is receiving its vascular supply from the vessels in the cartilage canals, and damage can lead to avascular necrosis of the cartilage [1]. Thus, the initial stage of the disease, the disturbance of enchondral ossification, also known as *osteochondrosis manifesta*, occurs within a specific time window. However, the progression of an *osteochondrosis manifesta* lesion to a clinical *osteochondrosis dissecans* lesion depends on local biomechanical factors and can occur at a later point in time [11].

As the subchondral bone density distribution reflects the long term loading history, the density distribution can be used to study the loading distribution within a joint non-invasively. When comparing the density distribution at 8 and 22 months in healthy Labrador Retrievers (**Chapter 7**), the location of the density maxima does not differ significantly, implying that the loading distribution remains similar during growth. The 'mismatch' between the onset of clinical signs and the initial development of the OC lesions is explained by the fact that initial formation of OC lesions can occur earlier, and be present as subclinical *osteochondrosis manifesta* lesions, that can progress to clinical osteochondrosis lesions several months later [1,14].

The main change in the period of skeletal maturation is an increase in overall density and maximum density (**Chapter 8**). This is most likely due to increased limb loading caused by an increase in body weight and physical activity. The density distribution itself is formed in the early post-natal months [8,15], so the density distribution found at 8 and 22 months of age is likely a reflection of the final joint loading distribution in the tarsal joint of healthy Labrador Retrievers. This also implies that during the time frame the cartilage canal vessels are most vulnerable to damage, the areas of maximum loading are similar to those found in adult dogs. This supports previous suggestions that biomechanical loading and repetitive micro damage play an important role in the development and progression of canine OC. Additionally, this is the first prospective, long-term follow-up study of subchondral bone density in dogs. Using the non-invasive methodology of CTOAM multiple follow-up studies of the same subjects are possible.

The density maximum on the lateral trochlear ridge is larger and shows more variation compared to the medial trochlear ridge (**Chapter 5**). Interestingly, the LTRT-OC lesions are also larger in comparison with MTRT-OC lesions and display a larger variation in size (**Chapter 3**). Furthermore, when looking at the subchondral bone density distribution, dogs with MTRT-OC lesions show typical changes that can be attributed to a true subchondral bone defect (**Chapter 8**), which is the classic definition of *osteochondrosis dissecans*. In LTRT-OC lesions, a different density distribution is seen, representing a transchondral fracture rather than a true

subchondral bone defect. In humans, transchondral fractures and osteochondrosis lesions of the talus are subsets of osteochondral lesions of the talus (OLT) [16], and a similar classification may be warranted in canine orthopedics.

The differences seen in subchondral bone density distribution between different breeds (**Chapter 9**) highlight that differences in joint loading do exist. The wild *Canidae* that were included in the comparison are the closest living relatives of the domestic dog. These kind of comparative studies can aid in the understanding of joint pathology in general, and the breed predisposition seen in many orthopaedic condition in specific. Since conformation and joint loading are closely connected, and genetic factors influence conformation, knowledge on breed-specific parameters regarding joint loading and conformation can be applied in an attempt to reduce the incidence of certain orthopaedic conditions in specific breeds.

Based on these results, it can be concluded that the location of the OC lesions correlates to density maxima found on the trochlear subchondral bone plate, evaluated by means of CTOAM. Since the subchondral bone density distribution is highly correlated to the long-term joint loading distribution, it is likely that the areas of high density are subjected to higher loading.

The chapters discussed above are based on the application of CTOAM to evaluate subchondral bone density distribution of a joint, which is an indirect way of evaluating joint loading. However, joint loading can also be evaluated directly, using pressure films (invasive technique) or musculoskeletal modeling. The use of musculoskeletal models (**Chapter 10**) provides the opportunity to study canine locomotion in more detail and has the potential to change the way orthopaedic conditions are diagnosed, to aid the veterinary surgeon in decision-making, to prevent certain orthopaedic injuries, and to improve the design of orthopaedic implants, as they can be tailored towards the dogs', or at least breeds', specific biomechanical needs [17]. The *in vivo* study of joint biomechanics have included the evaluation of kinetic and kinematic parameters using marker data and force plates [18-20] and more recently joint moments using inverse dynamics analysis [21-23]. The

transfer of these advanced biomechanical modeling techniques from human to veterinary biomechanical research will allow researchers to evaluate muscle forces and joint contact forces. This provides a direct evaluation of joint loading and will contribute to an improved understanding of normal and pathological gait [17].

The lack of breed-specific biomechanical data is an important aspect that currently holds back the use of advanced biomechanical modelling techniques in canine biomechanical research. Breed-specific biomechanical data should include different normal and abnormal gaits, and the boundaries that exist within different breeds [17]. Breed-related differences have been described in veterinary literature, and show major differences in parameters such as joint kinematics, joint moments, and joint power [10,22]. Although in human medicine gait parameters are variable and change in pathological circumstances, general comparisons of normal and affected joints can more readily be made because of the existence of large databases describing a variety of biomechanical parameters. However something similar in canine biomechanics does not exist. Therefore it is necessary to invest in breed-specific morphologic and biomechanical data, allowing canine biomechanical research to become the valuable tool it has proven to be in human medicine. The reason why breed-specific data is necessary can be understood when looking at the differences in conformation and size between different dog breeds. These have major implications on bone geometry, muscle moment arms, and joint moments [10,24], and therefore joint contact forces (i.e. joint loading). Additionally, standardised methods for the definition of joint angles and reporting of results are necessary, but currently do not exist in veterinary medicine [25]. Comparison of different studies reporting joint angles and joint moments are therefore complicated.

The calculation of joint angles (inverse kinematics) and joint moments (inverse dynamics) (**Chapter 10**) are based on experimental data from markers and force platforms, registering the movements of the different segments (hence, linked-segment model) and associated ground reaction forces (GRF's). In combination with a detailed musculoskeletal model, the data from the inverse kinematics and inverse dynamics can be used to estimate muscle forces and joint contact forces. The

current model allows the estimation of joint contact forces in the hip, stifle, and hock joint. The calculated joint angles and joint moments are similar to previous reports in both timing and magnitude [10,22,25]. For the joint angles, the reported absolute values differ because of differences in the definition of the neutral, or 0 degrees, joint angle. Due to the joint definitions used in the OpenSim model, the stifle joint moments are mirrored in comparison to values reported in literature.

The hip joint contact force curve in dogs shows a plateau just before mid-stance and a peak joint loading of around 2.5 times BW, which is quite similar to humans, where the peak hip contact force is around 2.1 - 2.8 times BW during normal walking [26]. However, in humans two distinct peaks can be seen [27], which were not present in the Labrador Retrievers.

The stifle joint contact force of Labrador Retrievers also shows a single peak around mid-stance of around 4 - 5 times BW. In contrast to humans, no second peak was seen in the stifle contact force curve, and the magnitudes of the peaks at 3 to 4 times BW in humans [27,28] appear to be a bit lower compared to the Labrador Retrievers. The angle of the stifle joint during stance phase is angled more in comparison to humans. To stabilize the joint, co-contraction of stifle flexors and extensors is likely, and will add to the joint contact force.

Further down, at the level of the hock joint, the joint contact force peaks at 2.5 - 3 times BW. In humans, the contact force varies between 2.5 and 3.6 times BW depending on the slope of the surface with 2.7 times BW at level walking [27].

To our knowledge, no published data exists describing the joint contact forces during the stance phase in walking dogs. In horses, joint contact forces in the fetlock joint (metacarpal-phalangeal joint) during walk are around 2-3 times BW, and during trot around 4-5 times BW [29,30]. The quadrupedal gait in both horses and dogs might lead to different joint contact forces compared to bipedal gait. Although the data from horses is from the front limb, they appear to be in the same order of magnitude as the canine hindlimb.

Finite element (FE) modeling allows the evaluation of the local stress and strain distribution at the level of the subchondral bone and cartilage and to relate the tissue-level response to the local mechanical environment it is subjected to during locomotion (**Chapter 11**). The application of FE models in canine biomechanical research has so far been limited to the bone end loads of the canine forelimb, the evaluation of hip prostheses, and fracture management [31-33]. In equine biomechanical research, the main application of FE models has been in the field of (micro)fractures and hoof biomechanics and morphology [34-37]. Also in equine biomechanics, the important message is that the combination of *in vivo* data, combined with computer models, can greatly improve our understanding of form, function and pathology [35,36].

The FE model of the tarsocrural joint presented in this work consists of bone geometry of the distal tibia, tarsal, and proximal metatarsal bones, in addition to cartilage geometry of the distal tibia and proximal talus. The boundary conditions applied to a finite element model are an important part of FE model design, and FE analysis is not possible without them [38]. The method of choice depends on the research question, and currently it is unknown how exactly bones are loaded and constrained *in vivo* [35]. Therefore, assumptions have to be made regarding the loading and constraining conditions. The definition of boundary conditions within a finite element model, especially when looking at clinical applications, requires rigorous sensitivity analysis [35,38]. Future development of the FE model should include sensitivity analysis on parameters such as material properties, different kinematic boundary conditions, and the effect of load application on the FEA results. Kinematic boundary conditions are largely determined by joint shape and ligaments. The incorporation of ligaments will aid in the kinematic boundary conditions of the model, however, these are also subject to sensitivity analysis on their modeling parameters (material properties). Currently, no data exists in literature describing the material properties of canine tarsocrural ligaments, although their functional morphology has been described [39].

The aim of the FE model (**Chapter 11**) was to evaluate the local stresses at the level of the subchondral bone and cartilage after the application of a load, consistent with the joint contact force. The applied loads, or loading conditions, are modeled as vectors and have a point of application, a direction and a magnitude. The applied load in the current model is the maximum joint contact force, as calculated with the musculoskeletal model (Chapter 8). These loading conditions can be combined with muscle forces, which can also be derived from the musculoskeletal model. These are not incorporated in the current model, but will provide a more realistic loading condition of the tarsocrural joint.

Currently there are still some modeling issues mainly regarding the last point discussed in Chapter 10, the numerical solution of the FE problem. The current setup has unfavorable, distorted elements when a load is applied, meaning the current model and applied load cannot reach a numerical solution. However, this is work in progress and with a working, validated model a more definitive answer on the role of biomechanical loading on the development of OC lesions can be formulated.

LIMITATIONS

CTOAM

The main limitation of CTOAM is that the 2D densitogram of the subchondral bone density is representing a 3D volume (voxels of the subchondral bone plate). For more or less flat surfaces, such as the radial head or the tibial plateau, this has no major implications. However, for more curved surfaces, such as the femoral head or the talus, it necessitates the use of multiple views, to allow the evaluation of the entire joint surface. In these cases, the values at the edge of the densitogram have to be interpreted carefully.

However, CTOAM has the major benefit that it is not invasive, and thus can be used in long-term follow-up studies and in patient populations. It allows the monitoring of (altered) joint loading and changes over time, making it an excellent addition to the field of veterinary biomechanics.

Musculoskeletal modeling

The estimations of joint contact forces reported in this work are based on several model assumptions. It is important to realise that to some degree, a computer model will always be a simplification of reality. Although advances in human musculoskeletal research have reached a point that detailed muscle-tendon parameters have been incorporated including temporal changes of these parameters during a full gait cycle, it remains an approximation of a biological system and therefore has its limitations.

For the musculoskeletal model presented here the muscles are assumed to work as an actuator (constant strength muscle model), which is obviously a simplification of the actual muscle function. More detailed methods to model muscle function exist, such as the Hill-type muscle model, but this requires the incorporation of muscle specific parameters such as optimal fiber length, tendon slack length, and pennation angle. These parameters are currently not available in literature and could not be included in the musculoskeletal model. Although this is a limitation, these parameters can be incorporated in the model as they become available.

Human musculoskeletal models can, at least in part, be validated using instrumented prosthetics. The use of instrumented hip prosthetics has provided a database on hip contact forces, which have been used to validate the results of hip biomechanics studies in a variety of experimental set-ups and different scientific aims [40,41]. Additionally, EMG data can also be used in model validation, to compare the model-based predictions of muscle or muscle-group activity to the measured EMG signals during gait. However, due to practical limitations, this was not included in the current study. The goal of the current model was to calculate 'ball-park' values of joint contact forces, and to evaluate the transfer of human biomechanical modeling techniques to veterinary medicine. For clinical use, and more detailed biomechanical research questions, validation studies should be carried out. However, these will be more relevant when muscle specific parameters are incorporated in the model, as these will provide a more realistic way of modeling the force generating capacities of the muscles.

The inclusion of surface EMG (sEMG) during gait analysis can further advance canine musculoskeletal models. Although the use of EMG in canine biomechanical research is still in its infancy, it can be used to validate muscle activation estimations from the musculoskeletal model output [42]. However, standardization protocols of sEMG need to be developed to allow comparison between different subjects and studies [43]. However, because maximum voluntary contraction (MVC), a parameter used in human medicine to normalise EMG signals, is not possible in animals, normalization is a challenge.

Joint definitions are currently simplified, and for the tarsocrural joint the degrees of freedom are limited to flexion and extension. The application of dynamic CT or MRI studies allows the incorporation of more detailed joint definitions based on experimental data, but this was beyond the scope of this work. The metatarsal-phalangeal and interphalangeal joints were locked, mainly because it is very difficult to measure the motion of these individual segments in dogs, encountering practical limitations due to their size. In human biomechanical research, specific foot musculoskeletal models incorporate different degrees of freedom at the subtalar, mid-tarsal, and tarsometatarsal joints [44-46]. Currently no data is available in canine literature on subtalar foot motion during gait, as data collection is challenging and has practical limitations. However, future advances can always be applied to the model and foot joint dynamics can be incorporated.

Finite element modeling

For the implementation of cartilage in the FE model, practical limitations have led to the implementation of a homogenous cartilage thickness, although anatomical studies have shown that cartilage thickness shows spatial variation [47]. However, the implemented cartilage thickness is consistent with reported values. How cartilage thickness, and thickness distribution might influence the resulting strain and stress distribution remains subject to further research.

Although the assignment of material properties is one of the strengths of FE modeling, it is also a very complex matter [38]. Ranging from the simplest isotropic material properties, with one Young's modulus and one Poisson's ratio, to complex anisotropic material properties with 21 independent elastic properties. Additionally, material properties can vary within individual bones [48]. In the FE model described in this work, two different 'materials' were defined, as isotropic materials with one Young's modulus and Poisson's ratio, i.e. bone and cartilage. The material properties used, were taken from literature as general material properties commonly used in vertebrate biomechanics.

FUTURE PERSPECTIVES

The differences in the current state-of-the-art in human musculoskeletal modeling versus veterinary musculoskeletal modeling illustrate the amount of research work that still has to be done in the field of veterinary biomechanical research. Human musculoskeletal modeling has aided in improved understanding of numerous orthopaedic conditions, as well as neurologic conditions with major orthopaedic implications such as cerebral palsy (CP) [41,49,50]. The use of musculoskeletal models in veterinary biomechanical research has the potential to make major contributions to reseach on mechanisms of joint pathology in cranial cruciate ligament rupture, hip dysplasia, and traumatic injuries but also to improved surgical treatment and implants design. Before extensive research projects on pathological gait can be done, knowledge on normal gait variation, and breed-specific gait parameters needs to be extended. Several studies have been looking at the description of joint angles, joint moments, and joint power, either in mixed breed dogs, or comparing different dog species [10,17-19,21,22,25,51]. All these studies highlight the need to invest in breed-specific biomechanical research. The comparison of kinematic and kinetic data from different breeds and evaluating joint contact forces will aid in the understanding of breed-specific gait, and gait abnormalities.

However, before musculoskeletal modeling can be applied to evaluate for instance surgical approaches, validation testing is necessary. Validation studies of human

musculoskeletal models include in vitro cadaver testing, which can also be applied to veterinary musculoskeletal models. The use of EMG can also aid in the validation of musculoskeletal models, although the practical applications may prove to be more challenging in comparison to humans [43]. Instrumented implants are the gold standard in validating joint contact force calculations [26,52], but are most likely out of reach for applications in canine orthopaedic research, at least in the near future.

In recent years, finite element modeling has sparked the interest of a broad research community, with important applications in the field of functional morphology [38,53]. It has been applied to the biting behavior in bats, suture morphology in dinosaurs, and beak evolution in Darwin's finches [54-56]. To investigate the form-function relationship, FE modeling has proven to be an excellent tool [38]. In equine biomechanical research, several publications look at the hoof and lower limb, and the impact of joint biomechanics and anatomy on mechanisms of injury or pathology [34,35,37,57]. Additionally, the results of FE analysis are used to improve training conditions for the equine athletes, very similar as has been done in humans. However, the use of FE models in canine biomechanical research is still in its infancy, and much more research, including detailed sensitivity analysis of parameters such as material properties, boundary conditions and loading conditions, are necessary before any results can be applied in a clinical setting.

Studies on the development of epiphyseal cartilage canals in dogs can elucidate the onset and early stages of OC, and may provide a definitive answer on the role of joint biomechanics in the development of canine osteochondrosis. Damage to the cartilage canals with disruption of the cartilage canal vessels lead to focal avascular necrosis of the epiphyseal cartilage and is considered to be the initiating step in the orthopaedic condition called osteochondrosis [1,6,14]. Studies in pigs and horses have evaluated the development of cartilage canals in different joints, specifically in relation to OC [6,14]. Transection of cartilage canal vessels resulted in ischaemic necrosis and a disturbance of enchondral ossification. The normal process of enchondral ossification at the level of the ischaemic necrosis is delayed compared to the viable growth cartilage [14].

Knowledge on subchondral bone density and density patterns can also form the base of screening protocols for orthopedic disease in dogs. Especially for conditions such as OC, it is likely that subchondral bone changes precede clinical signs. A prerequisite for such screening protocols is extensive knowledge of normal, physiological parameters affecting subchondral bone density and changes associated with pathology. This work presents this data for the tarsocrural joint in Labrador Retrievers (Chapter 4, 6, and 7), and forms the basis for a subchondral bone density based screening protocol for tarsocrural OC in Labrador Retrievers.

Finally, canine models can be used for human OA research. In dogs, clinical OA has similar causes and results in similar signs and symptoms as OA in humans [58]. The canine anterior cruciate ligament transsection (ACLT) – meniscectomy model is widely used as an animal model to study the pathophysiology of human OA [59,60]. The main focus of these studies is on subchondral bone pathology in the early stages of OA [58]. Some studies suggest that subchondral bone changes may even precede cartilage changes in the early stages of OA [61]. Subchondral bone evaluation is commonly done using histology, implying that experimental animals need to be sacrificed during the experiment at different time-point to evaluate temporal changes. Although subchondral bone density evaluation using CTOAM cannot supply all the same parameters as histological evaluation, it does offer the opportunity for longitudinal studies within the same animals. This can not only significantly reduce the amount of experimental animals needed, it can also add important information in cases where only endpoint histomorphometric assessment is possible [58].

CONCLUSION

Although the studies presented in this work do no provide conclusive answers on the role of biomechanical loading in the development of canine osteochondrosis, it does explain the predilection sites of tarsocrural osteochondrosis. The areas of high subchondral bone density are at the exact location where medial trochlear ridge lesions are found. However, not all dogs will develop osteochondrosis, even though the joint loading conditions, evaluated by means of CTOAM, appear to be similar within dogs of the same breed. In this perspective it is important to note that the focal area of avascular necrosis leading to a disruption of enchondral ossification (*osteochondrosis manifesta*) can heal spontaneously [11]. Although this has not yet been described in literature on canine osteochondrosis, it is reported in horses, pigs, and humans [62-64].

High, local joint loading can play a role in the development of OC lesions in two different ways. Firstly it can be the cause of damage to the cartilage canals, usually at the level they cross the enchondral ossification front. Secondly it can cause the progression of *osteochondrosis manifesta* lesions to *osteochondrosis dissecans* lesions, i.e. the rupture of the overlying cartilage and the formation of a cartilage flap. Based on the density distribution, is seems that MTRT-OC and LTRT-OC are two different conditions. However, the exact mechanism how these lesions occur remains subject to further research.

Through a combination of experimental data, such as subchondral bone density distribution, and advanced biomechanical modeling techniques, such as musculoskeletal modeling and finite element modeling, our knowledge on normal and pathological gait and joint loading can be improved. It allows the evaluation of parameters that cannot be measured non-invasively *in vivo*, such as muscle forces and joint contact forces [65-69], although thorough validation studies are necessary before the results can be applied clinically. When practical and technical difficulties are overcome, finite element analysis can provide important new insights in the local effect of joint loading on different articular structures. This will not only help to

understand the general form-function relationship, but also mechanisms of injury and joint pathology.

Joint loading does not only play a role in osteochondrosis, it has also been linked to a variety of other canine orthopaedic conditions, such as cranial cruciate ligament rupture and fragmented coronoid process. However, so far, most canine biomechanical research has been limited to invasive *in vitro* experiments. The use of musculoskeletal models has the potential to change the way orthopaedic conditions are diagnosed, to aid the veterinary surgeon in decision-making, to prevent certain orthopaedic injuries, and to improve the design of orthopaedic implants.

Additionally, the evaluation of subchondral bone density combined with the use of musculoskeletal models and FE models, can play a role in translational research in human OA using canine experimental models. The data collected in this work on normal and physiological changes of subchondral bone density play a key role in the application of CTOAM in canine experimental OA models. This potential CTOAM application can not only reduce the amount of experimental animals, it can also improve the efficacy of such translational studies by providing longitudinal data, instead of being limited to endpoint data.

REFERENCES

1. Ytrehus B, Carlson CS, Ekman S: Etiology and pathogenesis of osteochondrosis. Veterinary Pathology 44:429-448, 2007.

2. Richardson DC, Zentek J: Nutrition and osteochondrosis. Veterinary Clinics of North America-Small Animal Practice 28:115-135, 1998.

3. Ekman S, Carlson CS: The pathophysiology of osteochondrosis. Veterinary Clinics of North America-Small Animal Practice 28:17-29, 1998.

4. Carlson CS, Meuten DJ, Richardson DC: Ischemic Necrosis of Cartilage in Spontaneous and Experimental Lesions of Osteochondrosis. Journal of Orthopaedic Research 9:317-329, 1991.

5. Ytrehus B, Haga HA, Mellum CN, et al: Experimental ischemia of porcine growth cartilage produces lesions of osteochondrosis. Journal of Orthopaedic Research 22:1201-1209, 2004.

6. Olstad K, Ytrehus B, Ekman S, et al: Epiphyseal cartilage canal blood supply to the tarsus of foals and relationship to osteochondrosis. Equine Veterinary Journal 40:30-39, 2008.

7. Müller-Gerbl M, Putz R, Kenn R: Demonstation of subchondral bone density patterns by three-dimensional CT osteoabsorptiometry as a noninvasive method for in vivo assessment of individual long-term stresses in joints. Journal of Bone and Mineral Research 7:411-418, 1992.

8. Frost HM: A 2003 update of bone physiology and Wolff's Law for clinicians. Angle Orthodontist 74:3-15, 2004.

9. Colborne GR: Are sound dogs mechanically symmetric at trot? No, actually. Veterinary and Comparative Orthopaedics and Traumatology 21:294-301, 2008.

10. Colborne GR, Innes JF, Comerford EJ, et al: Distribution of power across the hind limb joints in Labrador Retrievers and Greyhounds. American Journal of Veterinary Research 66:1563-1571, 2005.

11. Mccoy AM, Toth F, Dolvik NI, et al: Articular osteochondrosis: a comparison of naturally-occurring human and animal disease. Osteoarthritis and Cartilage 21:1638-1647, 2013.

12. Gielen I, Van Bree H, Coopman F, et al: The value of computed tomography in the clinical course of canine tarsocrural osteochondrosis. Veterinary Radiology and Ultrasound 253:71-78, 2003.

13. Montgomery RD, Hathcock JT, Milton JL, et al: Osteochondritis dissecans of the canine tarsal joint. Compendium on Continuing Education for the Practicing Veterinarian 16:835-845, 1994.

14. Olstad K, Hendrickson EHS, Carlson CS, et al: Transection of vessels in epiphyseal cartilage canals leads to osteochondrosis and osteochondrosis dissecans in the femoro-patellar joint of foals; a potential model of juvenile osteochondritis dissecans. Osteoarthritis and Cartilage 21:730-738, 2013.

15. Holopainen JT, Brama PAJ, Halmesmaki E, et al: Changes in subchondral bone mineral density and collagen matrix organization in growing horses. Bone 43:1108-1114, 2008.

16. Talusan PG, Milewski MD, Toy JO, et al: Osteochondritis Dissecans of the Talus: Diagnosis and Treatment in Athletes. Clinics in Sports Medicine 33:267-278, 2014.

17. Colborne GR: Bringing canine biomechanics research out of the dark ages. Veterinary Journal 173:469-470, 2007.

18. Agostinho FS, Rahal SC, Miqueleto NSML, et al: Kinematic analysis of Labrador Retrievers and Rottweilers trotting on a treadmill. Veterinary and Comparative Orthopaedics and Traumatology 24:185-191, 2011.

19. Bertram JEA, Lee DV, Case HN, et al: Comparison of the trotting gaits of Labrador Retrievers and Greyhounds. American Journal of Veterinary Research 61:832-838, 2000.

20. Holler PJ, Brazda V, Dal-Bianco B, et al: Kinematic motion analysis of the joints of the forelimbs and hind limbs of dogs during walking exercise regimens. American Journal of Veterinary Research 71:734-740, 2010.

21. Nielsen C, Stover SM, Schulz KS, et al: Two-dimensional link-segment model of the forelimb of dogs at a walk. American Journal of Veterinary Research 64:609-617, 2003.

22. Ragetly CA, Griffon DJ, Mostafa AA, et al: Inverse Dynamics Analysis of the Pelvic Limbs in Labrador Retrievers With and Without Cranial Cruciate Ligament Disease. Veterinary Surgery 39:513-522, 2010.

23. Shahar R, Banks-Sills L: A quasi-static three-dimensional, mathematical, three-body segment model of the canine knee. Journal of Biomechanics 37:1849-1859, 2004.

24. Tomlinson J, Fox D, Cook JL, et al: Measurement of femoral angles in four dog breeds. Veterinary Surgery 36:593-598, 2007.

25. Headrick JF, Zhang SN, Millard RP, et al: Use of an inverse dynamics method to describe the motion of the canine pelvic limb in three dimensions. American Journal of Veterinary Research 75:544-553, 2014.

26. Bergmann G, Deuretzbacher G, Heller M, et al: Hip contact forces and gait patterns from routine activities. Journal of Biomechanics 34:859-871, 2001.

27. Alexander N, Schwameder H: Lower limb joint forces during walking on the level and slopes at different inclinations. Gait & Posture 45:137-142, 2016.

28. Meireles S, De Groote F, Reeves ND, et al: Knee contact forces are not altered in early knee osteoarthritis. Gait & Posture 45:115-120, 2016.

29. Noble P, Lejeune JP, Caudron I, et al: Heel effects on joint contact force components in the equine digit: a sensitivity analysis. Equine Veterinary Journal 42:475-481, 2010.

30. Merritt JS, Davies HMS, Burvill C, et al: Influence of muscle-tendon wrapping on calculations of joint reaction forces in the equine distal forelimb. Journal of Biomedicine and Biotechnology, 2008.

31. Coleman JC, Hart RT, Burr DB: Reconstructed bone end loads on the canine forelimb during gait. Journal of Biomechanics 36:1837-1844, 2003.

32. Shahar R, Banks-Sills L, Eliasy R: Mechanics of the canine femur with two types of hip replacement stems - Finite element analysis. Veterinary and Comparative Orthopaedics and Traumatology 16:145-152, 2003.

33. Shahar R, Shani Y: Fracture stabilization with type II external fixator vs. type I external fixator with IM pin - Finite element analysis. Veterinary and Comparative Orthopaedics and Traumatology 17:91-96, 2004.

34. Jansova M, Ondokova L, Vychytil J, et al: A Finite Element Model of an Equine Hoof. Journal of Equine Veterinary Science 35:60-69, 2015.

35. Panagiotopoulou O, Rankin JW, Gatesy SM, et al: A preliminary case study of the effect of shoe-wearing on the biomechanics of a horse's foot. Peerj 4, 2016.

36. McCarty CA, Thomason JJ, Gordon KD, et al: Finite-Element Analysis of Bone Stresses on Primary Impact in a Large-Animal Model: The Distal End of the Equine Third Metacarpal. Plos One 11, 2016.

37. O'hare LMS, Cox PG, Jeffery N, et al: Finite element analysis of stress in the equine proximal phalanx. Equine Veterinary Journal 45:273-277, 2013.

38. Richmond BG, Wright BW, Grosse L, et al: Finite element analysis in functional morphology. Anatomical Record Part a-Discoveries in Molecular Cellular and Evolutionary Biology 283A:259-274, 2005.

39. Aron DN, Purinton PT: Collateral Ligaments of the Tarsocrural Joint - an Anatomic and Functional-Study. Veterinary Surgery 14:173-177, 1985.

40. Wesseling M, Meyer C, Corten K, et al: Does surgical approach or prosthesis type affect hip joint loading one year after surgery? Gait & Posture 44:74-82, 2016.

41. Bosmans L, Jansen K, Wesseling M, et al: The role of altered proximal femoral geometry in impaired pelvis stability and hip control during CP gait: A simulation study. Gait & Posture 44:61-67, 2016.

42. Wibawa AD, Verdonschot N, Burgerhof JGM, et al: A validation study on muscle activity prediction of a lower limb musculoskeletal model using EMG during normal walking. Proceedings of 2013 3rd International Conference on Instrumentation, Communications, Information Technology, and Biomedical Engineering (Icici-Bme):260-264, 2013.

43. Valentin S, Zsoldos RR: Surface electromyography in animal biomechanics: A systematic review. Journal of Electromyography and Kinesiology 28:167-183, 2016.

44. Nichols JA, Roach KE, Fiorentino NM, et al: Predicting tibiotalar and subtalar joint angles from skin-marker data with dual-fluoroscopy as a reference standard. Gait & Posture 49:136-143, 2016.

45. Malaquias TM, Silveira C, Aerts W, et al: Extended foot-ankle musculoskeletal models for application in movement analysis. Computer Methods in Biomechanics and Biomedical Engineering 20:153-159, 2017.

46. Bruening DA, Cooney KM, Buczek FL: Analysis of a kinetic multi-segment foot model part II: Kinetics and clinical implications. Gait & Posture 35:535-540, 2012.

47. Brunnberg MM, Engelke E, Gielen IM, et al: Cartilage thickness of the trochlea of the talus, with emphasis on sites predisposed to osteochondrosis dissecans, in clinically normal juvenile and adult dogs. American Journal of Veterinary Research 72:1318-1324, 2011.

48. Peterson J, Dechow PC: Material properties of the human cranial vault and zygoma. Anatomical Record Part a-Discoveries in Molecular Cellular and Evolutionary Biology 274A:785-797, 2003.

49. Kiernan D, Malone A, O'Brien T, et al: "Children with cerebral palsy experience greater levels of loading at the low back during gait compared to healthy controls". Gait & Posture 48:249-255, 2016.

50. Bosmans L, Wesseling M, Desloovere K, et al: Hip Contact Force in Presence of Aberrant Bone Geometry During Normal and Pathological Gait. Journal of Orthopaedic Research 32:1406-1415, 2014.

51. Fu YC, Torres BT, Budsberg SC: Evaluation of a three-dimensional kinematic model for canine gait analysis. American Journal of Veterinary Research 71:1118-1122, 2010.

52. Bergmann G, Bender A, Dymke J, et al: Standardized Loads Acting in Hip Implants. Plos One 11, 2016.

53. Ross CF: Finite element analysis in vertebrate biomechanics. Anatomical Record Part a-Discoveries in Molecular Cellular and Evolutionary Biology 283A:253-258, 2005.

54. Dumont ER, Piccirillo J, Grosse LR: Finite-element analysis of biting behavior and bone stress in the facial skeletons of bats. Anatomical Record Part a-Discoveries in Molecular Cellular and Evolutionary Biology 283A:319-330, 2005.

55. Rayfield EJ: Using finite-element analysis to investigate suture morphology: A case study using large carnivorous dinosaurs. Anatomical Record Part a-Discoveries in Molecular Cellular and Evolutionary Biology 283A:349-365, 2005.

56. Soons J, Herrel A, Genbrugge A, et al: Mechanical stress, fracture risk and beak evolution in Darwin's ground finches (Geospiza). Philosophical Transactions of the Royal Society B-Biological Sciences 365:1093-1098, 2010.

57. Harrison SM, Whitton RC, Kawcak CE, et al: Evaluation of a subject-specific finite-element model of the equine metacarpophalangeal joint under physiological load. Journal of Biomechanics 47:65-73, 2014.

58. Kuroki K, Cook CR, Cook JL: Subchondral bone changes in three different canine models of osteoarthritis. Osteoarthritis and Cartilage 19:1142-1149, 2011.

59. Intema F, Hazewinkel HAW, Gouwens D, et al: In early OA, thinning of the subchondral plate is directly related to cartilage damage: results from a canine ACLT-meniscectomy model. Osteoarthritis and Cartilage 18:691-698, 2010.

60. Brandt KD, Braunstein EM, Visco DM, et al: Anterior (Cranial) Cruciate Ligament Transection in the Dog - a Bona-Fide Model of Osteoarthritis, Not Merely of Cartilage Injury and Repair. Journal of Rheumatology 18:436-446, 1991.

61. Intema F, Sniekers YH, Weinans H, et al: Similarities and Discrepancies in Subchondral Bone Structure in Two Differently Induced Canine Models of Osteoarthritis. Journal of Bone and Mineral Research 25:1650-1657, 2010.

62. Ytrehus B, Grindflek E, Teige J, et al: The effect of parentage on the prevalence, severity and location of lesions of osteochondrosis in swine. Journal of Veterinary Medicine Series a-Physiology Pathology Clinical Medicine 51:188-195, 2004.

63. Cahill BR: Osteochondritis Dissecans of the Knee: Treatment of Juvenile and Adult Forms. J Am Acad Orthop Surg 3:237-247, 1995.

64. Carlson CS, Hilley HD, Meuten DJ, et al: Effect of Reduced Growth-Rate on the Prevalence and Severity of Osteochondrosis in Gilts. American Journal of Veterinary Research 49:396-402, 1988.

65. Brand RA, Crowninshield RD, Wittstock CE, et al: A model of lower-extremity muscular anatomy Journal of Biomechanical Engineering-Transactions of the ASME 104:304-310, 1982.

66. Crowninshield RD, Johnston RC, Andrews JG, et al: Biomechanical investigation of the human hip. Journal of Biomechanics 11:75-85, 1978.

67. Seireg A, Arkivar RJ: A mathemathical model for evaluation of forces in lower extremities of the musculo-skeletal system. Journal of Biomechanics 6:313-326, 1973.

68. Prinold JAI, Mazza C, Marco R, et al: A Patient-Specific Foot Model for the Estimate of Ankle Joint Forces in Patients with Juvenile Idiopathic Arthritis. Annals of Biomedical Engineering 44:247-257, 2016.

69. Lerner ZF, Browning RC: Compressive and shear hip joint contact forces are affected by pediatric obesity during walking. Journal of Biomechanics 49:1547-1553, 2016.

SUMMARY

Osteochondrosis (OC) is a multifactorial orthopaedic condition that is an important cause of lameness in dogs. The exact pathophysiology remains unclear, but several factors indicate that biomechanical loading of the joint plays an important role.

The general aim of this PhD was to gain more insight in the role of biomechanical loading in the development of OC lesions in dogs, more specifically at the level of the tarsocrural joint.

In **Chapter 1**, a general introduction about bone and bone adaptation is given. Additionally, it is explained why subchondral bone density distribution is an interesting parameter to study, and how this can be visualised using CTOAM.

In **Chapter 2**, a review of literature on canine osteochondrosis in general and tarsocrural osteochondrosis in specific was provided. In addition to a general background of tarsocrural OC, different diagnostic techniques, including clinical examination, radiography, CT, and arthroscopy are discussed. The diagnosis of tarsocrural OC is complicated due to superposition of bony structures on radiography, and CT is often needed to obtain a definitive diagnosis. Different treatment options are available, with the arthroscopic removal of the fragment being the surgical method of choice in most cases. The prognosis differs among various cited studies, however, with the use of minimally-invasive technique such as arthroscopy, improvement or full recovery is seen in the majority of cases.

Tarsocrural osteochondrosis can occur on the medial (MTRT-OC) or lateral (LTRT-OC) trochlear ridge. In **Chapter 3**, clinical and morphological parameters were compared between MTRT-OC and LTRT-OC. Clinical parameters included breed, age, gender, weight, and duration of clinical symptoms and morphological data included size, location, and number of fragments as determined by CT. The LTRT-OC lesions were found to be bigger and had a larger variation in size compared to MTRT-OC lesions. Additionally, dogs with LTRT-OC lesions were younger and tended to have a shorter duration of clinical signs before presentation compared to dogs with MTRT-OC. These findings might support existing hypotheses about differences in aetiology

between MTRT-OC and LTRT-OC lesions, with the first one being true OC lesions, in which micro-damage plays in important role, and the latter being traumatic, transchondral fractures, similar to those seen in humans.

To explore the role of biomechanical loading in the development of OC lesions, a combination of non-invasive *in vivo* evaluation of subchondral bone density distribution is combined with advanced biomechanical modeling techniques, more specifically image-based musculoskeletal modeling, dynamic motion analysis and finite element analysis. The scientific aims (**Chapter 4**), were formulated around the central hypothesis of a clear correlation between a high, experimentally determined subchondral bone density, high model based strains, and the location of OC lesions in the tarsocrural joint.

The subchondral bone density is highly correlated with the joint loading distribution and can be used to study joint biomechanics non-invasively. First, subchondral bone density distribution of the talus in healthy Labrador Retrievers was evaluated (**Chapter 5**) as a parameter reflecting the long-term joint loading in the tarsocrural joint. This resulted in a non-homogenous density distribution with two density maxima, one on the proximal aspect of the medial trochlear ridge, and one more distally on the lateral trochlear ridge. No differences were found between left and right limbs, and the subchondral bone density distribution was very similar between different dogs of the same breed. The lateral trochlear ridge had a higher apparent density compared to the medial trochlear ridge, as the lateral trochlear ridge is more pronounced and likely to endure increased loads during gait.

The location of the density maximum on the medial trochlear ridge is the same location where MTRT-OC lesions are found, supporting previous studies suggesting that repetitive micro-damage is an important factor in the development of OC. Additionally, the use of CTOAM in the field of veterinary biomechanics has significant advantages compared to more traditional and invasive techniques used to evaluate joint loading.

To investigate the material properties of the subchondral bone plate, the subchondral bone density was correlated with the strength of the subchondral bone plate determined by indentation testing (**Chapter 6**). High correlations were found between the density values and the measured mechanical strength with a mean r^2 of 0.89. This shows that CTOAM in dogs can be used to evaluate the mechanical strength of the subchondral bone plate, and provides the opportunity to do so in longitudinal studies.

During growth, the supporting skeletal structures mature and continually adapt to the loading conditions. The evaluation of age-dependent changes in subchondral bone density during skeletal maturation (**Chapter 7**), shows a general increase in density with in creasing age. This is expected and most likely an adaptive response to increased bodyweight and physical activity. Interestingly, the subchondral bone density distribution was very similar between 8 months of age and 20 months of age, indicating that the joint loading distribution also remains very similar. So although the overall density increased, the density distribution was preserved over time. This provides important information for the evaluation of subchondral bone density in the tarsocrural joint of Labrador Retrievers.

Because the subchondral bone density distribution is likely to change in case of joint pathology, and joint pathology itself is likely to change joint loading, several dogs with tarsocrural OC were evaluated using CTOAM at the time of diagnosis and in some cases during long-term follow-up (**Chapter 8**). The subchondral lesions show a low density and are surrounded by a high-density ring. Density changes are not limited to the affected joint, as the contralateral joint shows an increase in subchondral bone density. This is most likely a reflection of weight-shift and changes in loadbearing on the hind limbs in dogs with MTRT-OC.

The subchondral bone density differences found between different dog breeds (*Canis familiaris*), and between other *Canidae* (*Canis lupus* and *Canis aureus*), indicate differences in joint loading of the hock joint (**Chapter 9**). For the domestic dogs, these differences can be attributed to conformational differences, which are

especially obvious when comparing Labrador Retrievers and German Shepherds. Differences between domestic dogs and other *Canidae* were also seen, however, how these differences relate to diffences in pelvic limb loading remains subject to further research.

Another way to evaluate joint loading is the use of musculoskeletal modeling. Using a breed-specific musculoskeletal model of the pelvis and hind limbs of a Labrador Retriever, the joint kinematics, kinetics, muscle forces, and joint contact forces were evaluated (**Chapter 10**). Geometry was derived from CT images, and model input came from marker data combined with force-plate data, providing an integrated dataset. Although the current model has several assumptions and limitations, it can be used to explore canine joint loading and can be further refined as more morphological data becomes available.

The combination of musculoskeletal modeling and finite element modeling (**Chapter 11**) provides the opportunity to investigate the strains and stresses at the level of the subchondral bone and articular cartilage. It enables us to evaluate the tissue response to the local mechanical environment and to link the results to joint pathology. Although thorough sensitivity analysis and validation studies are necessary before the model can be applied in a clinical setting, it holds promising results and definitely deserves a place in the field of canine orthopaedic research.

The general discussion is given in **Chapter 12**. The results of the different chapters are discussed in light of the research question of this PhD.

SAMENVATTING

Osteochondrose (OC) is een multifactoriele aandoening en een belangrijke oorzaak van manken bij de hond. De exacte pathofysiologie is nog onduidelijk, maar verschillende factoren wijzen erop dat de biomechanische belasting van het gewricht een belangrijke rol speelt.

In **Hoofdstuk 1** wordt een kort overzicht gegeven van bot en de aanpassingen die op weefselniveau kunnen plaatsvinden. Daarnaast wordt besproken waarom de densiteitsdistributie van het subchondrale bot een interessante parameter is om te bestuderen en hoe we dit door middel van CTOAM kunnen evalueren.

In **Hoofdstuk 2** wordt een literatuur overzicht gegeven van osteochondrose bij de hond in het algemeen, en meer specifiek ter hoogte van het tarsocrurale gewricht. Naast een algemene achtergrond van tarsocrurale OC, komen verschillende diagnostische technieken, zoals klinisch onderzoek, radiografie, CT en arthroscopie aan bod. De diagnose van tarsocrurale OC is moeilijk door de superpositie van de verschillende botten op radiografie, en CT is een veel gevallen noodzakelijk voor een definitieve diagnose. Er zijn verschillende behandelingen, maar arthroscopische verwijdering van het fragment is in de meeste gevallen de beste keus. De prognose varieert naargelang verschillende bronnen, maar met minimaal invasieve technieken, zoals arthroscopie, wordt er verbetering of volledig herstel bekomen in de meerderheid van de gevallen.

Tarsocrurale osteochondrose kan voorkomen op de mediale en laterale taluskam. In **Hoofdstuk 3** worden klinische en morfologische parameters vergeleken tussen mediale en laterale OC letsels. De klinische parameters zijn ras, leeftijd, geslacht, gewicht en duur van de symptomen, en de morfologische parameters zijn grootte, locatie en aantal fragmenten, op basis van de CT beelden. De laterale letsels zijn groter en vertonen een grotere variatie in grootte in vergelijking met de mediale letsels. Daarnaast zijn honden met laterale letsels jonger en hebben ze in veel gevallen minder lang symptomen vooraleer ze worden aangeboden bij de dierenarts. Deze bevindingen zijn in lijn met bestaande hypotheses dat mediale en laterale letsels mogelijk een andere etiologie hebben, waarbij de mediale letsels echte

osteochondrose letsels zijn, waarbij micro-schade een belangrijke rol speelt, en de laterale letsels eerder traumatische, transchondrale fracturen, zoals bij de mens.

Om de rol van biomechanische belasting in het ontstaan van OC letsels te onderzoeken, is er gebruik gemaakt van een combinatie van niet-invasief, *in vivo* onderzoek van de subchondrale bot densiteit in combinatie met geavanceerde biomechanische modelleringstechnieken, meer specifiek muskuloskeletale modellering, dynamische bewegingsanalyse en eindige elementen modellering. De wetenschappelijke doelstellingen (**Hoofdstuk 4**) werden geformuleerd rond de centrale hypothese dat er een duidelijke correlatie bestaat tussen een hoge, experimenteel bepaalde densiteit van het subchondrale bot, hoge modelgebaseerde spanningen, en de locatie van OC letsels in het tarsocrurale gewricht.

Er is een hoge correlatie van de densiteit van het subchondrale bot met de distributie van de gewrichtsbelasting en dit kan gebruikt worden om de gewrichtsbiomechanica op een niet-invasieve manier te bestuderen. Om te beginnen werd de densiteitsdistributie van het subchondrale bot van de talus van gezonde Labrador Retrievers geëvalueerd (**Hoofdstuk 5**). Hieruit bleek dat er een heterogene distributie is van de densiteit, waarbij er twee maxima te onderkennen zijn, een op het proximale aspect van de mediale taluskam, en een op distale aspect van de laterale taluskam. Er werden geen verschillen gevonden tussen linker en rechter talus en de distributie van de densiteit van het subchondral bot was zeer gelijkaardig tussen honden van hetzelfde ras. De laterale taluskam had een hogere densiteit in vergelijking met de mediale taluskam, omdat de laterale taluskam hoger is, en waarschijnlijk een hogere belasting ondergaat tijdens beweging.

De locatie van het densiteitsmaximum is dezelfde als waar de OC letsels op de mediale taluskam worden gevonden, hetgeen eerdere suggesties dat herhaalde micro-schade een belangrijke rol speelt in het ontstaan van OC bevestigd. Daarbij heeft het gebruik van CTOAM in veterinair biomechanisch onderzoek belangrijke voordelen ten opzichte van de meer traditionele en invasieve onderzoekstechnieken om gewrichtsbelasting te evalueren.

De materiaaleigenschappen van de subchondrale beenplaat werden onderzocht door de densiteit van het subchondrale bot te correleren met de mechanische sterkte van het subchondrale bot, door middel van indentatie testen (**Hoofdstuk 6**). Er werden hoge correlaties gevonden tussen de densiteit en de gemeten mechanische sterkte met een gemiddelde r^2 van 0.89. Dit toont aan dat CTOAM bij honden ook gebruikt kan worden voor het evalueren van de mechanische sterkte, en het geeft de mogelijkheid om dit te doen in longitudinale studies vanwege het niet-invasieve karakter van CTOAM.

Tijdens de groei ontwikkelt het skelet zich voortdurend en past zich continue aan, aan de belasting. De leeftijdsafhankelijke verandering van de densiteit van het subchondral bot tijdens het opgroeien (**Hoofdstuk 7**), is voornamelijk een toegenomen densiteit met toenemende leeftijd. Dit is hetgeen we verwachten en is waarschijnlijk een aanpassing aan een hogen lichaamsgewicht en meer fysieke activiteit. Interessant is dat de densiteitsdistributie van het subchondral bot vrijwel gelijk tussen honden van 8 tot 20 maanden. Dit toont aan dat de distributie van de gewrichtsbelasting waarschijnlijk erg gelijkaardig blijft. Dus hoewel de algemene densiteit toeneemt, blijft de densiteitsdistributie behouden. Dit geeft belangrijke informatie voor het evalueren van de densiteit van het subchondrale bot in het tarsocrurale gewricht van Labrador Retrievers.

Omdat het subchondrale bot waarschijnlijk veranderingen ondergaat op vlak van densiteit bij honden met gewrichtspathologie, werden verschillende honden met tarsocrurale OC geëvalueerd door middel van CTOAM op het moment van diagnose, en in enkele gevallen ook op langere termijn (**Hoofdstuk 8**). De letsels hebben een lage densiteit en zijn omringd door een zone met hoge densiteit. De densiteitsveranderingen zijn niet beperkt tot het aangetaste lidmaat, het contralaterale gewricht toont een toename in de densiteit van het subchondrale bot. Dit komt waarschijnlijk door een verandering in steunname op de achterpoten bij honden met MTRT-OC.

De densiteit van het subchondrale bot van de talus verschilt tussen honden van verschillende rassen (*Canis familiaris*), en andere *Canidae* (*Canis lupus* en *Canis aureus*). Dit wijst op verschillen in gewrichtsbelasting van het enkelgewricht (**Hoofdstuk 9**). Bij de hond kunnen de verschillen verklaard worden door verschillen in conformatie. Deze zijn vooral uitgesproken wanneer de vergelijking wordt gemaakt tussen Labrador Retrievers en Duitse Herders. Er warden ook duidelijke verschillen gezien tussen de hond en andere *Canidae*, maar hoe deze verschillen verklaard kunnen worden en gerelateerd kunnen worden aan gewrichtsbelasting van de achterpoot moet nog verder onderzocht worden.

Een andere manier om de gewrichtsbelasting te evalueren is door gebruik te maken van musculoskeletale modellering. Door middel van een ras-specifiek muskuloskeletaal model van het bekken en de achterpoten van een Labrador Retriever, werden de gewrichts-kinematica, -kinetica, spierkrachten en gewrichtscontactkrachten geëvalueerd (**Hoofdstuk 10**). De geometrie is gebaseerd op CT beelden en de kinematische en kinetische input voor het model kwam uit marker-data gecombineerd met krachtenplaten, wat zorgt voor een geïntegreerde dataset. Hoewel er voor het bestaande model een aantal beperkingen zijn, kan het gebruikt worden in verder onderzoek naar gewrichtsbelasting bij de hond en het kan verder worden verfijnd van zodra er meer morfologische data beschikbaar is.

De combinatie van muskuloskeletale modelering en eindige elementen modellering (**Hoofdstuk 11**) zorgt ervoor dat spanningen op het niveau van het subchondrale bot en het overliggende kraakbeen geëvalueerd kunnen worden. Het geeft de mogelijkheid om te kijken naar weefselrespons op basis van de lokale mechanica en daarbij de link te maken met gewrichtspathologie. Hoewel uitgebreide sensitiviteitsanalyses en validatie nodig zijn voordat musculoskeletale modelering en eindige elementen modelering gebruikt kan worden in een klinische setting, zijn de resultaten veelbelovend en verdient het zeker een plek in het onderzoeksgebied van orthopedische aandoeningen bij de hond.

In **hoofdstuk 12** wordt een algemene discussie gegeven. Hierbij worden de resultaten van de verschillende hoofdstukken besproken en gerelateerd met de onderzoeksvraag van dit doctoraat.

BIBLIOGRAPHY

Publications in International Journals

W. Dingemanse, I. Gielen, H. van Bree. Diagnosis and treatment of tarsocrural osteochondrosis in dogs. Vlaams Diergeneeskundig Tijdschrift (Flemish Veterinary Journal) 80. (2011). 223-232.

W. Dingemanse, I. Gielen, L. Duchateau, H. van Bree. Comparison of morphological and clinical features between medial and lateral trochlear ridge talar osteochondritis dissecans in dogs. Veterinary Surgery 42 (2013). 340-345.

N. Smits, I. Gielen, L. Mosselmans, **W. Dingemanse**, T. Bosmans, E. Van der Vekens, B. Van Ryssen. Bilateral osteochondritis dissecans of the lateral trochlear ridge in a young Rottweiler. Vlaams Diergeneeskundig Tijdschrift (Flemish Veterinary Journal) 82 (2013). 275-281.

L. M. De Rycke, I.M. Gielen, **W. Dingemanse**, K. Kromhout, H. van Bree. Computed Tomographic and Low-Field Magnetic Resonance Arthrography: A Comparison of Techniques For Observing Intra-Articular Structures of the Normal Canine Shoulder. Veterinary Surgery 44 (2015). 704-712.

A. Villamonte-Chevalier, H. van Bree, B.J.G. Broeckx, **W. Dingemanse**, M. Soler, B. Van Ryssen, I. Gielen. Assessment of medial coronoid disease in 180 canine lame elbow joints: a sensitivity and specificity comparison of radiographic, computed tomographic and arthroscopic findings. BMC Veterinary Research 11 (2015). 243.

B.J.G. Broeckx, F. Coopman, G. Verhoeven, T. Bosmans, I. Gielen, **W. Dingemanse**, J.H. Saunders, D. Deforce, F. Van Nieuwerburgh. An heuristic filtering tool to identify phenotype-associated genetic variants applied to human intellectual disability and canine coat colors. BMC Bioinformatics 16 (2015). 391.

A. Villamonte-Chevalier, **W. Dingemanse**, B.J. Broeckx, A. Van Caelenberg, A. Agut, L. Duchateau, H. van Bree, I. Gielen. Bone density of elbow joints in Labrador retrievers and Golden retrievers: Comparison of healthy joints and joints with medial coronoid disease. Veterinary Journal 216 (2016). 1-7

W. Dingemanse, M. Müller-Gerbl, I. Jonkers, J. Vander Sloten, H. van Bree, I. Gielen. Subchondral bone density distribution of the talus in clinically normal Labrador Retrievers. BMC Veterinary Research 12 (2016). 56.

B. Dries, I. Jonkers, **W. Dingemanse**, B. Vanwanseele, J. Vander Sloten, H. van Bree, I. Gielen. Musculoskeletal modelling in dogs: Challenges and future perspectives. Veterinary Comparative Orthopaedics and Traumatology 29 (2016) 3. 181-187.

W. Dingemanse, M. Müller-Gerbl, I. Jonkers, J. Vander Sloten, H. van Bree, I. Gielen. A prospective follow up of age related changes in the subchondral bone density of the talus of healthy Labrador Retrievers. BMC Veterinary Research 13 (2016). 57.

C. P. Crijns, H. J. Van Bree, B. J. G. Broeckx, S. Schauvliege, G. Van Loon, A. Martens, K. Vanderperren, **W. B. Dingemanse**, I. M. Gielen. The Influence of the Size, Age and Sex on the Computed Tomographic Measured Size of the Pituitary Gland in Normal Horses. Anatomia, Histologia, Embryologia. 2017.

Publications in Proceedings of International Scientific Meetings

H. van Bree, **W. Dingemanse**, I. Gielen. MRI and arthroscopy for evaluation of shoulder joint pathology. 20th Annual Scientific Meeting, European College of Veterinary Surgery, 8-10 July, 2011, Ghent, Belgium. p. 101-103.

I. Gielen, K. Kromhout, **W. Dingemanse**, H. van Bree. Update on diagnostic imaging in elbow disease. 27th Annual Meeting International Elbow Working Group , April 11th, 2012, Birmingham, UK. p. 13-15.

W. Dingemanse, M. Müller-Gerbl, I. Jonkers, J. Vander Sloten, H. van Bree, I. Gielen. Subchondral bone density of the normal canine talus. 3h CT-User Meeting. Ghent, Belgium. 30th November – 1st December 2013. p. 24.

W. Dingemanse, M. Müller-Gerbl, I. Jonkers, J. Vander Sloten, H. van Bree, I. Gielen. Age-related changes in subchondral bone density in the talus of healthy Labrador Retrievers. EVDI 2014 Conference. Utrecht, the Netherlands. 27th – 30th August, 2014. p. 67.

W. Dingemanse, I. Jonkers, L. Bosmans, M. Müller-Gerbl, J. Vander Sloten, I. Gielen. A three-dimensional musculoskeletal model of the Labrador Retriever (Canis familiaris) pelvis and hind limbs. 25th Congress of the International Society of Biomechanics. Glasgow, UK. 12th-16th July 2015. p. 990-991.

B. Dries, I. Jonkers, W. Van Den Broeck, **W. Dingemanse**, I. Gielen. JSAP5: What scaled canine muscle parameters can tell about their functional properties. International Conference on Canine and Equine Biomechanics, London, UK. 17th-19th August 2016. Journal of Small Animal Practice 57. Supplement S2.

W. Dingemanse, I. Jonkers, M. Müller-Gerbl, L. Bosmans, J. Vander Sloten, I. Gielen. JSAP9: Calculation of muscle forces in Labrador Retriever hind legs during stance. International Conference on Canine and Equine Biomechanics, London, UK. 17th-19th August 2016. Journal of Small Animal Practice 57. Supplement S2.

Presentations

Subchondral bone density distribution of the canine talus. Dingemanse W., Müller-Gerbl M., van Bree H., Gielen I. 3rd International Veterinary CT-User Meeting. 30th November – 1st December, 2013. Poster presentation.

Age-related changes in subchondral bone density in the talus of healthy Labrador Retrievers. EVDI 2014 Conference. Utrecht, the Netherlands. 27th – 30th August, 2014. Oral presentation.

A three-dimensional musculoskeletal model of the Labrador Retriever (Canis familiaris) pelvis and hind limbs. 25th Congress of the International Society of Biomechanics. Glasgow, UK. 12th-16th July 2015. Oral presentation.

Calculation of muscle forces in the Labrador Retriever (Canis familiaris) hind legs during stance. ICEL 8. International Conference on Canine and Equine Biomechanics, London, UK. 17th-19th August 2016. Oral presentation. Awarded with Qualisis award for best oral presentation.

Correlation of subchondral bone density and mechanical strength in the canine talus. Dingemanse W., Müller-Gerbl M., Jonkers I., Vander Sloten J., van Bree H., Gielen I.. 6rd Veterinary CT-User Meeting 2016. Ghent, Belgium. December 9th-10th, 2016. Poster presentation.

Awards

Best oral presentation (Qualisis award)

Calculation of muscle forces in the Labrador Retriever (Canis familiaris) hind legs during stance. ICEL8. International Conference on Canine and Equine Biomechanics, London, UK. 17th-19th August 2016. Oral presentation.

Best poster presentation

Correlation of subchondral bone density and mechanical strength in the canine talus 6rd Veterinary CT-User Meeting 2016. Ghent, Belgium. December 9th-10th, 2016. Poster presentation.

DANKWOORD

De enige tekst die iedereen effectief leest, in plaats van enkel doorheen bladert om naar de plaatjes te kijken, is de tekst die nog het moeilijkst is om te schrijven van allemaal. De voorgaande hoofdstukken zijn het wetenschappelijke resultaat van onze reis van grofweg zes jaar. Onze reis, want het is een reis die ik zeker niet alleen heb gemaakt. Ik heb het geluk gehad om omringd te zijn met een geweldige groep mensen.

Een reis die ook niet mogelijk was geweest zonder de financiele steun van het IWT. Want zoals alle zaken in het leven, ook een doctoraatsonderzoek doen kost geld. Ik ben een van de gelukkigen geweest om een doctoraatsbeurs te behalen, dus via deze weg wilde ik het IWT nog eens expliciet bedanken.

Zoals iedereen kan zien, staan er vier promotoren op de kaft van dit doctoraatsboekje. Mensen met verschillende achtergronden, vanuit verschillende disciplines, en het is juist deze diversiteit van de mensen dat de grote sterkte is van dit project en de reden dat we dit allemaal hebben kunnen bereiken. Een belangrijke naam ontbreekt echter, en daar begin ik dan nu mee.

Professor van Bree, dat uw naam niet op de voorkant van het boekje staat is een groot gemis. U heeft zonder twijfel een van de belangrijkste rollen gespeeld in de ontwikkeling van dit doctoraat en ik ben u enorm dankbaar voor alle kansen die u mij gegeven heeft. Het doctoraat dat hier voor ons ligt is geen op zichzelf staand werk, het is eigenlijk een volledig nieuwe onderzoekslijn, waar heel veel toekomst in zit. En hoewel niet iedereen het zo ziet, ben ik er van overtuigd dat het afronden van dit project zeker niet het einde betekend van dit onderzoek.
De onderzoeksgroep die we de laatste jaren hebben opgebouwd en de mensen die we rondom ons hebben verzameld, is van onschatbare waarde. Met de recente ontwikkelingen, en de samenwerkingen in de rest van Europa en de rest van de wereld, zal al het werk zeker niet verloren gaan. Dat is een van de waarden die we delen en waar we samen voor zullen strijden, dat dit werk niet ergens in de kast belandt en er niet meer naar gekeken wordt.

Beste Piet, bedankt voor uw geloof en vertrouwen in mij. Bedankt om mij de vrijheid te geven om dit project uit te werken en tegelijkertijd de begeleiding en sturing te voorzien die nodig was. Dat u er niet veel om gaf dat uw naam niet op de voorkant van dit boekje staat, siert u, maar ik wilde uw bijdrage zeker niet onopgemerkt voorbij laten gaan.

Dan mijn promotor, dr. Gielen. Beste Dr. Gielen, beste Ingrid, hoeveel ik hier ook schrijf, het zal nooit genoeg zijn om mijn dankbaarheid te beschrijven voor alles wat u voor mij gedaan heeft de afgelopen jaren. U en prof. van Bree hebben mij de kans gegeven om een onderzoeksonderwerp uit te werken rond tarsocrurale osteochondrose bij de hond. Wie had kunnen denken dat het zou uitgroeien tot het doctoraat wat nu voor ons ligt? Het is uw onderzoek dat de aanzet heeft gegeven, en de gezamenlijke inzet van het hele team dat in de loop van de jaren is opgebouwd dat het heeft verder gezet. Ik denk dat we enorm trots mogen zijn op het eindresultaat. Ik weet nog dat verschillende mensen ons voor gek verklaarden met de hoeveelheid werk dat we wilden verzetten, en ook al zijn we niet 100% rond geraakt, we zijn toch gigantisch ver gekomen. Dream big, aim high! Ingrid, mijn vertrek naar Engeland zal zeker niet het einde betekenen van dit onderzoek. Er ligt nog zoveel in het verschiet… Ik ben er van overtuigd dat we nog vele mooie onderzoeken kunnen afronden, nieuwe kunnen starten, en hopelijk een nieuwe lichting doctoraatsstudenten hierbij kunnen betrekken. Duizend maal dank voor alles, voor alle steun, alle adviezen en alle opbeurende woorden.

Via via zijn we, prof. van Bree, dr. Gielen en ikzelf, dan in Leuven beland, bij de onderzoeksgroep van professor Jonkers. Beste Ilse, ik weet nog goed hoe ik vol trots de eerste versie van mijn IWT beurs-aanvraag doorstuurde. Een gedetailleerde beschrijving van de probleemstelling, en alle onderdelen van het doctoraatsonderzoek dat ik wilde gaan doen. Nadat ik de versie terug kreeg met de eerste commentaren en een voorbeeld versie doorgestuurd kreeg van een eerder ingediend project, was duidelijk dat er nog veel werk aan was. Vele versies later en na een aantal goed gedrilde ‘proef-verdedigingen’, was het dan tijd om ons project te gaan verdedigen in Brussel. Hoewel de resultaten na de eerste keer teleurstellend

waren, heeft u altijd 200% achter het project gestaan. Ik kreeg de kans om nog een jaar langer op de faculteit te blijven en het het jaar daarna nog eens te proberen. In dat jaar zijn we er gewoon aan begonnen alsof we het project ook effectief zouden kunnen afmaken. Honden naar Leuven gebracht om in het bewegingslabo alle kinetische en kinematische data te verzamelen en alvast een begin gemaakt met het musculoskeletaal model. Ik ben er van overtuigd dat al het werk dat we dat jaar gedaan hebben ervoor gezorgd heeft dat we de tweede keer wel succesvol waren in de aanvraag van een beurs. In de jaren daarna hadden we gelukkig steeds kleine en grotere mijlpalen… Gewrichten in het musculoskeletaal model, inverse kinematica, inverse dynamica, en in het laatste jaar ook de laatste stap naar de statische optimalisatie.
Ondanks uw drukke schema stond u altijd klaar met raad en opbouwende commentaren. Uw ruime onderzoeksinteresse en de visie dat we de technieken vanuit humaan biomechanisch onderzoek konden overbrengen naar de diergeneeskunde, heeft een heel belangrijke rol gespeeld in het behalen van de doctoraatsbeurs en de invulling van het onderzoek. Ilse, enorm bedankt voor alles!

Profesorry Van Ryssen, Bernadette, bedankt voor de jarenlange samenwerking en interessante discussies. De samenwerking met de orthopedie was een essentieel deel van dit hele project en uw kijk op dit project heeft zeker bijgedragen aan de succesvolle afronding ervan.

Dear professor Müller-Gerbl, Frau Professor, thank you for getting on board on this project. From the first time I introduced our research ideas to you to our first trip to Basel, and all the time spend working on the CTOAM images and interpreting the results. Your guidance and experience in CTOAM have made a major contribution to the results that we can present here today. The technique you have developed has the ability to do some amazing research projects, and I hope that with the work presented here, CTOAM will become a little more known in the world of veterinary biomechanical research. Thank you very much for everything you have done!

Professor Vanwanseele, Benedicte, ook u wil ik bedanken voor alle tijd die u gestoken heeft in mijn onderzoeksproject, en uiteraard dat van Billy. De vele uren die we tijdens de meetings in Leuven hebben samengezeten en verschillende spierparameters hebben bekeken, functionele implicaties van resultaten die we niet altijd 123 konden verklaren. Dit leverde altijd boeiende en leerrijke discussies op. Samen met professor Jonkers en professor Vander Sloten maakt u deel uit van het geweldige team dat mij, of beter gezegd ons, begeleid heeft in de wereld van gewrichtsbelasting en biomechanica.

Geachte professor Vander Sloten, Beste Jos, ook u bent vanaf het prille begin bij dit onderzoeksproject betrokken geweest en u was van onschatbare waarde. Zowel voor het uitschrijven van de project aanvraag als de daarop volgende proefverdediging en uiteraard het uiteindelijke onderzoekswerk. Uw verhelderende inzichten rond gewrichtsbiomechanica hebben dit werk tot een veel hoger niveau getild dan ik had kunnen hopen. Het blijft mij keer op keer verbazen hoe breed uw interesse en kennisdomein is. Heel hard bedankt voor alles en ik kijk uit naar de voortzetting van de onderzoekslijn die we met z'n allen hebben uitgebouwd.

Ik zou ook graag alle andere leden van de examencommissie willen bedanken voor hun tijd en energie die ze gestoken hebben in het verbeteren van de teksten, en de waardevolle commentaren die dit werk zonder twijfel tot een hoger niveau hebben gebracht.

Professor de Rooster, beste Hilde, u heeft uw taak als voorzitster van de examencommissie glansrijk volbracht. Ik wil u bedanken voor de jarenlange fijne samenwerking, voor het vertrouwen dat u altijd in mij gesteld hebt en voor uw hulp achter de schermen. Ik vind het jammer dat ik weg ga, maar ik kijk uit naar de nieuwe uitdagingen die de toekomst brengt.

Beste professor Van den Broeck, u was een van de mensen die ik graag in mijn examencommissie wilde hebben. Ik heb altijd veel respect voor u gehad omwille van uw kennis en brede interesses. Jaren geleden heb ik als student een Masterproef bij

u gedaan over het zicht bij roofvogels en uilen, een onderwerp waar u onmiddellijk mee instemde toen ik het aan u voorstelde. Het is een mooie cirkel dat u nu, aan het einde van mijn onderzoeksloopbaan aan de faculteit, terug een belangrijke rol speelt in mijn onderzoek.

The person who has literally gone to great lengths and distances, to be part of this exam committee is without a doubt professor Colborne. Dear professor, I am honoured that you are a member of my exam committee. Your publications on canine biomechanics are one of my main inspirations for this research project and your experience on biomechanical research and the applications in canine and equine orthopaedics is amazing. It was a privilege to be part of a select group of researchers at the Horse and Hounds workshop in Denmark this summer. I am looking forward to what the future will bring in terms of cooperation and research projects. Thank you for making time in your busy schedule to stop in Belgium form my internal defence.

Beste Evelien, bedankt voor je tijd en alle tekstuele verbeteringen die je hebt aangebracht. Ook bedankt voor de jarenlange samenwerking op de vakgroep, we zullen elkaar ongetwijfeld nog wel eens tegenkomen.

En dan van kleine naar grote huisdieren. Dr. Oosterlinck, beste Maarten, met uw inzichten en ervaring met bewegingsonderzoek bij paarden was u een perfecte kandidaat om in mijn examencommissie te zetelen. Merci voor uw tijd en opbouwende commentaren. Het doet goed om te weten dat het werk van de afgelopen jaren gewaardeerd wordt, hartelijk dank daarvoor.

Uiteraard was het luik van de musculoskeletale modellering niet mogelijk geweest zonder de hulp van verschillende mensen van de KUL. De eerste stappen zette ik onder het toeziend oog van Lode en Mariska. Lode, bedankt voor alle tijd die je in dit project gestoken hebt, de vele regels code die je hebt aangepast, en hoe je me wegwijs hebt gemaakt in al de verschillende programma's die ik onder de knie moest krijgen om vanaf een reeks CT beelden een musculoskeletaal model op te bouwen.

Hetzelfde geldt voor jou, Mariska, altijd heb ik op je hulp kunnen rekenen, en mede dankzij jou ben ik als simpele dierenarts zo ver gekomen met het model. En enorm bedankt voor alle hulp en antwoorden op mijn last-minute vragen.

Maarten, ook jou wil ik bedanken voor je al de tijd die je gestoken hebt om mij te trachten wegwijs te maken in Matlab. Ik ben geen Matlab-superster geworden, maar ik kan toch soms zelf al de fout in de code vinden en oplossen. Voor alle andere gevallen heb ik altijd een beroep op je kunnen doen, waarvoor heel veel dank!

En dan is er nog de eindige elementen modellering. Pim, enorm bedankt om mij te introduceren in de wereld van de eindige elementen. Hoewel we niet helemaal zijn rond geraakt, denk ik dat we trots mogen zijn op wat we hebben bereikt. De vele uren die je hebt gestoken in brainstormen over de best mogelijke aanpak heb ik zeer gewaardeerd. Ik wens je een gelukkige toekomst toe samen met Lianne en jullie kleine spruit.

Een welgemeende merci aan alle andere mensen van Leuven die rechtstreeks of onrechtstreeks geholpen hebben met dit doctoraat. Sam en Hannelore, bedankt voor jullie hulp bij het opmeten van de bewegingsdata. Ik waardeer het zeer dat jullie hiervoor tijd hebben vrijgemaakt in het weekend, om alles mee in goede banen te leiden.

Zonder bewegingsdata geen inverse kinematica of inverse dynamica, daarom een dikke merci aan de mensen van Hachico, in het bijzonder Elke en Annelies, om verschillende keren naar Leuven te komen met de Labradors, en geduldig mee te helpen met het bevestigen van al de markers.

Hoewel de resultaten van de bewegingsanalyse van de Mechelse Herder niet meer tot in dit doctoraatsboekje zijn geraakt, wil ik hiervoor toch een aantal mensen speciaal voor bedanken. In de eerste plaats alle eigenaren die zich hebben vrijgemaakt en in de weekenden zijn afgezakt naar Leuven. Cathy en Manu, Elke, Annick, Natacha en Fabien, Elke, en Marie zonder jullie was er geen kinematische en

kinetische data om verder mee te werken. Jullie inzet is van onschatbare waarde voor het toekomstige werk rond rasverschillen op vlak van beweging en gewrichtsbelasting.

En daarnaast natuurlijk 'mijn' Masterproefstudenten uit Leuven. Charlotte en Mayke, bedankt voor jullie interesse in dit onderzoeksproject, jullie inzet en al de tijd die jullie gestoken hebben in het labellen en verwerken van de bewegingsdata.

Sebastian, a big thanks to you for helping me out with all the practical CTOAM stuff. I really appreciated that I could stay at your house, and I will always remember all the daytime and late-night laughs and the tours around Basel. And a massive thank you for helping me with the indentation testing. Without your help, getting through the hundreds or test point would have taken days longer. The basement of the Engineering Faculty was like home for almost 2 weeks. I look forward to our future research projects together and I am sure we will stay in touch.
I would also like to thank Mira for all her time explaining the CTOAM workflow and getting me familiar with using the software.

En dan mijn 'onderzoeks-collega's', Casper, Aqui en Billy. De doctoraatsstudenten van de medische beeldvorming, allemaal met een eigen weg en een eigen verhaal.

Casper, we kennen elkaar al lang en onze Hollandsche roots zitten er ongetwijfeld voor iets tussen dat we altijd goed overeen zijn gekomen. Het is spijtig dat je niet de kansen hebt gekregen die je verdiende, maar ik denk dat je nu op een mooie plek terecht bent gekomen en ik hoop dat je toekomstplannen zoals ze er nu liggen werkelijkheid worden. Bedankt voor alle discussies, op wetenschappelijk en privé vlak, het waren mooie tijden als bureaugenoten. We houden contact en kijk uit naar de volgende 'case' die we samen bespreken en de ideeën die we heen en weer sturen.

Aqui, Mandingo! Thank you for everything the last years. It has been a pleasure getting to know you, both at work and outside work. All the laughs, crazy jokes and

videos made the long days of data collection a little more bearable. I hope everything with the house will work out the way you want it to. I wish you and Sofie all the best, and you know you are always welcome in the UK. Cuidate.

Billy, bedankt om jarenlang bureaugenoot te zijn. Ook al heeft het niet altijd mee gezeten met het verzamelen van data, en het verwerken van de grote hoeveelheid stalen, het is een heel mooi onderzoek. Ik ben er zeker van dat alle op zijn pootjes terecht komt, de aanhouder wint! Hoewel we er helaas niet meer toe gekomen zijn om jouw resultaten in het musculoskskeletale model te verwerken, zal dit zeker iets zijn dat in de toekomst zal gebeuren. Nog veel succes met het afronden van je doctoraat, en ik kijk uit naar je verdediging!

In de jaren op de faculteit heb ik vele bureaus mogen 'bewonen', en deze gedeeld met evenveel verschillende mensen.
Annemie, op dag 1 werd ik in je bureau gedropt. Bedankt voor de vele gesprekken en het delen van leuke, en minder leuke momenten. Ik heb je altijd graag gemogen en waardeer je interesse in wat ik doe en waar ik mij mee bezig hou, ook nu ik niet meer veel op de faculteit te vinden ben. We zullen elkaar nog wel eens tegenkomen in de toekomst. Voor nu, het allerbeste en veel succes met alle uitdagingen in de kliniek en daarbuiten.
Kaatje, bedankt voor de jarenlange samenwerking in de kliniek, het brainstormen over cases, en de wederzijdse klaagmuur functie. Het ga je goed.
Eva, ook al ben ik de laatste tijd niet meer op de bureau te vinden, sterker nog, al mijn spullen zijn al weg, er was altijd tijd voor een leuke babbel. Bedankt daarvoor, en wie weet komen we elkaar nog eens tegen.
Emmelie, nu je doctoraat achter de rug is, heb je weer wat ademruimte. Bedankt voor alle babbels, het delen van doctoraatsfrustraties en de hulp bij de laatste puzzelstukjes van mijn doctoraat. Ik wens je al het goede voor de toekomst.

Kim, ook al zat je meestal aan de andere kant van de gang bij de grote huisdieren, toch hebben we altijd een leuke tijd gehad. Bedankt voor alle babbels tussendoor en wie weet komen we elkaar nog eens tegen ☺.

Marnix, wat zou de vakgroep doen zonder u… De grote steun van alle projecten, groot en klein. Bedankt voor alles, en in het bijzonder voor alle praktische hulp bij de verschillende projecten die we gedaan hebben.

Alle andere collega's van de vakgroep, Yves, Stijn, Eva, Evelien, Elke, Els, Katrien, Kathelijne, bedankt voor de prettige samenwerking al die jaren. The imaging residents, Laure, Olivia, Blandine, Mileva, Lise, and Tibor, I would have loved to be part of the team, but the universe decided otherwise. I wish you all the best with the exams, the cases, and all the work you put into it, and I am sure you will all be great radiologists!
Professor Saunders, Jimmy, veel succes met het leiden van de diversiteit aan mensen en karakters binnen de vakgroep. Ik wens u en de vakgroep een mooie toekomst.

Professor Simoens, bedankt voor alle interessante discussie doorheen de jaren en voor het ter beschikking stellen van de snijzaal voor al het dissectie werk dat gedaan moest worden. Uw hulp met het prepareren van de ontkalkte tali, om zo een gefundeerde, wetenschappelijke basis te geven aan de CTOAM analyses was zeer waardevol.

Naast mijn doctoraat heb ik ook de kans gekregen om mij verder te verdiepen in de beeldvorming, meer specifiek CT en MRI. De vele nuttige ochtend meetingen met de CT-MRI unit zal ik mij altijd herinneren. Doorheen de jaren is mijn interesse in de beeldvorming alsmaar groter geworden, en hopelijk kan ik mij ook in de toekomst daar op richten.

Een speciaal woordje van dank ook voor de anesthesisten, zonder jullie geen honden op de CT en MRI. Ingeborg, Bossie, Inge, Virginie, Caroline, Alix, Ilaria, Anna, Tim Waelbers en Koen Piron, het was altijd fijn samenwerken. Bedankt voor jullie geduld tijdens de vele uren scannen.

De collega's van neurologie, professor Van Ham, Sophie, Valentine, Ine, Kenny, Emilie, Kimberley, Marios bedankt voor alles. Ik heb veel geleerd van jullie allemaal,

en bewonder wat jullie doen voor alle neurologische patiënten die we zien. Ik wens jullie en het Epicentrum al het goede voor de toekomst!

Professor Janssens, beste Geert, hartelijk dank voor de samenwerking op vlak van botdensiteit en allerhande biochemische bepalingen. De resultaten hiervan zullen zeker nog herwerkt worden tot een publicatie, want het is te mooi om verloren te laten gaan. Met de 'bouillon-theorie', is er een einde gekomen aan de initiële tegenstrijdige resultaten.

Alle andere collega's van verschillende vakgroepen over heel de faculteit, ik ga geen namen noemen uit schrik iemand over te slaan, maar ik heb met plezier met iedereen samengewerkt en nieuwe dingen geleerd. Bedankt aan iedereen!

Beste Siegfried Jaecques, een welgemeende merci voor de waardevolle oefenverdedigingen voor mijn beursaanvraag. Uw inzichten en tips hebben mij zeker geholpen beter voorbereid te zijn en op een heldere manier mijn antwoorden op de vragen van de jury te kunnen formuleren.

Hilde de Cock, bedankt voor alle pathologische rapporten en verhelderende inzichten.

De collega's van de microCT, in het bijzonder Manuel Dierick, bedankt voor al het werk dat jullie gedaan hebben voor het scannen van de tarsi. Het is deze data dat de basis heeft gelegd voor het eindige elementen model.

En dan zijn er natuurlijk nog de mensen buiten het werk en het onderzoek, en die zijn minstens even belangrijk. Zonder ontspanning is het niet mogelijk om jarenlang intensief aan iets als dit te werken.

Imme, ook al zien we elkaar niet zo veel, we hebben altijd een sterke band gehad. Bedankt voor je jarenlange vriendschap en steun in moeilijke tijden. Ik wens jou en

Chenzi een prachtige toekomst! En we zullen er zeker proberen bij te zijn in september!

Elise, ik ben blij dat je er vandaag ook bij bent. We hebben zoveel meegemaakt samen, leuke en minder leuke dingen, maar dat maakt onze vriendschap alleen maar sterker. Zoals je in Antwerpen en Gent altijd welkom was, geldt dit voor Engeland ook. Het is niet het eind van de wereld ☺. En als wij op 'het vaste land' zijn, plannen we zeker nog eens een wandeling door de Biesbosch met alle honden. Dikke knuffel voor jou en Bailey, BB4L!
David en Elien, door de jaren heen zijn we hechte vrienden geworden. Ik hoop dat we onze oudjaar-tradities kunnen voortzetten, ook nu we naar Engeland verhuizen. Het logeerbed staat al klaar en David, Oxford is maar een half uurtje rijden ☺. Alle geluk van de wereld voor jullie beiden en natuurlijk voor Marie. Ik kijk uit naar nog vele avonden flauwe, droge humor.

Iedereen die mij een beetje kent weet dat ik 1 grote passie heb, agility. Dat is dan ook waar ik mijn ontspanning en heel veel voldoening uit haal.
Andy, merci voor alle uren training en begeleiding. De laatste tijd niet veel tijd meer om tot Venlo te komen om te trainen, maar ik heb veel van je geleerd de afgelopen jaren.
Dave, thank you for all your training advice, and the hours of training videos you have reviewed over the last years. The training camps with you and Dan are always amazing, and we have learned so much!
En aan iedereen die ik via de agility heb leren kennen, merci voor de geweldige jaren! Als we nog eens terug in België zijn en hier een wedstrijd lopen, zullen we elkaar ongetwijfeld nog eens tegenkomen.

Papa en mama, het is niet in woorden uit te drukken wat jullie allemaal voor mij gedaan hebben. Het is geen gemakkelijke weg geweest om te komen tot waar ik nu ben. Bedankt om mij doorheen alles te steunen. Jarenlang van hot naar her gereden voor al mijn hobby's en verzameldrang, de vele ritten over en weer naar België, en de gigantische hoeveelheid levenswijsheid die jullie over de jaren met mij gedeeld

hebben. Zonder jullie zou alles er heel wat anders uit zien. Mama, wie had kunnen denken dat toen u jaren geleden een carrière switch maakte, dat u zou eindigen met een extra Master diploma. Ik ben enorm trots op alles wat u heeft bereikt en ben er zeker van dat de lijst zeker nog zal groeien! Papa, bedankt voor alles wat u gedaan heeft, ik kan mij geen betere papa wensen! Het is mede dankzij u dat ik de moed heb om alles te pakken en naar Engeland te vertrekken.

Stefan, mijn kleine broertje, ik ben trots op je! Helpen verhuizen en klussen gaat iets moeilijker worden nu we naar Engeland vertrekken, maar ik denk dat je voorlopig wel zal blijven wonen waar je woont. Het is toch in ieder geval op de groei gekocht ☺. Bedankt voor alles, en uit het oog is zeker niet uit het hart. Ik wens jou en Joyce alle geluk van de wereld samen!

Mijn schoonouders, Erna en Guy, ook jullie bedankt voor de steun en alles wat jullie voor mij, en ons, gedaan hebben de afgelopen jaren. Van de basis in de agility, tot het uitzoeken van een caravan die ons inmiddels al op heel wat schitterende plekken gebracht heeft. De vele barbecues, vakanties die ingepland worden rond agility wedstrijden, en de vele ovenschotels en lasagnes hebben de afgelopen jaren heel wat draaglijker gemaakt.

Mousti, Xanthy en Noa, bedankt om mij met andere ogen naar honden te doen kijken. Dat waren grote stappen, heel grote stappen, met een enorme impact op mijn leven. En natuurlijk Litch, Sim, Pixie en Yoko, toch stiekem ook een klein beetje mijn hondjes.

En om af te sluiten, mijn grote liefdes. Khai, Dice en Dobby. De een nog specialer dan de ander, wat zou ik zonder jullie moeten doen? Bedankt voor alle levenslessen die jullie mij geleerd hebben. Ik zal er over waken dat jullie het best mogelijke leven hebben.

Op een gedeelde eerste plaats, mijn andere grote liefde. Debby, schatje, merci om er altijd voor mij te zijn. Bij jou kan ik mezelf zijn, kan ik tot rust komen, en ik weet dat

het niet evident is om zo iemand te vinden. Sorry voor alle ametante momenten van de laatste maanden/jaren, ik weet dat ik niet altijd de gemakkelijkste ben. Ik ben een gelukkig man, en ik hoop dat ik jou zo gelukkig kan maken als jij mij maakt. Het feit dat we samen onze agility passie delen, maakt ons alleen maar sterker. Je hebt Dobby opgeleerd tot een geweldig hondje en ik ben ongelooflijk trots op wat je allemaal bereikt hebt!

Ik kijk er naar uit om ons leven samen verder te zetten in Engeland. Een groot avontuur wat ongetwijfeld niet altijd gemakkelijk gaat zijn, maar ik denk dat het geweldig gaat zijn daar.

WHAT WOULD YOU DO IF YOU WEREN'T AFRAID?